AD-A090 895 AIR FORCE INST OF TECH WRIGHT-PATTERSON AFB OH F/G 1/3
A FLIGHT INVESTIGATION OF DIGITAL CONTROL USING MICROPROCESSOR --ETC(U)
JUN 79 J C SEAT
UNCLASSIFIED AFIT-CI-79-188T NL

1 OF 2

AD A
090895

LEVEL II

1

AD A090895

Princeton University

DEI SUB NUMINE VIGET

Department of
Mechanical and
Aerospace Engineering

DTIC
ELECTE
OCT 23 1980
S D
D

DISTRIBUTION STATEMENT A
Approved for public release;
Distribution Unlimited

DDC FILE COPY

80 10 14 175

Accession For
NTIS GRA&I ☒
DTIC TAB ☐
Unannounced ☐
Justification
By
Distribution/
Availability Codes
Avail and/or
Dist Special
A

79-188T

A FLIGHT INVESTIGATION OF DIGITAL CONTROL USING MICROPROCESSOR TECHNOLOGY

by

James C. Seat

Princeton University
School of Engineering and Applied Science
Department of Mechanical and Aerospace Engineering

Submitted in partial fulfillment of the requirements for the degree of Master of Science in Engineering from Princeton University, 1978.

Prepared by:

James C. Seat

Approved by:

Professor R. F. Stengel

April 1979

DTIC
ELECTE
OCT 23 1980
S D
D

DISTRIBUTION STATEMENT A
Approved for public release;
Distribution Unlimited

UNCLASS

SECURITY CLASSIFICATION OF THIS PAGE (When Data Entered)

REPORT DOCUMENTATION PAGE		READ INSTRUCTIONS BEFORE COMPLETING FORM
1. REPORT NUMBER 79-188T	2. GOVT ACCESSION NO. AD-A090 895	3. RECIPIENT'S CATALOG NUMBER
4. TITLE (and Subtitle) A Flight Investigation of Digital Control Using Microprocessor Technology		5. TYPE OF REPORT & PERIOD COVERED Thesis
		6. PERFORMING ORG. REPORT NUMBER
7. AUTHOR(s) James C. Seat		8. CONTRACT OR GRANT NUMBER(s)
9. PERFORMING ORGANIZATION NAME AND ADDRESS AFIT Student at: Princeton University		10. PROGRAM ELEMENT, PROJECT, TASK AREA & WORK UNIT NUMBERS
11. CONTROLLING OFFICE NAME AND ADDRESS AFIT/NR WPAFB OH 45433		12. REPORT DATE June 1979
		13. NUMBER OF PAGES 162
14. MONITORING AGENCY NAME & ADDRESS (if different from Controlling Office)		15. SECURITY CLASS. (of this report) UNCLASS
		15a. DECLASSIFICATION/DOWNGRADING SCHEDULE

16. DISTRIBUTION STATEMENT (of this Report)

Approved for public release; distribution unlimited

17. DISTRIBUTION STATEMENT (of the abstract entered in Block 20, if different from Report)

APPROVED FOR PUBLIC RELEASE AFR 190-17.

FREDRIC C. LYNCH, Major, USAF
Director of Public Affairs

23 SEP 1980

18. SUPPLEMENTARY NOTES

Approved for public release: IAW AFR 190-17
Air Force Institute of Technology (ATC)
Wright-Patterson AFB, OH 45433

19. KEY WORDS (Continue on reverse side if necessary and identify by block number)

20. ABSTRACT (Continue on reverse side if necessary and identify by block number)

[redacted]

DD FORM 1 JAN 73 1473 EDITION OF 1 NOV 65 IS OBSOLETE

UNCLASS

SECURITY CLASSIFICATION OF THIS PAGE (When Data Entered)

ABSTRACT

A microprocessor-based digital flight control system (Micro-DFCS) is implemented in Princeton's Variable-Response Research Aircraft (VRA), and evaluated through flight testing. The flight control computer program, CAS-1, provides three longitudinal control options; direct (unaugmented) command, pitch rate command, and normal acceleration command. The latter two options are Type 0 systems designed by linear-quadratic control theory. The flight tests are designed to investigate the characteristics of these control laws in flight, to provide experimental evidence for sampling rate requirements, and to demonstrate digital flight control of the VRA with the Micro-DFCS.

The Micro-DFCS is installed in the VRA and functions properly. The qualitative and quantitative flight tests indicate that sampled-data regulator theory adequately accounts for the phase lags associated with sampling and holding continuous signals. Low sampling rates, of 10 samples per sec (sps) or less, can be used as a consequence. The controllability and responsiveness resulting at each of the three command modes are good at 10 sps. The pitch rate command option is considered to give good response down to 7 sps, although the vibrations generated by the discrete elevator movements sound somewhat like the stall buffet, which is disconcerting to the pilot. For all sampling rates tested (except 5 sps), pitch rate and normal acceleration control improves response over the direct command option; however, the discrete

movements of the elevator are more apparent for 7 sps and below.

Experimental results indicate that the Micro-DFCS provides a practical way to implement digital flight control. More research is necessary to investigate digital flight control using advanced command and control modes.

FOREWORD

I wish to express my appreciation and gratitude to Professor Stengel for his guidance and supervision during this investigation.

Further appreciation is extended to technical staff member George E. Miller for his invaluable advice and support throughout every phase of the project. I also wish to thank safety pilot Barry W. Nixon, aircraft mechanic Barton Reavis, and electronics technician Don Carter whose experience and expertise is reflected by the successful conduct of this project.

I wish to acknowledge the Office of Naval Research, which provided funding for this study under Contract No. N00014-78-C-0257.

I am most grateful to Sharon Matarese and Marion Sandvik for their time and patience in typing this thesis.

This thesis carries the report number 1411-T in the records of the Department of Mechanical and Aerospace Engineering.

TABLE OF CONTENTS

	Page
ABSTRACT	i
FOREWORD	iii
LIST OF FIGURES	vi
LIST OF TABLES	viii
LIST OF SYMBOLS	ix
1. INTRODUCTION	1-1
1.1 Advantages of Digital Flight Control Using Modern Control Theory	1-2
1.2 Research Objectives and Summary of Major Results	1-5
1.3 Organization of the Thesis	1-7
2. DEVELOPMENT OF THE CONTROL LAW	2-1
2.1 Derivation of the Type 0 Digital CAS	2-1
2.2 Effects of the Sampling Interval	2-9
2.3 Objectives of Control Design	2-12
2.4 Pitch Rate Command Control Structure	2-15
2.5 Normal Acceleration Command Control Structure	2-28
2.6 Dynamic Model Matching	2-34
3. CONTROL LAW IMPLEMENTATION AND HYBRID TESTING	3-1
3.1 Equipment Configuration of the Micro-DFCS	3-1
3.2 The Operational Microcomputer Software	3-4
3.3 Hybrid Simulation Tests and Results	3-9
4. FLIGHT TESTING	4-1
4.1 Test Objectives and Procedures	4-1
4.2 Flight Test Results and Analysis	4-6
5. CONCLUSIONS AND RECOMMENDATIONS	5-1
5.1 Conclusions	5-1
5.2 Recommendations	5-5

TABLE OF CONTENTS

(cont)

		Page
APPENDIX A:	Derivation of Discrete Weighting Matrices From Continuous Implicit Model-Following Weighting Matrices	A-1
APPENDIX B:	Description of APL Functions for Generating Optimal Gains and Time Histories	B-1
APPENDIX C:	Research Systems	C-1
	C.1 Variable-Response Research Aircraft (VRA)	C-1
	C.2 Experimental Facilities	C-6
APPENDIX D:	The Micro-DFCS Hardware	D-1
	D.1 Description of Microcomputer Components	D-1
	D.2 Directions for Using Control Display Unit	D-4
APPENDIX E:	The Micro-DFCS Software	E-1
	E.1 Description of CAS-1 Routines	E-1
	E.2 Software Development	E-9
	E.3 Adding Flight Control Routines to CAS-1	E-9
REFERENCES		R-1

LIST OF FIGURES

No.		Page
2-1	Type 0 CAS Structure	2-6
2-2	Frequency Ratio Versus Phase Lag for 20 dB Attenuator	2-9
2-3	Short-Period Frequency Requirements - Category B Flight Phase	2-16
2-4	Sequence for Finding Optimal Gains	2-20
2-5	Relation Between Weighting and Time Response - q CAS	2-23
2-6	Open-Loop Step Response for $y_d = 5^o$/sec (105 KIAS)	2-25
2-7	Pitch Rate Command Step Response for Q Weightings 25,25 ($y_d = 5^o$/sec, 10 sps, 105 KIAS)	2-25
2-8	Pitch Rate Command Step Response for Q Weightings 50,50 ($y_d = 5^o$/sec, 10 sps, 105 KIAS)	2-26
2-9	Pitch Rate Command Step Response for Q Weightings 75,25 ($y_d = 5^o$/sec, 10 sps, 105 KIAS)	2-26
2-10	Pitch Rate Command Step Response for Q Weightings 25,25 ($y_d = 5^o$/sec, 20 sps, 105 KIAS)	2-27
2-11	Pitch Rate Command Step Response for Q Weightings 75,25 ($y_d = 5^o$/sec, 20 sps, 105 KIAS)	2-27
2-12	Relation Between Weightings and Time Response - n_z CAS	2-32
2-13	Open-Loop Step Response for $y_d = .25g$ (105 KIAS)	2-33
2-14	Normal Acceleration Step Response for Q Weightings 5,10, R = 33 ($y_d = .25g$, 10 sps, 105 KIAS)	2-33
2-15	Normal Acceleration Step Response for Q Weightings 5,10 R = 250 ($y_d = .25g$, 10 sps, 105 KIAS)	2-35
2-16	Normal Acceleration Step Response for Q Weightings 5,10 R - 33 ($y_d = .25g$, 20 sps, 105 KIAS)	2-35
2-17	Sequence for Implicit Model-Following	2-39
3-1	Micro-DFCS Microcomputer Configuration	3-3
3-2	Overview of the VRA/Micro-DFCS System	3-4
3-3	CAS-1 Program Organization	3-7
3-4	Equipment Layout for Micro-DFCS Software Development	3-8
3-5	Hybrid Simulation Step Responses	3-15

LIST OF FIGURES

(cont)

No.		Page
4-1	Breakdown of Test Methods Used	4-5
4-2	Short-Period Frequency Requirements with All Control Modes Marked	4-9
4-3	Flight Test Step Responses	4-18
B-1	Sequence for Calculating Gains by Changing Weighting Matrices	B-13
B-2	Sequence for Calculating Gains Using Implicit Model-Following	B-17
C-1	Variable-Response Research Aircraft (VRA)	C-2
C-2	Major Components of VRA	C-3
C-3	Instrument Panel and Controls of VRA	C-5
C-4	FRL Ground Station	C-7
C-5	Schematic of Simulated VRA at 105 Kts With Scaling for Microcomputer Interface	C-8
D-1	Components of the Micro-DFCS and Software Development System	D-3
D-2	Control Display Unit (CDU)	D-4
D-3	Levels of Entry on CDU	D-5
E-1	Flowchart of Executive for CAS-1	E-2
E-2	Formating and Scaling of Sensor and Pilot Inputs	E-7
E-3	Sequence for Developing Microcomputer Routines	E-10
E-4	Flowchart for Typical Mode Set-Up Routine	E-12
E-5	Flowchart for Typical Flight Control Interrupt Service Routine	E-13

LIST OF TABLES

No.		Page
2-1	Gains, Predicted Step-Response and Eigenvalues for q CAS (105 KIAS)	2-28
2-2	Closed-Loop $\omega_{n_{sp}}$ and ζ_{sp} for q CAS (105 KIAS)	2-29
2-3	Gains, Predicted Step-Response and Eigenvalues for n_z CAS (105 KIAS)	2-34
2-4	Weighting Matrices and Gains for Implicit Model-Following Example	2-41
3-1	CAS-1 Program Table of Contents and Memory Requirements	3-6
3-2	Control Modes Used in Hybrid Tests	3-11
3-3	Optimal Gains for the Control Configurations	3-12
4-1	Results for Tracking Task	4-10
4-2	Results for Landing Approach Using the Direct Mode	4-14
4-3	Results for Banked Turn Test	4-15
B-1	Listing of APL Functions	B-3
C-1	VRA Control Characteristics	C-4
C-2	Computer Potentiometer Settings for VRA Longitudinal Model (105 KIAS)	C-9

LIST OF SYMBOLS

Variables	Description
C	Optimal Gains
D	Aerodynamic drag force
e	2.71828 . . . . .
F	System dynamics matrix (continuous-time system)
f	Frequency in Hz
$\underline{f}$	Nonlinear functions for vehicle equations of motion
G	Control effect matrix (continuous-time system)
g	Gravitational acceleration
H	• Observation matrix • Hexadecimal number
I	Identity matrix
J	Scalar cost funtional
L	Aerodynamic lift force
M	• Pitch moment • State and control weighting matrix
n_z	Normal acceleration
P	• Riccati equation solution • State covariance matrix
p	Roll Rate
Q	State weighting matrix
q	Pitch rate
R	Control weighting matrix
r	Yaw rate

S_{12}	Steady-state state vector mapping matrix
S_{22}	Steady-state control vector mapping matrix
s	Laplace transform variable
T	• Sampling interval • Thrust
t	Time
u	x-axis velocity
$\underline{u}$	Control vector
V	Total velocity
v	y-axis velocity
W	• Implicit model-following weighting matrix • Disturbance covariance matrix
w	z-axis velocity
$\underline{x}$	State vector
$\underline{y}$	Command vector
Z	Aerodynamic force along the z-axis

Variables (Greek)

α	Angle of attack
Γ	Control effect matrix (discrete-time system)
γ	Vertical flight path angle
δ_A	Aileron deflection
δ_E	Elevator deflection
δ_F	Flap deflection
δ_R	Rudder deflection

δ_s	Longitudinal stick deflection
δ_{SF}	Side-force panel deflection
δ_T	Throttle deflection
ζ	Damping ratio
θ	Pitch attitude angle
λ	Eigenvalue
Σ	Summation
Φ	State transition matrix (discrete-time system)
ϕ	Roll attitude angle
ψ	Yaw attitude angle
ω_n	Natural frequency

Subscripts

CL	Closed-loop
d	Desired value
i	Element index for vectors and matrices
k	Sampling instant index
M	Model
o	Nominal value
q	Sensitivity to pitch rate
SP	Short-period
V	Sensitivity to total velocity
α	Sensitivity to angle of attack
δ_E	Sensitivity to elevator deflection

Punctuation

$(\dot{\ })$	Derivative of quantity with respect to time
$(\underline{\ \ })$	Vector quantity
$\partial(\ )/\partial(\ )$	Partial derivative of one variable with respect to another
$\Delta(\ )$	Perturbation variable
$(\ )^*$	Steady-state value
$(\ )^T$	Transpose of a vector or matrix
$(\ )^{-1}$	Inverse of a matrix
$(\hat{\ })$	Discrete weighting matrix

Acronym

A/D	Analog to digital
APL	A programming language
ASCII	American standard code for information interchange
CAS	Command augmentation system
CDU	Control display unit
CPU	Central processing unit
D/A	Digital to analog
DFC	Digital flight control
DFCS	Digital flight control system
FBW	Fly-by-wire
FCCU	Flight control computer unit
FRL	Flight Research Laboratory
IAS	Indicated air speed

I/O	Input/output
KIAS	Knots, indicated air speed
LQ	Linear-quadratic
Micro-DFCS	Microprocessor based digital flight control system
MSL	Mean sea level
PDM	Pulse duration modulation
PROM	Programmable read-only memory
RAM	Random access memory
RF	Radio frequency
SBC	Single board computer
sps	Samples per second
VRA	Variable-response research aircraft

1. INTRODUCTION

A properly implemented Command Augmentation System (CAS) provides stability and control augmentation which can significantly improve the basic aircraft handling qualities. A digitally mechanized CAS, as opposed to one which uses analog components, allows advanced concepts of control theory to be easily reduced to practice. Using the computational capabilities of digital computers, advanced control modes can be implemented and scheduled according to the task and flight condition.

Digital microprocessors and modern control theory are two relatively new areas for research in the Digital Flight Control (DFC) context. The application of both technologies to DFC will help realize the full potential of flight control. To date, few aircraft have been flown under digital control and none have used a microprocessor based digital flight control system (Micro-DFCS) for a manned vehicle. Likewise, the use of modern control theory for DFC in actual flight tests has been limited. More flight testing of DFC using these concepts is necessary to fully understand the relationships between theory and practice.

This thesis describes an experimental program for investigating DFC using a Micro-DFCS. Simple Type 0 longitudinal control laws, designed with modern control theory, are implemented on a Micro-DFCS installed in the research aircraft. Actual flight tests are conducted

to provide results and experimental evidence for DFC and modern control theory.

1.1 ADVANTAGES OF DIGITAL FLIGHT CONTROL USING MODERN CONTROL THEORY

Modern control theory combines state space, time domain, and optimal control concepts with earlier frequency domain methods in the design of control systems. The procedure uses high-speed digital computers to generate control gains and parameters. This method allows easy development of advanced control modes such as controllers with state and control rate restraint, control decoupling, interconnects, and Type 1 CAS structures (although this study examines none of these advanced modes). For a Digital Flight Control System (DFCS), it is important to minimize sampling rates to reduce computational requirements. High sampling rates will be required unless care is taken in the modeling and design process (Ref. 1); hence, modern digital control design techniques, including both time-domain and frequency-domain methods, generally model the sampling effects well enough to allow low rates to be used without loss of stability or performance.

Some of the major advantages of using a digital computer for flight control are the following:

- Ease of scheduling gains and changing control modes
- Ability to implement advanced control modes easily (Ref. 2)
- Ease of changing performance characteristics
- Ability to time share logic to serve a number of other functions (such as navigation or fuel management) (Ref.3)
- Ability to perform in-line self testing, resulting in improved performance (Ref. 2)

The first advantage listed is attributed to the digital computer's conditional logic. By monitoring the aircraft's flight condition and pilot's requests, the computer can make decisions to change the parameters of the presently running control law or can implement a completely different CAS structure. The last four points listed are due mainly to the flexibility of designing with software. Once the pilot's commands and the feedback variables are interfaced with the computer's analog input channels, the software can be developed to manipulate the input data in a variety of ways to perform the desired functions. Advanced control modes would require different sets of calculations in software, but no increase in hardware complexity. Performance characteristics of the DFCS can be changed by simple software modifications instead of a complete redesign of hardware. The computer can be programmed to diagnose malfunctions in the control system and take corrective action. For instance, the computer can compare the output from feedback sensors with the values expected, given by a state estimator. If a sensor's value is completely different from the expected value, a back-up sensor can be brought on line.

It is becoming increasingly apparent that the principal means of implementing the DFCS in the future will be with microprocessor technology. Great advances within the last few years in the development of large-scale-integrated circuits enable these small, inexpensive components to perform the arithmetic logic, data storage, control sequencing, and input/output functions necessary for the DFCS. A Micro-DFCS

will give a significant reduction in cost, size, weight, and power usage for the flight control hardware. These four characteristics will probably have the most direct impact on cost/performance criteria and therefore will be the immediate stimulus for using the Micro-DFCS. The present major limitation of microprocessors is the small data word length. Most microprocessors on the market today, have word lengths of four or eight bits (although a few have 16 bit words). This reduces the computational speed relative to minicomputer systems, increasing the need for low sampling rates.

Very few flight test programs have been done to research digital flight control. To date, the tests used aircraft and experimental equipment with high operating costs (due to their large size, high fuel use, and complexity). References 2 and 4 to 10 describe flight test programs that used a DFCS. Because of the high cost of these programs, the data on actual implementation of digital flight control is understandably limited. No flight tests prior to this study have used microprocessor technology for digital flight control in manned vehicles.

Similarly, the availability of flight test results for a DFCS designed with modern control theory is small (References 4, 5, 10 and 11 document investigations that have used modern control laws in flight, and there may be other examples not cited here). Past programs have

usually used the conservative approach of digitizing an analog control law which leads to high sampling rates (usually 50 per sec or higher). Sampled-data regulator theory (Ref. 12) gives control law designs that take into account the discrete-time nature of the calculations and makes more efficient use of digital systems by allowing lower sampling rates. More experimental data is required through flight testing to define the methodologies and verify the concepts of digital flight control using microprocessor technology and modern control theory. Such testing will promote the practical acceptability of digital flight control and modern control theory in the future.

1.2 RESEARCH OBJECTIVES AND SUMMARY OF MAJOR RESULTS

The flight testing of this investigation is conducted using Princeton's Variable-Response Research Aircraft (VRA) operating from the Flight Research Laboratory (FRL). See Appendix C for a description of the VRA and FRL. The analog Fly-by-Wire (FBW) system of the VRA is augmented with the Micro-DFCS described in Chapter 3 and Appendices D and E. Qualitative and quantitative data are collected on the performance of the system operating with simple Type 0 control laws where the optimal gains are not scheduled. Pitch rate and normal acceleration CAS structures with two-state feedback, one control input to elevator, and one pilot input of longitudinal stick are tested.

The testing is constructed to allow three primary objectives to be met:

- Provide results for the investigation of optimal control laws in flight
- Provide experimental evidence for sampling rate requirements
- Successfully demonstrate the VRA FBW system augmented with the Micro-DFCS

The first and second objectives are aimed at answering some basic questions about implementing a Micro-DFCS. They are accomplished by setting a variation of sampling rates and optimal gains for the pitch rate control mode, the normal acceleration control mode, and a direct (open-loop) mode. The different control configurations are evaluated in the landing approach, in a tracking task at altitude, and by examining the step response of the commanded state to a step input with longitudinal stick. The telemetry records and pilot's comments for each variation are examined to demonstrate flying qualities and to define advantages and limitations of the Micro-DFCS using optimal control laws. The test results are used also to establish some lower limits on sampling rate for these particular control configurations. The third objective is intended to demonstrate that the Micro-DFCS equipment and related software function in actual flight as designed. Of course, the successful completion of the first two objectives depend on accomplishment of the third objective.

Many results were obtained from the development and testing of the Micro-DFCS; a few major ones are summarized here. The hardware of the Micro-DFCS is completely installed and working. No hardware problems were encountered except for a structural vibration that needed to be filtered out of the normal accelerometer. A sampling rate of 10 samples per

second (sps) is very acceptable for the pitch rate control laws studied. At sampling rates of 7 sps and below, the step movements of the elevator are very annoying and sound somewhat like a stall buffet. The present results indicate that for any given sampling rate, the pitch rate CAS improves the response over that obtained with open-loop control. Sampling rates of 3 sps and above are acceptable for the flare maneuver of the landing, but the short final approach segment requires 10 sps for good control. Telemetry records show that, as expected, decreasing sampling rates do not affect the step response of the commanded state when the gains are calculated using sampled-data regulator theory.

1.3 ORGANIZATION OF THE THESIS

The thesis is organized into five chapters and five appendices. In Chapter 2, the control laws are developed with linear-optimal control theory. The optimal gains are calculated by a linear-quadratic weighting method and an implicit model-following technique. The response of the augmented system, as predicted by the analytical study, is presented for different control laws, sampling rates, and gains. In Chapter 3, the basic aspects of the Micro-DFCS equipment and software are outlined to show how the control laws are actually implemented. Results from hybrid tests (where the VRA is simulated on an analog computer) are presented and compared to the analytic results of the previous chapter.

Chapter 4 gives results and analysis of the actual flight tests.

The theory and designs discussed in Chapters 2 and 3 are evaluated in the actual environment for which they are intended. Comparisons with analytic and hybrid test results are made. Chapter 5 draws conclusions from this work and makes recommendations for further study. Appendices A through E provide details of the VRA and FRL facilities, a derivation of digital weighting matrices, instructions for using the APL functions for generating optimal gains, and a detailed description of the Micro-DFCS equipment and related software.

2. DEVELOPMENT OF THE CONTROL LAW

This chapter describes the optimal control theory, control design objectives, and analytical results for the Micro-DFCS. Pitch rate and normal acceleration command control laws are developed with a second-order reduced model of the VRA. An easy extension of the linear-quadratic (LQ) regulator methods used here, to dynamic model matching is presented.

2.1 DERIVATION OF THE TYPE 0 DIGITAL CAS

The development of the digital CAS in this report uses sampled-data regulator theory. In this case the selected control law drives a continuous system using piecewise - constant inputs that change only at the sampling intervals (zero-order hold). The objective of the sampled-data regulator is to control the system to be as close as possible to the trajectory obtained by using a continuous controller (Ref. 12). The derivation proceeds as follows.

The design of the digital CAS starts with specification of the continuous-time system dynamics. Neglecting disturbance inputs, the non-linear equations of motion for the flight vehicle (Ref. 13) can be written as a vector differential equation:

$$\dot{\underline{x}}(t) = \underline{f}[\underline{x}(t), \underline{u}(t)] \tag{1}$$

The state vector $\underline{x}(t)$ is, in general, of length n and specifically contains three components each of translational rate, angular rate, and attitude,

$$\underline{x}^T = [u\ v\ w\ p\ q\ r\ \theta\ \phi\ \psi] \tag{2}$$

where (u, v, w) are body-axis velocities, (p, q, r) are body-axis rotational rates, and (θ, ϕ, ψ) are Euler angles of the body-axes with respect to an Earth-fixed frame. The control vector $\underline{u}(t)$ is of length m and includes deflections of the elevator, throttle, flaps, ailerons, rudder, and side force panels:

$$\underline{u}^T = [\delta_E\ \delta_T\ \delta_F\ \delta_A\ \delta_R\ \delta_{SF}\ ] \tag{3}$$

In order to linearize the equations for use in designing the control laws, it is necessary to divide the states and controls into nominal and perturbation components,

$$\underline{x}(t) = \underline{x}_o(t) + \Delta\underline{x}(t) \tag{4}$$

$$\underline{u}(t) = \underline{u}_o(t) + \Delta\underline{u}(t) \tag{5}$$

The linearization is accomplished by taking a first-order Taylor series expansion of Eq. 1:

$$\dot{\underline{x}}_o(t) = \underline{f}\ [\underline{x}_o(t),\ \underline{u}_o(t)\ ] \tag{6}$$

$$\Delta\dot{\underline{x}}(t) = F(t)\ \Delta\underline{x}(t) + G(t)\ \Delta\underline{u}(t) \tag{7}$$

where

$$F(t) = \frac{\partial}{\partial\underline{x}}\underline{f}\ [\underline{x}_o(t),\ \underline{u}_o(t)] \tag{8}$$

$$G(t) = \frac{\partial}{\partial \underline{u}} \underline{f} \, [\underline{x}_o(t), \, \underline{u}_o(t)] \tag{9}$$

The F matrix is (n x n) and will be referred to as the system dynamics matrix. G is (n x m) and is called the control effectiveness matrix. The calculation of $\underline{x}_o$ is still a non-linear problem, so the CAS will be designed with one specific $\underline{x}_o$ in mind. F(t) and G(t) are functions of $\underline{x}_o$ and $\underline{u}_o$; as long as the vehicle flies within close proximity to the flight condition specified, F(t) and G(t) change very little (Ref. 13). This leads to control laws based on linear time-invariant models which could be adapted to changing flight conditions by gain scheduling.

The linear differential equations of motion (Eq. 7) are converted to difference equations which take the form,

$$\Delta \underline{x}_{k+1} = \Phi \, \Delta \underline{x}_k + \Gamma \, \Delta \underline{u}_k \tag{10}$$

where Φ is the aircraft's state transition matrix and Γ is the discrete control effectiveness matrix (Ref. 12),

$$\Phi = e^{FT} = I + FT + \frac{(FT)^2}{2} + \frac{(FT)^3}{6} + \ldots \tag{11}$$

$$\Gamma = F^{-1}(I - \Phi^{-1}) \, G \tag{12}$$

where T is the sampling interval.

To complete the state space representation of the aircraft's dynamics, the output of the system is defined as:

$$\Delta \underline{y}_k = H_x \, \Delta \underline{x}_k + H_u \, \Delta \underline{u}_k \tag{13}$$

The Type 0 control law takes the form,

$$\Delta \underline{u}_k - \Delta \underline{u}^* = - C\ (\Delta \underline{x}_k - \Delta \underline{x}^*) \tag{14}$$

where a starred vector represents the steady-state value of that vector when the input to the CAS commanded by the pilot is attained. Examining Eq. 14, it is seen that when $\Delta \underline{x}_k$ reaches its steady-state value, the output of the controller, $\Delta \underline{u}_k$, will be equal to the proper steady-state deflections. The steady-state vectors $\Delta \underline{x}^*$ and $\Delta \underline{u}^*$ are functions only of the pilot's commanded inputs and are independent of what feedback gains are used or how the loop is closed. They are simply the calculated values of $\Delta \underline{x}_k$ and $\Delta \underline{u}_k$ for a particular commanded input.

The states or controls to be commanded by the pilot are specified in the control law by defining values for H_x and H_u of the output equation, Eq. 13 (Ref. 14). In this way, the pilot's inputs are defined as the system's outputs to be controlled by the CAS. In other words, the aircraft's motions are the variables commanded by the pilot's controls rather than the control surface positions. Since the pilot's inputs will be considered, the system's outputs after the selection of H_x and H_u, Eq. 13 can be rewritten,

$$\Delta \underline{y}_{d_k} = H_x\ \Delta \underline{x}_k + H_u\ \Delta \underline{u}_k \tag{15}$$

where $\Delta \underline{y}_{d_k}$ contains the pilot's commanded inputs.

The relations between $\Delta \underline{y}_{d_k}$, $\Delta \underline{x}^*$, and $\Delta \underline{u}^*$ are described by

Eqs. 7 and 15 when $\Delta\dot{\underline{x}} = 0$, defining the trim condition:

$$\begin{bmatrix} F & G \\ H_x & H_u \end{bmatrix} \begin{bmatrix} \Delta\underline{x}^* \\ \Delta\underline{u}^* \end{bmatrix} = \begin{bmatrix} 0 \\ \Delta\underline{y}_{d_k} \end{bmatrix} \tag{16}$$

If the number of commands and controls is equal, and the compound matrix in Eq. 16 is nonsingular, then it can be inverted, and $\Delta\underline{x}^*$ and $\Delta\underline{u}^*$ are defined by

$$\begin{bmatrix} \Delta\underline{x}^* \\ \Delta\underline{u}^* \end{bmatrix} = \begin{bmatrix} F & G \\ H_x & H_u \end{bmatrix}^{-1} \begin{bmatrix} 0 \\ \Delta\underline{y}_{d_k} \end{bmatrix} \tag{17}$$

or

$$\Delta\underline{x}^* = - F^{-1}G(-H_xF^{-1}G + H_u)^{-1}\ \Delta\underline{y}_{d_k} \tag{18}$$

$$\Delta\underline{u}^* = (- H_xF^{-1}G + H_u)^{-1}\ \Delta\underline{y}_{d_k} \tag{19}$$

Throughout this report, the relations in Eqs. 18 and 19 will be written as

$$\Delta\underline{x}^* = S_{12}\ \Delta\underline{y}_{d_k} \tag{20}$$

$$\Delta\underline{u}^* = S_{22}\ \Delta\underline{y}_{d_k} \tag{21}$$

for reasons explained in Ref. 15.

Substituting Eqs. 20 and 21 into Eq. 14 and rearranging, the control inputs (as functions of the pilot's inputs) are

$$\Delta \underline{u}_k = S_{22}\, \underline{y}_{d_k} - c(\Delta \underline{x}_k - S_{12} \underline{y}_{d_k}) \tag{22}$$

A block diagram of this system is shown in Fig. 2-1.

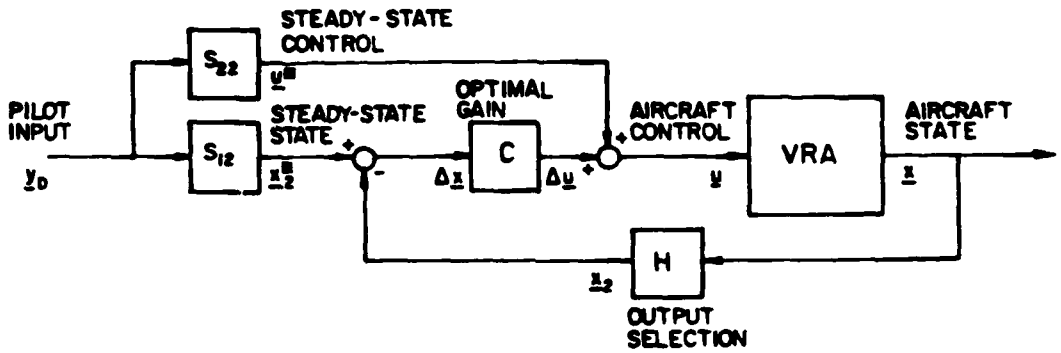

Figure 2-1. Type 0 CAS Structure

It is interesting to note that due to the feedforward of $\underline{y}_{d_k}$ through S_{22}, it is possible to have zero "hang-off" error even though this is a Type 0 system. A condition of zero hang-off depends, however, on no disturbances and knowing the exact system parameters when calculating S_{12} and S_{22}.

The gains, C, are calculated using linear quadratic (LQ) regulator theory (Ref. 12). The objective of this method is to find the feedback gains which allow the control law to minimize the quadratic cost functional,

$$J = \int_0^\infty (\Delta \underline{x}^T Q \Delta \underline{x} + \Delta \underline{u}^T R \Delta \underline{u})\, dt \tag{23}$$

where Q is positive semi-definite and R is positive definite. Matrices Q and R weight the importance of suppressing perturbations in states and control inputs away from the commanded values. Therefore Q and R are design parameters which provide flexible and efficient means of changing closed-loop response to satisfy the response criteria.

Gains calculated to minimize Eq. 23 will not minimize its sampled-data counter-part,

$$J = \sum_{i=o}^{N-1} (\Delta \underline{x}_i^T Q \Delta \underline{x}_i + \Delta \underline{u}_i^T R \Delta \underline{u}_i) \tag{24}$$

for the same Q and R. Reference 12 outlines a method of picking continuous-time weighting matrices that minimize the continuous-time cost functional even though a sampled-data regulator is used. In this case the cost functional for the sampled-data case penalizes the system continuously in time, i.e., not just at the sampling instances. Minimizing a continuous cost functional with a sampled-data regulator is equivalent to making the state trajectory obtained from the digital CAS as close as possible to that obtained with a continuous controller. This is true because both controllers are derived from the same performance criterion, J. Using the method of Ref. 12, Eq. 23 is set equal to the sampled-data cost functional:

$$J = \sum_{k=o}^{\infty} [\Delta \underline{x}_k^T \hat{Q} \Delta \underline{x}_k + 2\Delta \underline{x}_k^T \hat{M} \Delta \underline{u}_k + \Delta \underline{u}_k^T \hat{R} \Delta \underline{u}_k] \tag{25}$$

The discrete weighting matrices are found to be:

$$\hat{Q} = \int_{t_k}^{t_{k+1}} \Phi^T(T)\ Q\ \Phi(T)\ dt \tag{26}$$

$$\hat{M}^T = \int_{t_k}^{t_{k+1}} \Phi^T(T)\ Q\ \Gamma(T)\ dt \tag{27}$$

$$\hat{R} = \int_{t_k}^{t_{k+1}} [R + \Gamma^T(T)\ Q\ \Gamma(T)\ dt \tag{28}$$

The matrices $\hat{Q}$ and $\hat{R}$ are, respectively, positive semi-definite and positive definite. The steady-state discrete Riccati equation is,

$$P = \Phi^T P \Phi - (\Gamma^T P \Phi + \hat{M})^T (\hat{R} + \Gamma^T P \Gamma)^{-1} (\Gamma^T P \Phi + \hat{M}) + \hat{Q} \tag{29}$$

where P is the equation's steady-state solution. The gains C, are given by:

$$C = (\hat{R} + \Gamma^T P \Gamma)^{-1} (\Gamma^T P \Phi + \hat{M}) \tag{30}$$

To find the gain matrix C for a certain Q and R, $\hat{Q}$, $\hat{M}$ and $\hat{R}$ must be calculated using Eqs. 26-28. Equation 29 then is solved, and these results are used in the gain equation (Eq. 30) to compute C.

In summary, this section has presented a way to control a continuous-time system with a discrete-time Type 0 CAS. The weighting matrices Q and R can be specified for a continuous-time cost functional but implemented with a discrete-time control law (Eq. 22). This is easier than trying to specify $\hat{Q}$, $\hat{M}$, and $\hat{R}$ directly, because Q and R

can be based on state-control tradeoffs in the continuous-time problem. Also, Q and R can be picked as diagonal matrices whereas $\hat{Q}$ and $\hat{R}$ would not normally be diagonal.

2.2 EFFECTS OF THE SAMPLING INTERVAL

As mentioned in Chapter 1, a digitized analog control law normally requires very high sampling rates which could put excessive computational burden on a microprocessor-based system. High sampling rates are necessary for mimicked analog systems because of the phase lags associated with zero-order hold sampling. Reference 16 presents a graph (Fig. 2-2) that shows the relation between phase lag and sampling frequency when the signal is first passed through a second-order anti-aliasing filter with 20 dB attenuation at the sampling frequency, f_{sample}.

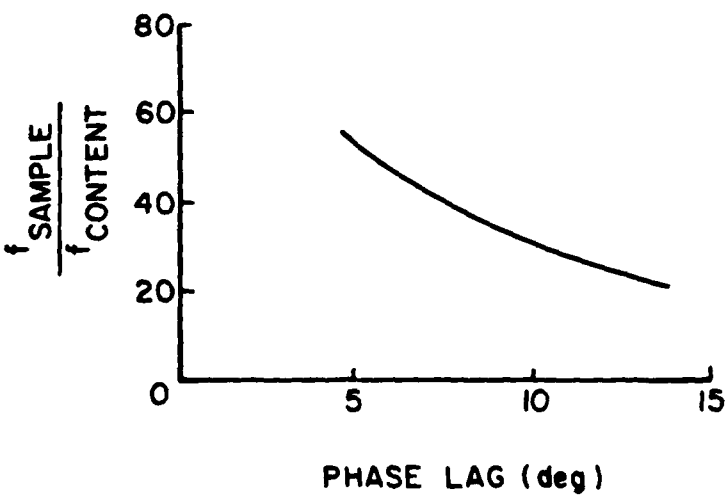

Figure 2-2. Frequency Ratio Versus Phase Lag for 20 dB Attenuator.

For instance, if a phase shift of 10 deg is tolerable, the sampling frequency should be approximately 30 times the highest frequency of interest, according to Fig. 2-2.

The constraints imposed by the phase lag problem are eliminated when the sampled-data regulator theory of Section 2.1 is used in the controller's design. It is not too difficult to see that sampling lag effects are taken into account with a sampled-data regulator because the cost functional is being minimized in continuous-time and not just at discrete instances. Not quite so obvious is why it is not necessary to sample at higher than twice the highest frequency mode to be controlled. This constraint is avoided by taking advantage of our prior knowledge of the system in developing the control law. As can be seen from Eqs. 22-30, the aircraft's dynamics and control effects are included right in the control law. For any given control input, the digital CAS "knows" what the aircraft's response will be and controls it to match $\underline{y}_{d_k}$ to the degree specified by the weighting matrices.

There is, of course, a maximum value for the sampling interval for any given system to be controlled. This maximum can be dictated by one of two different constraints. The two constraints are 1) error build-up between samples, and 2) pilot acceptance. These two limiting factors are explained below.

Error Build Up Between Samples

If there were no disturbance inputs to the system and the dynamic and control parameters of the system were known exactly, then this constraint would not be present. But in the real world there are disturbances and parameter variations, so errors between the desired and actual states of the aircraft can build up while the system is running "open-loop" between the discrete control inputs. The sampling interval should, therefore, be selected so that error build up is limited to acceptable values under "worst case" conditions (Ref. 17). The error buildup can be described by propagating the state covariance with the differential equation,

$$\dot{P} = FP + PF^T + W \tag{31}$$

where P is the state covariance matrix and W is the disturbance covariance matrix (Ref. 18).

Error build-up because of too long a sampling interval can lead to large control change increments, which may be damaging to the control surface actuators and associated mechanisms. These large changes are commanded instantaneously, which causes the actuators to deflect the controls at the maximum rate. These quick, pulsing movements may set up vibrations and high stresses on the actuators and linkage. This may effectively reduce the operating life of these components.

Pilot Acceptance

Because a DFCS changes its output only at discrete instants,

the plane's motions set by a pilot's commands may not occur until up to one sampling interval after the command. If the pilot moves a control and the aircraft's response is delayed perceptably, his ability to control is degraded. The sampling rate must be at least high enough so the pilot perceives no appreciable time delay in response to his inputs, as defined for each phase of flight. It is necessary to conducted piloted experiments, either in flight or in ground-based simulators, to determine this significance of time-delay effects.

2.3 OBJECTIVES OF CONTROL DESIGN

Two different design objectives for the control law are addressed, both aimed at modifying the basic short-period response of the aircraft in straight-and-level flight. The first is to improve the response of the commanded state to a step input from the pilot. An improved response is judged by a decrease in rise time and overshoot (an increase in the longitudinal, closed-loop, short-period natural frequency and damping). The degree to which the response can be improved is constrained by the maximum rate of deflection of the control surface and the requirement to satisfy "Level 1" flying quality specifications for the short-period, as defined by MIL-F-8785B(ASG) (Ref. 19). The FBW system in the VRA is set to disengage automatically if the error between actual and commanded deflections of elevator is greater than approximately 5 deg. The error to be tolerated in the analytic study is taken to be this value.

The specifications for the short-period motion in the Military Specification on Flying Qualities are stated as constraints on the natural frequency and damping of that mode. For cruise, the minimum damping ratio is 0.3 and the maximum is 2.0. Natural frequency limitations are expressed in a graph with the frequency,($\omega_{n_{sp}}$) related to normal acceleration (n_z) per angle of attack (α) (Fig. 2-3). The basic VRA is marked on Fig. 2-3 and is in the Level 1 flying qualities area.

It is not always desirable to speed up the response and reduce overshoot of the commanded inputs. Sometimes it is necessary to slow the response down because the basic aircraft is too quick and oversensitive to commanded inputs. The weighting matrices can be found to do this by a method of model following explained in Section 2.6. Therefore, the second design objective for the control law is to allow simulation of another aircraft's dynamics by matching the closed-loop short-period modal characteristics of the VRA with the aircraft to be modeled. Success of the match is checked analytically by comparing stability derivatives of the closed-loop and model F matrices.

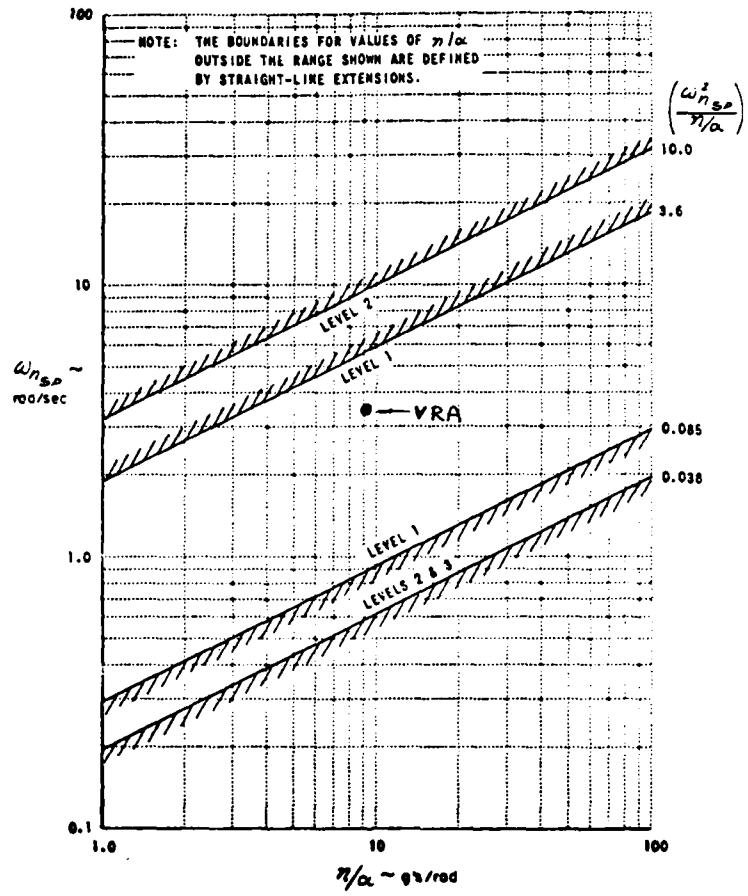

Figure 2-3. Short-Period Frequency Requirements - Category B Flight Phase (from Ref. 19).

In this case, the design objective for augmenting the short-period is not to increase the natural frequency or damping ratio, but to show that, in fact, the short-period poles can be arbitrarily placed in the left-half-plane as required using the LQ control methods.

2.4 PITCH RATE COMMAND CONTROL STRUCTURE

Pitch rate (q) is a desirable state for longitudinal stick (δ_s) to command because at low speeds, when performing some sort of tracking task, q is the motion cue the pilot senses for a deflection of δ_s. The simple Type 0 control law derived in Section 2.1 is now applied so the response of Δq to $\Delta\delta_s$ can be modified as required. The procedure begins by defining the dynamics that give changes in q.

No coupling between the longitudinal and lateral-directional dynamics will be considered, so the state and control vectors of Eqs. 2 and 3 reduce to:

$$\underline{x}^T = [\ u\ w\ q\ \theta\ ] \tag{32}$$

$$\underline{u}^T = [\ \delta_E\ \delta_T\ \delta_F\ ] \tag{33}$$

States u and w are not directly measurable by the sensors of the VRA, so $\underline{x}$ is redefined as,

$$\underline{x}^T = [\ V\ \gamma\ q\ \alpha\ ] \tag{34}$$

where the velocity, V, and climb angle, γ are taken from the velocity-axis, and α is taken from the wind-axes. The F matrix associated with

the above state vector is derived from the nonlinear equations of motion (Ref. 13) as in Eq. 8 and is,

$$F = \begin{bmatrix} D_V & -g\cos\gamma_o & D_q & D_\alpha \\ L_V & g/V_o\sin\gamma_o & L_q & L_\alpha \\ M_V & 0 & M_q & M_\alpha \\ L_V & -g/V_o\sin\gamma_o & (1-L_q) & -L_\alpha \end{bmatrix} \tag{35}$$

where the elements of F are stability derivatives and inertial effects that represent the sensitivity of state rates to state perturbations. At 105 KIAS in straight-and-level flight, the VRA's F matrix is:

$$F = \begin{bmatrix} -.073 & -32.2 & 0 & 0 \\ .002 & 0 & 0 & 2 \\ .002 & 0 & -2.08 & -8.35 \\ -.002 & 0 & 1 & -2 \end{bmatrix} \tag{36}$$

where angles are in radians, velocity in fps, and acceleration is in fps^2. The F matrix can be divided into four (2 x 2) matrices that contain the parameters for the short-period and phugoid modes:

$$F = \left[\begin{array}{c:c} \text{Phugoid Parameters} & \text{Short-Period to Phugoid Coupling} \\ \hdashline \text{Phugoid to Short-Period Coupling} & \text{Short-Period Parameters} \end{array}\right] \tag{37}$$

Since the off-diagonal matrices have elements with values of near zero, the short-period is described mostly by changes in q and α, and the phugoid is described mostly by changes in V and γ. This implies control

of q response can be accomplished by examining a reduced second-order model of the VRA, using the (2 x 2) submatrix of Eq. 37 with the short-period parameters. The controls vector is reduced to δ_E in order to simplify the initial control law design. The G matrix is (2 x 1) and has the elements,

$$G = \begin{bmatrix} M_{\delta_E} \\ -L_{\delta_E} \end{bmatrix} = \begin{bmatrix} -12.5 \\ -.125 \end{bmatrix} \tag{38}$$

for the same flight condition as Eq. 36. The resulting model used for the design of the pitch rate controller is:

$$\Delta\dot{\underline{x}} = \begin{bmatrix} -2.08 & -8.35 \\ 1 & -2 \end{bmatrix} \begin{bmatrix} \Delta q \\ \Delta\alpha \end{bmatrix} + \begin{bmatrix} -12.5 \\ -.125 \end{bmatrix} \Delta\delta_E \tag{39}$$

$$\Delta\underline{y} = H_x \, \Delta\underline{x} + H_u \, \Delta\delta_E \tag{40}$$

The reduced-order VRA dynamics along with a choice of weighting matrices, Q and R, can be used to generate the gains C and matrices S_{12} and S_{22}. Appendix B contains an explanation of the APL functions used to find and evaluate C, S_{12} and S_{22}. Essentially the procedure is as shown in Fig. 2-4. First, matrices H_x and H_u are defined to specify what variables the pilot will command with δ_s. In this case:

$$H_x = [1 \;\; 0] \tag{41}$$

$$H_u = 0 \tag{42}$$

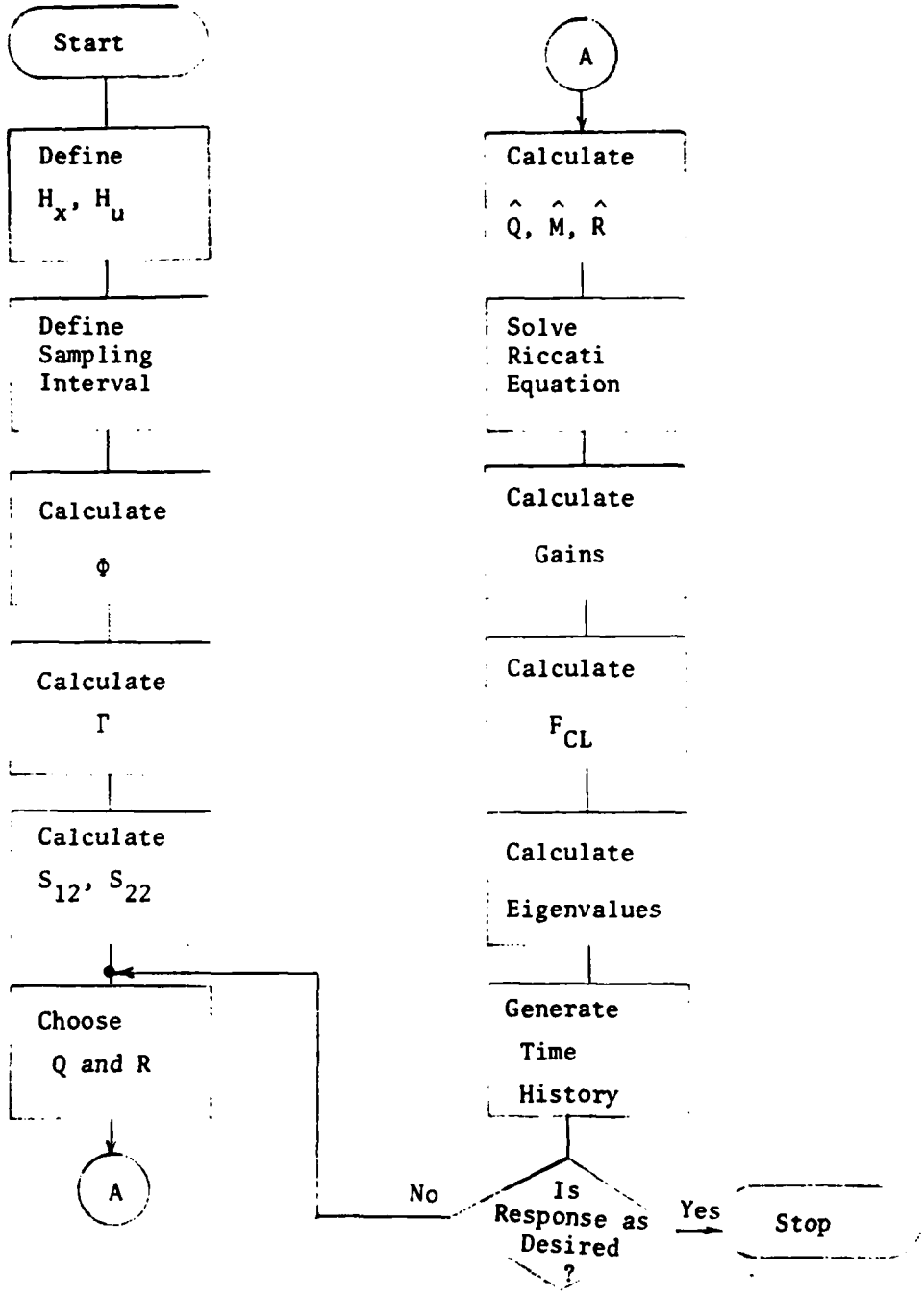

Figure 2-4. Sequence for Finding Optimal Gains.

The sampling rate is chosen next because it is used in Eqs. 11 and 12 to find Φ and Γ. S_{12} and S_{22} are calculated from Eqs. 18 and 19 next since they do not depend on how the states and controls are weighted. For the pitch rate CAS these matrices are:

$$S_{12} = \begin{bmatrix} 1 \\ .5 \end{bmatrix}, \quad S_{22} = -.5$$

Choosing Q and R will set the closed-loop response of the system, and changing the elements of these matrices allows the desired response to be attained. An appropriate starting choice for the weighting factors in Q and R is the inverse of the maximum allowable mean-square values of the states and control (Ref.20):

$$Q = \begin{bmatrix} 1/\Delta q^2 & 0 \\ 0 & 1/\Delta\alpha^2 \end{bmatrix}_{max}, \quad R = 1/\Delta\delta_{E_{max}}^2 \qquad (43),(44)$$

In the iterative technique of developing the desired time response, the weighting factors can be changed higher or lower than the initial set as necessary. Matrices $\hat{Q}$, $\hat{R}$, and $\hat{M}$ are found by performing an Euler integration of Eqs. 26-28. The Riccati equation (Eq. 29) is solved, yielding the matrix P necessary to derive the gains from Eq. 30. The closed-loop F matrix, F_{CL}, is the continuous-time equivalent of Φ_{CL}, and can be calculated from the expansion of (Ref.21),

$$F_{CL} = \frac{1}{T} \ln \Phi_{CL} \qquad (45)$$

which is

$$F_{CL} = \frac{1}{T}\left[(\Phi_{CL}-I) - 1/2(\Phi_{CL}-I)^2 + 1/3\,(\Phi_{CL}-I)^3 - \ldots\right] \tag{46}$$

By substituting Eq. 14 into Eq. 10, Φ_{CL} can easily be found to be:

$$\Phi_{CL} = \Phi - \Gamma\, C \tag{47}$$

The eigenvalues of the closed-loop system are the roots of the characteristic equation specified by the determinant:

$$|sI - F_{CL}| = 0 \tag{48}$$

Continuing the procedure, time histories are generated using Eqs. 10 and 14. If examination of the time response and closed-loop eigenvalues does not show the desired response, it is necessary to go back and re-choose the matrices Q and R.

As mentioned previously in Section 2.3, there is no established general relation between quadratic weightings and time response for any given controller or plant. The particular relation between response to a step input (measured in rise time to 95 percent of commanded value, and percent overshoot of commanded value) and the Q matrix weightings is shown in Fig. 2-5. Matrix R is held constant with a value of $1/(.17\text{rad})^2 = 32.8$, and the sampling rate is 10 sps. The curves radiating outward correspond to decreasing rise times and increasing initial control deflections. The straight lines intersecting the origin represent decreasing overshoots when approaching the Δq axis. The dotted line represents the approximate boundary between a closed-loop system with complex eigenvalues (below the line) and one with real eigenvalues. About 25 data points were used to derive the curves of Fig. 2-5 using

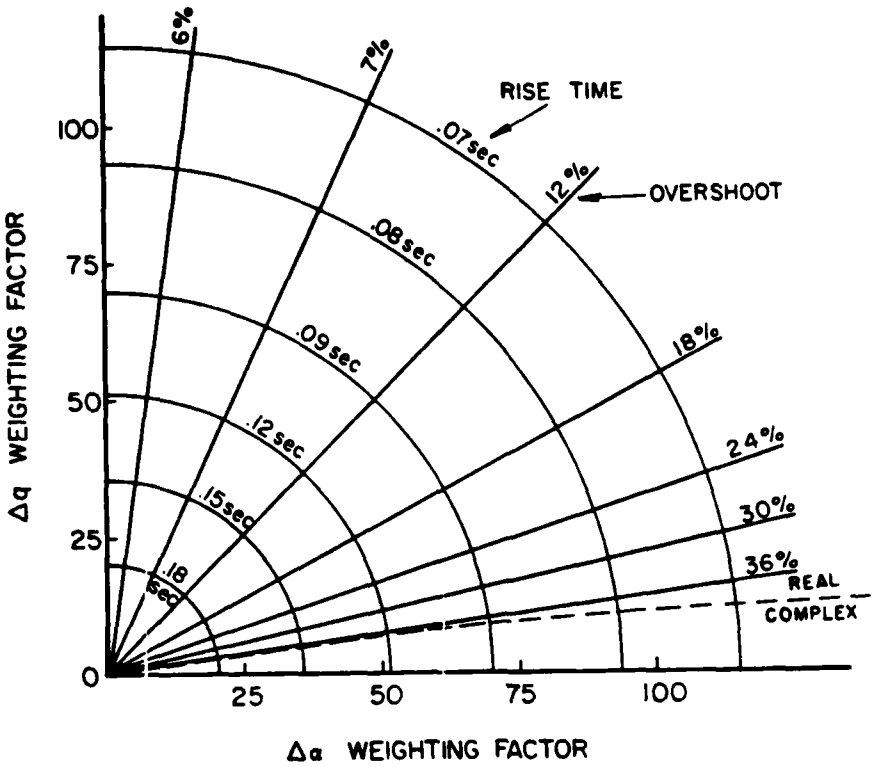

Figure 2-5. Relation Between Weighting and Time Response - q CAS; R = 32.8.

interpolation. The general relationship is shown, and if a particular response is desired of this CAS, Fig. 2-5 can give very good starting values for the weightings, requiring only a few iterations to find the necessary Q. The relation between weightings and response does not vary much at all for different sampling rates because sampled-data control methods minimize the cost functional continuously in time regardless of the sampling interval. Figure 2-5 can therefore be used for sampling rates other than 10 sps.

Time history plots for a few representative weightings were generated on Princeton University's IBM 370/158 time=sharing computer

(Figs. 2-6 through 2-11). All plots are for a step command input of 5 deg/sec using a full fourth-order model of the VRA's longitudinal dynamics. The Δq response on the open-loop aircraft (Fig. 2-6) has a 47.5% overshoot and 0.19 sec rise time. As the velocity decreases, Δq falls off because there is no throttle input. Angle of attack shows the expected initial increase as the phugoid oscillation sets in. Weighting factors in the Q matrix of (25,25) show a definite improvement in rise time and overshoot of the Δq response (Fig. 2-7). Because the CAS is Type 0, and there is no feedback to throttle, Δq again shows a decrease but not quite as much as the open-loop case. The elevator initially attains a larger than steady-state deflection to improve rise time, but then dips below steady-state value to control the overshoot. Finally, the elevator assumes the steady-state deflection for Δq = 5 deg/sec. The plots for weightings of (50,50) and (75,25) (Figs. 2-8 and 2-9) show further improvements in time response, but the initial elevator deflection is larger. The time responses with weightings (25,25) and (75,25) are also plotted (Figs. 2-10 and 2-11) for a sampling rate of 20 sps. It can be seen that they have the same state trajectories as the 10 sps plots of the same weightings. The control trajectories are different because the CAS is taking into account the difference in phase lag between the two sampling rates.

The gains, resulting step responses, and closed-loop eigenvalues obtained from the simulation are given in Table 2-1. A negative gain implies negative feedback while positive gains give positive feedback. The phugoid eigenvalues change very little for different

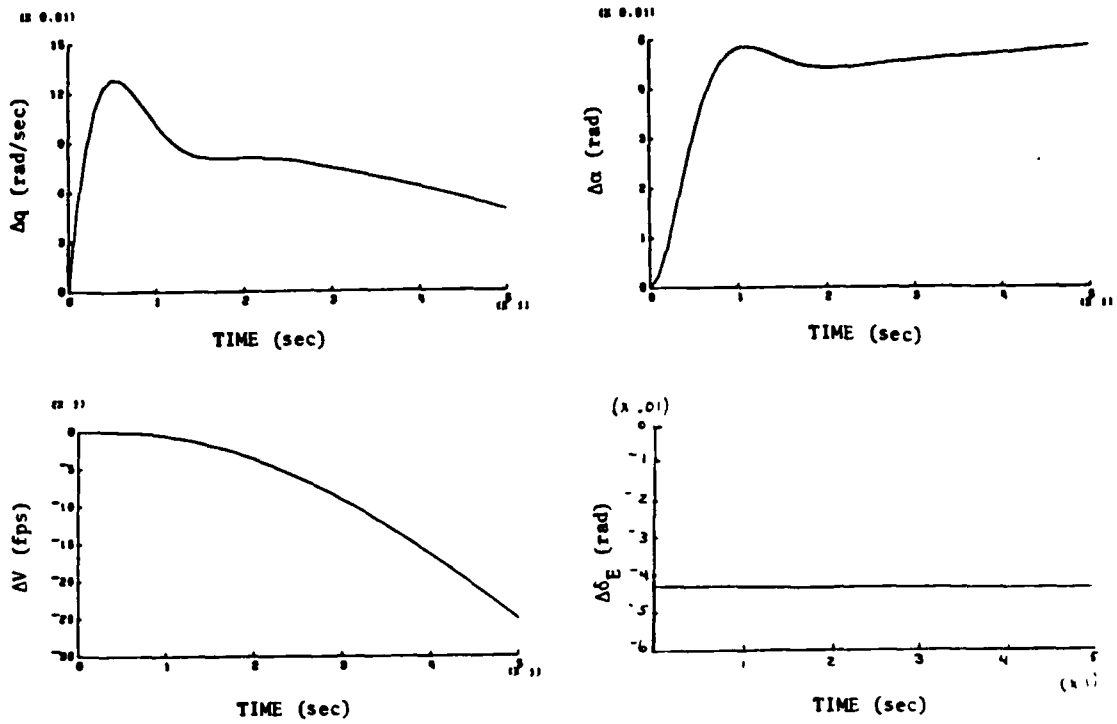

Figure 2-6. Open-Loop Step Response for y_d = 5°/sec (105 KIAS).

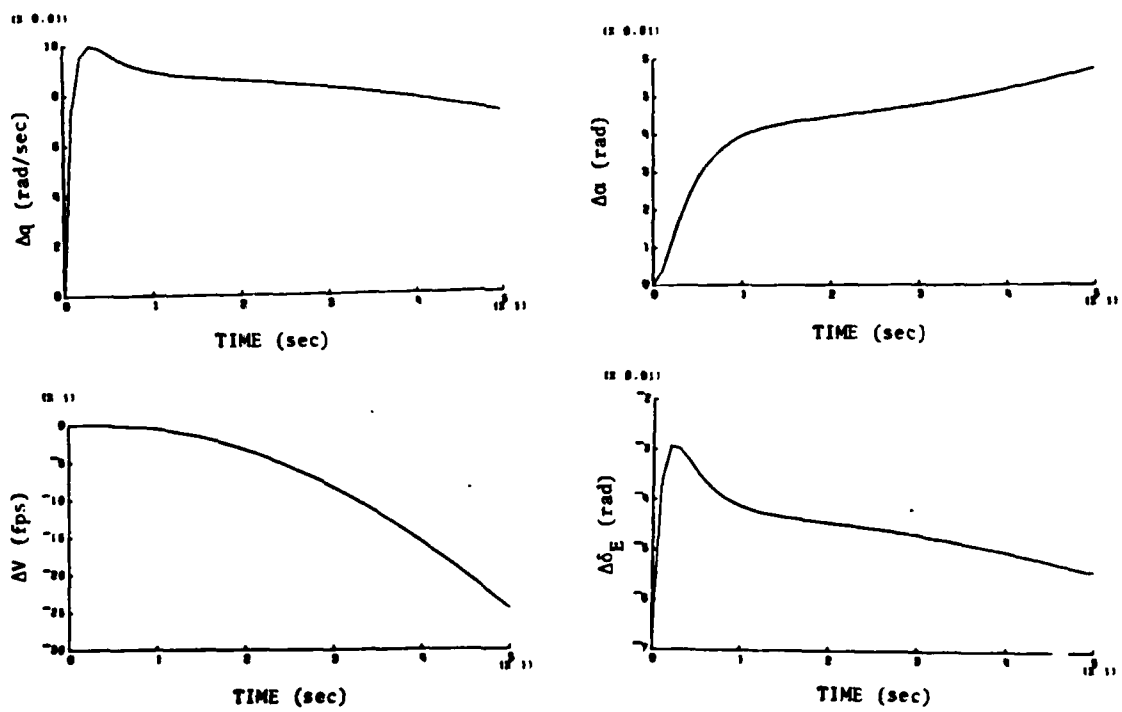

Figure 2-7. Pitch Rate Command Step Response for Q Weightings 25,25 (y_d = 5°/sec, 10 sps, 105 KIAS).

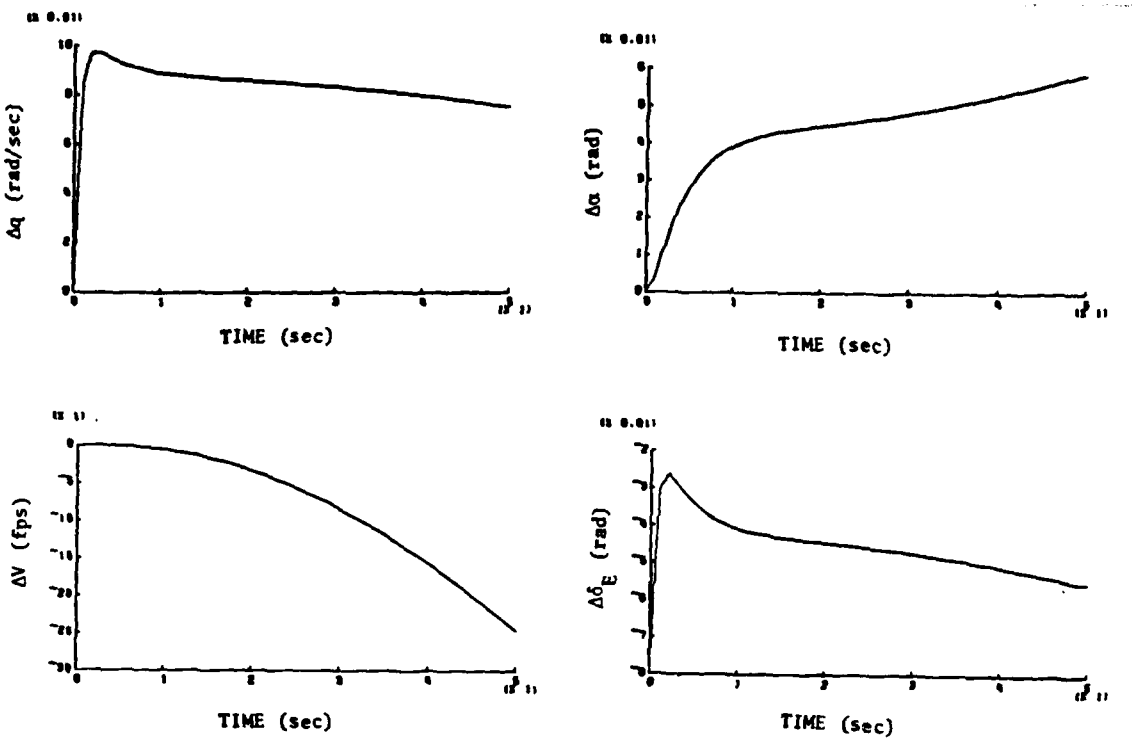

Figure 2-8. Pitch Rate Command Step Response for Q Weightings 50,50 (γ_d = 5°/sec, 10 sps, 105 KIAS).

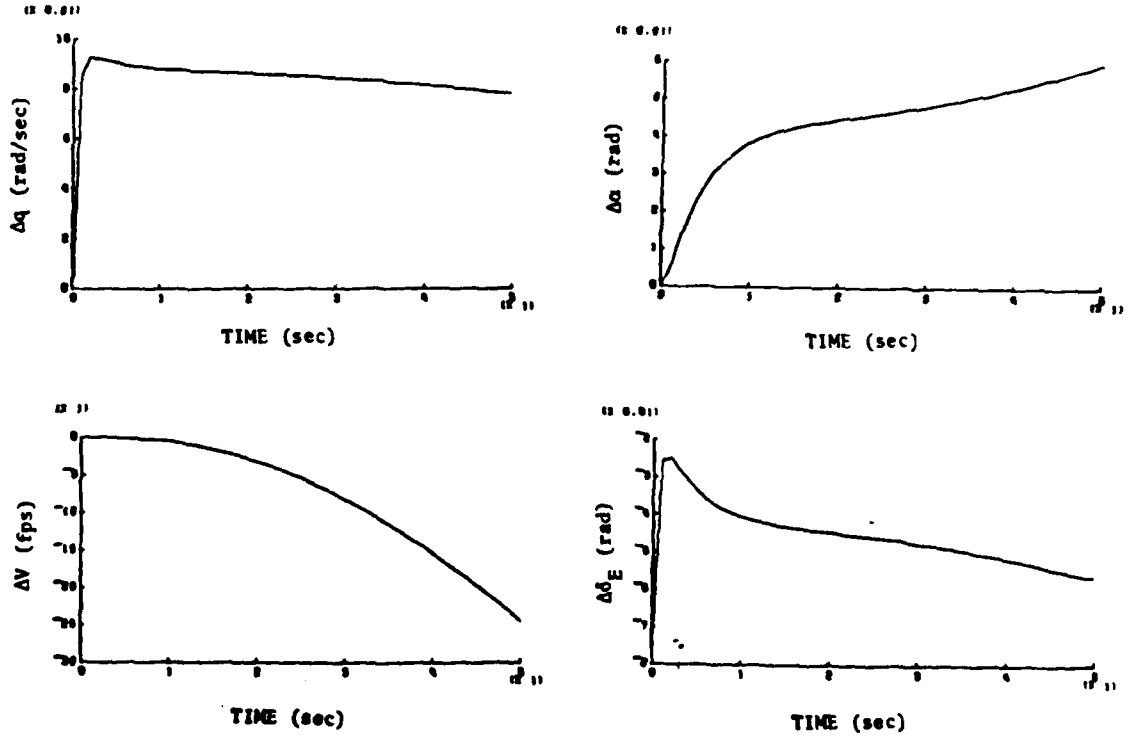

Figure 2-9. Pitch Rate Command Step Response for Q Weightings 75,25 (γ_d = 5°/sec, 10 sps, 105 KIAS).

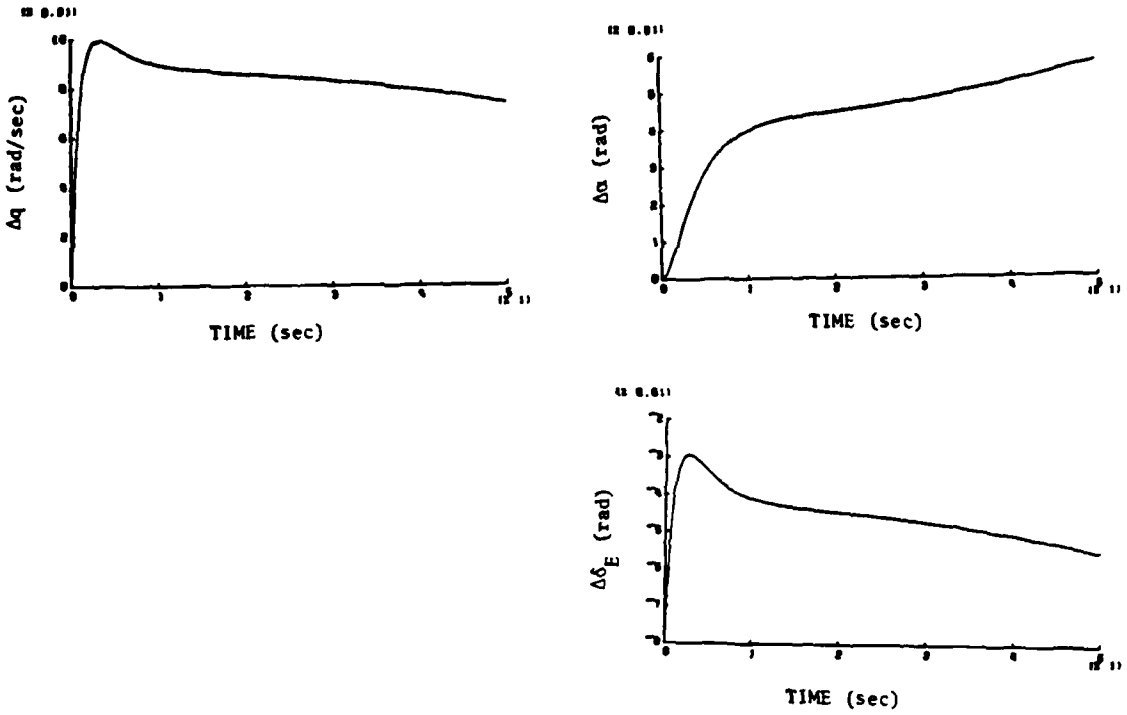

Figure 2-10. Pitch Rate Command Step Response for Q Weightings 25,25 (y_d = 5°/sec, 20 sps, 105 KIAS).

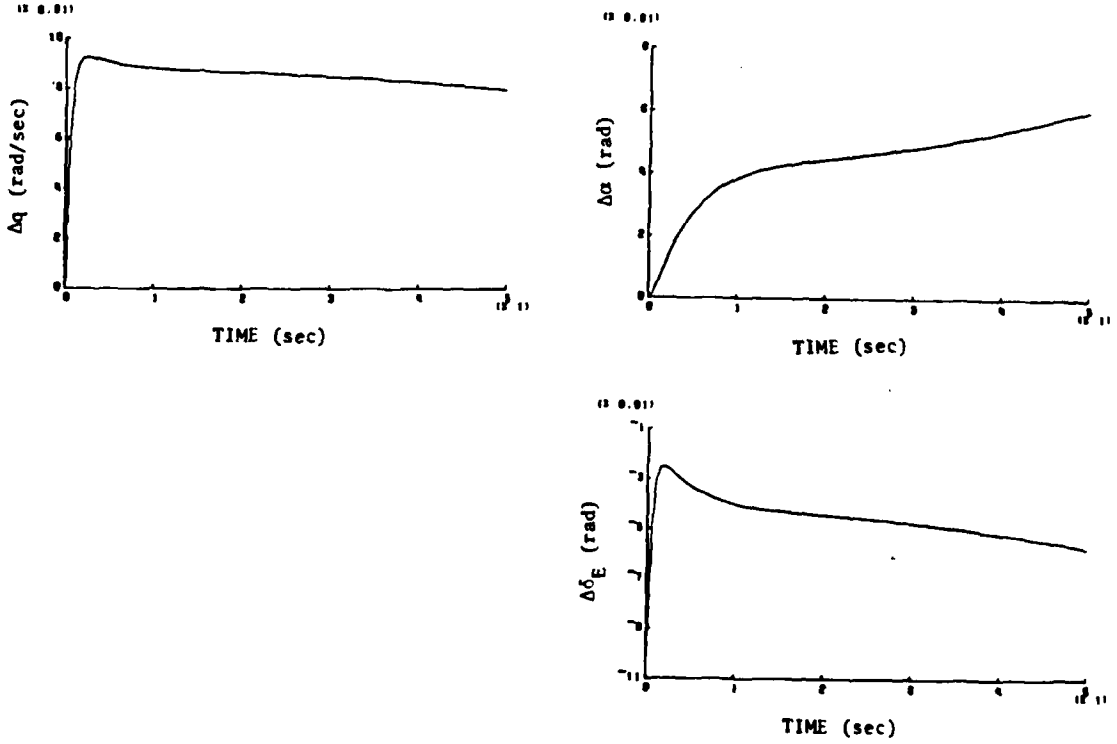

Figure 2-11. Pitch Rate Command Step Response for Q Weightings 75,25 (y_d = 5°/sec, 20 sps, 105 KIAS).

TABLE 2-1

Gains, Predicted Step-Response and Eigenvalues for q CAS (105 KIAS)

	Q Weightings	Gains q	Gains α	Eigenvalues Short-Period, Phugoid	Response Rise Time, Sec	Response Overshoot, %
Open Loop		-	-	-2.04±j2.89 -.033±j.228	0.19	47.5
10 sps	[25,25]	-.427	.324	-10.74,-2.68 -0.45±j.139	0.15	14.7
	[50,50]	-.554	.360	-16.96,-2.43 -.046±j.123	0.09	11.8
	[75,25]	-.620	.468	-23.24,-2.20 -.048±j.104	0.08	6.7
20 sps	[25,25]	-.541	.283	-10.30,-2.68 -.045±j.133	0.14	14.3
	[75,25]	-.876	.439	-19.31,-2.20 -.049±j.092	0.1	6.4

gains due to the weak coupling between short-period and phugoid modes. The $\omega_{n_{sp}}$ is increased from the open-loop value of 3.54 rad/sec (Table 2-2) for the 3 weightings examined. This increase is primarily seen in the decrease in rise time for the commanded state, Δq, and is considered an improvement by the time response criterion. However, referring to Fig. 2-3, the closed-loop $\omega_{n_{sp}}$ for weightings of (50,50) and (75,75) is outside the Level 1 area for n/α constant at 9.3 g/rad. This implies the flying qualities of the VRA may be unsatisfactory in actual flight tests if gains calculated from these weightings are used.

TABLE 2-2

Closed-Loop $\omega_{n_{sp}}$ and ζ_{sp} for q CAS (105 KIAS)

Q Weightings	$\omega_{n_{sp}}$ (rad/sec)	ζ_{sp}
Open Loop	3.54	0.576
[25,25]	5.39	1.25
[50,50]	6.45	1.51
[75,25]	7.19	1.77

Examination of F_{CL}, calculated from Eq. 46, will show how the stability derivatives have been augmented for the particular weightings chosen. For example, the second-order F_{CL} for weightings of (75, 25) is:

$$\begin{bmatrix} M_q & M_\alpha \\ 1-L_q & -L_\alpha \end{bmatrix} = \begin{bmatrix} -23.5 & -4.48 \\ 1.40 & -1.93 \end{bmatrix} \tag{49}$$

Comparing this to the open-loop F matrix of Eq. 39, M_q has increased by approximately a factor of 10, M_α has decreased by a factor of two, and some negative lift due to q has developed. The stability derivative, L_α has not changed much because the only control surface used by the CAS is elevator and L_{δ_E} is very small. To augment L_α, direct lift control from the flaps is needed. The F_{CL} for weightings of

(25,25) and (50,50) are,

$$\begin{bmatrix} -11.5 & -5.93 \\ 1.09 & -1.96 \end{bmatrix} \quad \text{and} \quad \begin{bmatrix} -17.5 & -6.56 \\ 1.22 & -1.92 \end{bmatrix}$$

respectively.

2.5 NORMAL ACCELERATION COMMAND CONTROL STRUCTURE

Normal acceleration commanded by δ_s is the next CAS structure examined. The development is very similar to that of the pitch rate CAS of Section 2.4; hence, the principal differences are given here. The gains are again calculated with a second-order model but using the states q and n_z. Using the relation,

$$n_z = Z_\alpha \alpha + Z_{\delta_E} \delta_E , \tag{50}$$

the model represented by Eq. 39 can be used if the correct substitution for $\Delta\alpha$ is made. Since the effects of Z_{δ_E} are so small, the second term of Eq. 50 is dropped to make the substitution easier. Making the change, the second-order F matrix is:

$$\begin{bmatrix} M_q & M_\alpha/L_\alpha V \\ VL_\alpha & -L_\alpha \end{bmatrix} = \begin{bmatrix} -2.08 & -.0235 \\ 354.9 & -2 \end{bmatrix} \tag{51}$$

Normalizing acceleration by the force of gravity, the resulting model

is given as:

$$\Delta\dot{\underline{x}} = \begin{bmatrix} -2.08 & -.758 \\ 11.02 & -2 \end{bmatrix} \begin{matrix} \Delta q \\ \Delta n_z \end{matrix} + \begin{bmatrix} -12.5 \\ -.125 \end{bmatrix} \Delta\delta_E \tag{52}$$

$$\Delta\underline{y} = H_x \, \Delta\underline{x} + H_u \, \Delta\delta_E \tag{53}$$

To select n_z as the state commanded by δ_s, the H_x and H_u matrices are given the values:

$$H_x = [0 \quad 1] \tag{54}$$

$$H_u = 0 \tag{55}$$

Following the procedure of Section 2.4, gains and resulting time responses and eigenvalues are generated. The matrices S_{22} and S_{12} are found to be:

$$S_{22} = -.091 \quad , \quad S_{12} = \begin{bmatrix} .181 \\ 1 \end{bmatrix} \quad .$$

The general relationship between Q weightings for R = 32.8 and a sampling rate of 10 sps is presented in Fig. 2-12. The straight lines relate rise time to weightings and the curves, connected at the origin, relate overshoot to weightings. The dotted line separates closed-loop systems with complex short-period eigenvalues on the top and real eigenvalues on the bottom. The relations in Fig. 2-12 are not exact, but can be used to find good starting values for weightings. As explained in Section 2.4, Fig. 2-12 is the same for other sampling rates.

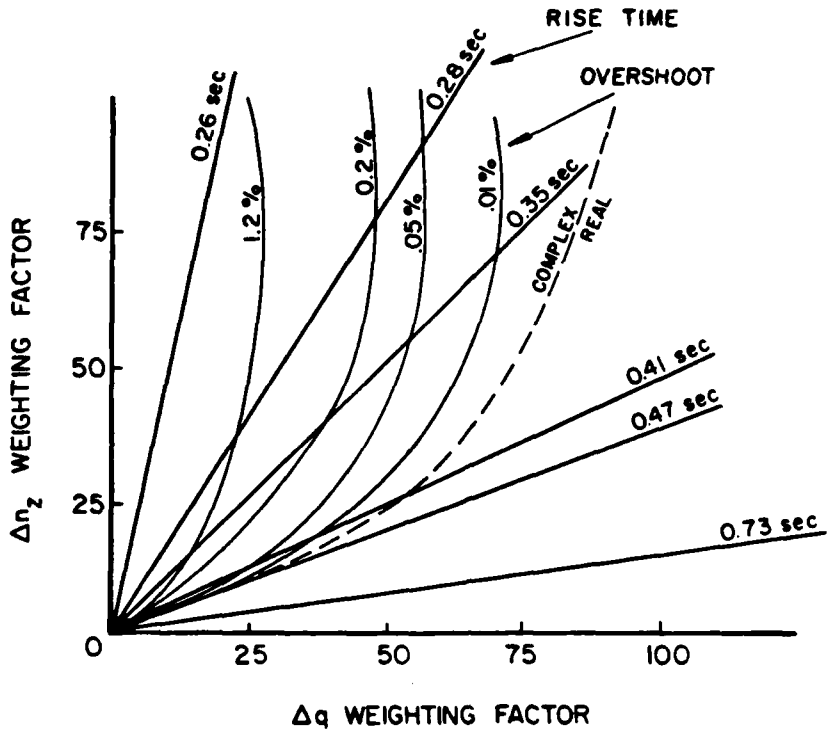

Figure 2-12. Relation Between Weightings and Time Response - n_z CAS; R = 32.8.

Time history plots for a few representative weightings are presented in Figs. 2-13 through 2-16. All plots are generated with a step command input of 0.25g using a full fourth-order model of the VRA's longitudinal dynamics. The Δn_z response for the open-loop aircraft (Fig. 2-13) has a 10.8% overshoot and 0.7 second rise time. Velocity is falling off and $\Delta\delta_E$ holds constant at 1.3 deg because its position is only a function of the step input on $\Delta\delta_s$. Weightings of (5,10) in the Q matrix and R = 33 (Fig. 2-14) shows a large improvement in rise time for Δn_z response. However, now Δq overshoots its steady-state value quite a bit more than the open-loop case. The elevator initially deflects more than 5 deg, which indicates the FBW

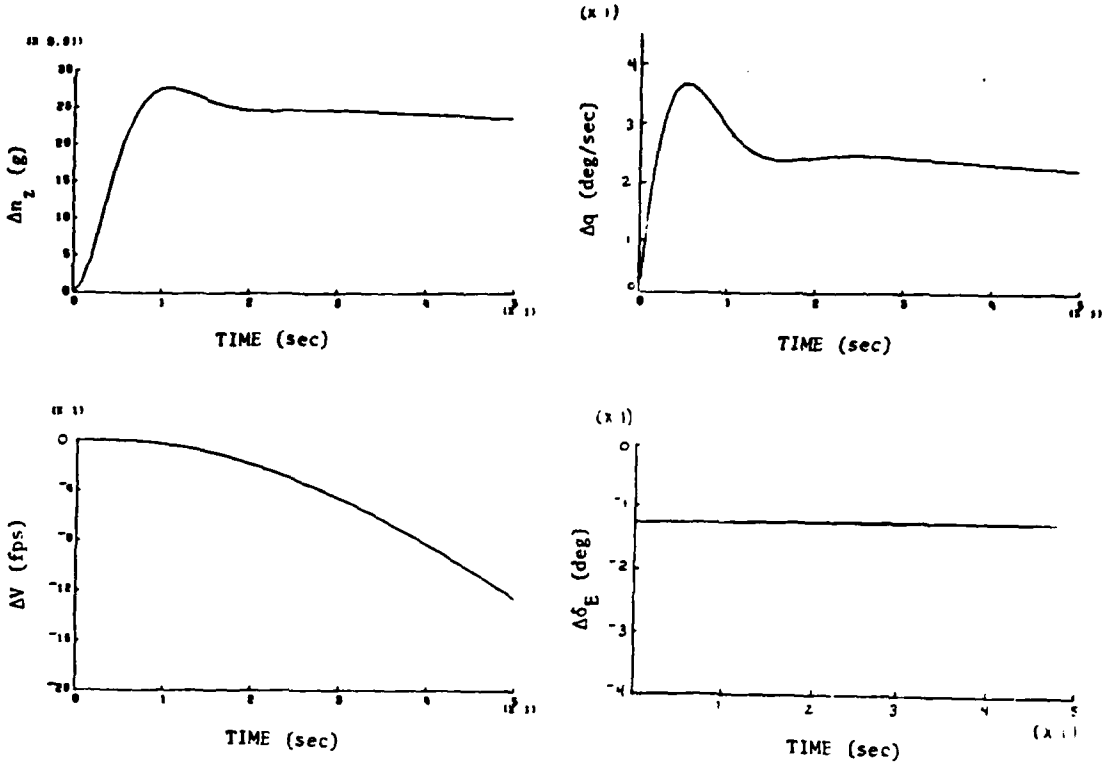

Figure 2-13. Open-Loop Step Response for y_d = .25g (105 KIAS).

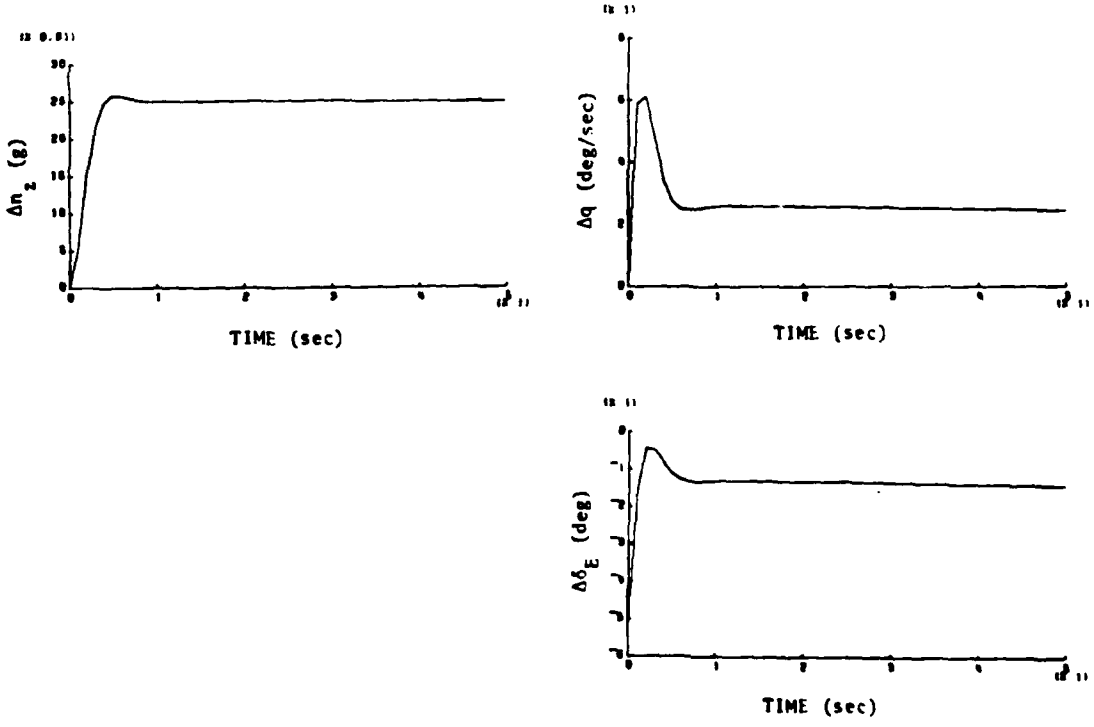

Figure 2-14. Normal Acceleration Step Response for Q Weightings 5,10, R = 33 (y_d = .25g, 10 sps, 105 KIAS)

system of the VRA will disengage for a .25g true step input. Figure 2-15 shows the response for a heavier weighting (R=250) on Δu. The initial step of $\Delta\delta_E$ is now less than 3 deg but rise time on Δn_z has been slowed by 0.2 sec. The peak on the Δq overshoot also is less with the heavier control weighting. A set of plots drawn for the same weightings as Fig. 2-14, but a sampling rate of 20 sps (Fig. 2-16), shows once again that a change in sampling rate does not effect the state trajectories if new gains are calculated to take into account the change in phase lag of the inputs to the digital CAS. The control trajectory is different from Fig. 2-14 as a result.

The gains, resulting step responses, and closed-loop eigenvalues obtained from the computer simulation are given in Table 2-3.

TABLE 2-3

Gains, Predicted Step-Response and Eigenvalues for n_z CAS (105 KIAS)

Weightings Q, R	Gains q	Gains n_z	Eigenvalues Short Period, Phugoid	Response Rise Time, Sec	Response Overshoot, %
Open Loop	-	-	-2.04±j2.89 -.033±j.228	0.7	10.8
[5,10] 33	-.533	-.181	-6.47±j6.04 -.036±j.252	0.35	3.0
[5,10] 250	-.238	-.0535	-3.71±j4.09 -.0360±j.257	0.52	5.6
[5,10] 33	-.620	-.250	-6.52±j5.95 -.0364±j.252	0.35	3.15

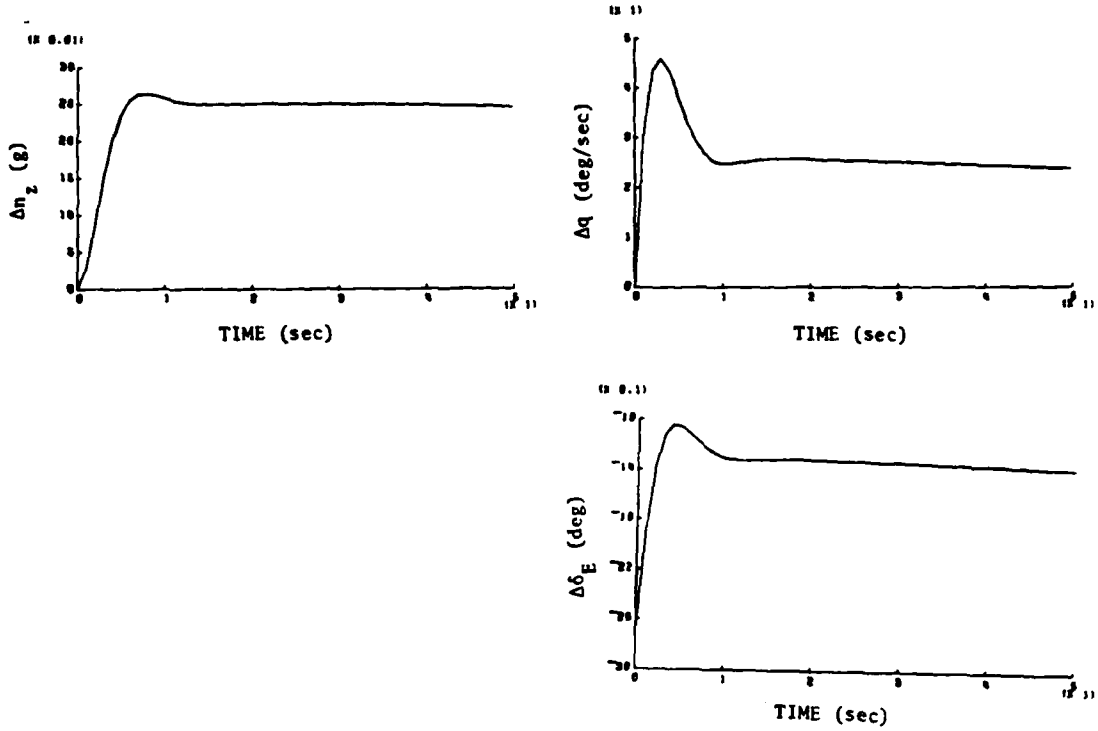

Figure 2-15. Normal Acceleration Step Response for Q Weightings 5,10 R = 250 (y_d=.25g, 10 sps, 105 KIAS).

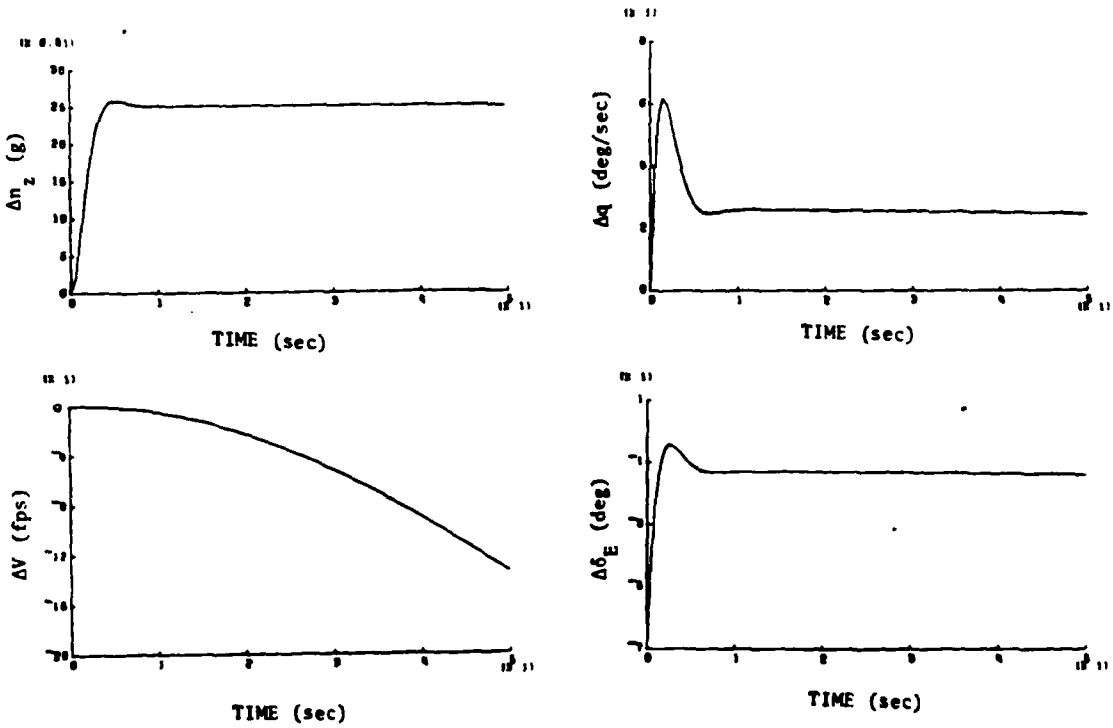

Figure 2-16. Normal Acceleration Step Response for Q Weightings 5,10 R = 33 (y_d=.25g, 20 sps, 105 KIAS).

The $\omega_{n_{sp}}$ for the weightings with R = 32.8 and 250 is 8.85 rad/sec and 5.52 rad/sec respectively. This increase in $\omega_{n_{sp}}$ from open-loop (3.54 rad/sec) accounts for the decrease in rise time for Δn_z. This is considered an improvement by the time response criterion but for the case where $\omega_{n_{sp}}$ = 8.35, it no longer meets the requirement set by the Military Specification on Flying Qualitites (Ref.20). Referring to Fig. 2-3, the augmented $\omega_{n_{sp}}$ puts the aircraft in the Level 2 area of the chart for n/α still equal to 9.3 g/rad. This indicates the control law, with gains calculated from weightings of $Q = \begin{bmatrix} 5 & 0 \\ 0 & 10 \end{bmatrix}$ and R = 32.8, may not be satisfactory to the pilot in the actual flight tests.

The closed-loop stability derivatives may be examined by calculating F_{CL} from Eq. 46. The F_{CL} for the systems with R = 32.8 and R = 250 are

$$\begin{bmatrix} -11.5 & -5.33 \\ 11.53 & -1.48 \end{bmatrix} \quad \text{and} \quad \begin{bmatrix} -5.49 & -1.80 \\ 11.09 & -1.93 \end{bmatrix}$$

respectively. These can be compared to the open-loop F matrix of Eq. 52 to see how the stability derivatives have changed.

2.6 DYNAMIC MODEL MATCHING

The method of choosing weighting matrices Q and R described in the preceding two sections can result only in decreases in overshoot and rise time for the time response of the commanded state; however, it may be desirable to change the modal characteristics of

an aircraft in the opposite way if the basic plane's response is too fast or too well damped. This can be done with the previously described LQ control methods by using, in addition , the method of implicit model-following.

The procedure begins by defining the eigenvalues desired for the closed-loop system. Next, the F matrix associated with the eigenvalues through Eq. 48 is found. By the method of implicit model-following, it is possible to find the weightings which give the closed-loop system the correct F matrix (Ref. 22). Just as in Section 2-1 the design is posed as a linear-quadratic control problem, but with a different quadratic cost functional

$$J = \int_0^\infty (\Delta\underline{x}^T Q \Delta\underline{x} + 2\ \Delta\underline{x}^T M \Delta\underline{u} + \Delta\underline{u}^T R \Delta\underline{u})\ dt \tag{56}$$

where

$$Q = (F-F_M)^T W\ (F-F_M) \tag{57}$$

$$M = (F-F_M)^T\ W\ G \tag{58}$$

$$R = G^T\ W\ G \tag{59}$$

The matrix W is a diagonal weighting matrix and F_M is the F matrix to be modeled. If the modeling was to be done in continuous-time, the Riccati equation would be solved next and the feedback gains calculated. However, in the discrete-time case, the weightings must be modified to account for the effective lag of the sampling process. Unlike the cost functional of Eq. 23, there is a cross weighting, M, in Eq. 56

which cannot be transformed to its discrete counterpart just by using Eqs. 26-28 of the procedure outlined in Section 2.1. Following the development in Ref. 15, a transformation from the continuous-time weighting matrices (Q, M, and R) to the discrete-time matrices ($\hat{Q}$, $\hat{M}$, and $\hat{R}$) was derived (see Appendix A). The discrete weighting matrices are found to be

$$\hat{Q} = \int_{t_k}^{t_{k+1}} \Phi^T Q \Phi \, dt \tag{60}$$

$$\hat{M} = \int_{t_k}^{t_{k+1}} (\Gamma^T Q\Phi + M\Phi)dt \tag{61}$$

$$\hat{R} = \int_{t_k}^{t_{k+1}} (R + \Gamma^T Q\Gamma + 2 M\Gamma)dt \tag{62}$$

The gains are calculated (Eq. 30) from the solution of the Riccati equation (Eq. 29), and F_{CL} is found with Eq. 44. If F_{CL} is not exactly as desired, then matrix W should be changed and a new set of quadratic weightings calculated (Fig. 2-17). If changing W does not yield satisfactory results, the F_M used in the calculation can be changed. APL functions to perform these calculations are listed and explained in Appendix B.

For example, say it is necessary to find the feedback gains for a closed-loop system with $\omega_{n_{sp}} = 1.56$ and $\zeta_{sp} = 0.76$. The corresponding eigenvalues are $-1.18 \pm j\ 1.02$. The F_M matrix which gives these eigenvalues must be found with the constraint that some elements of F for the VRA cannot be changed much with only elevator control. Specifically, L_q and L_α cannot be augmented with only δ_E, so the top

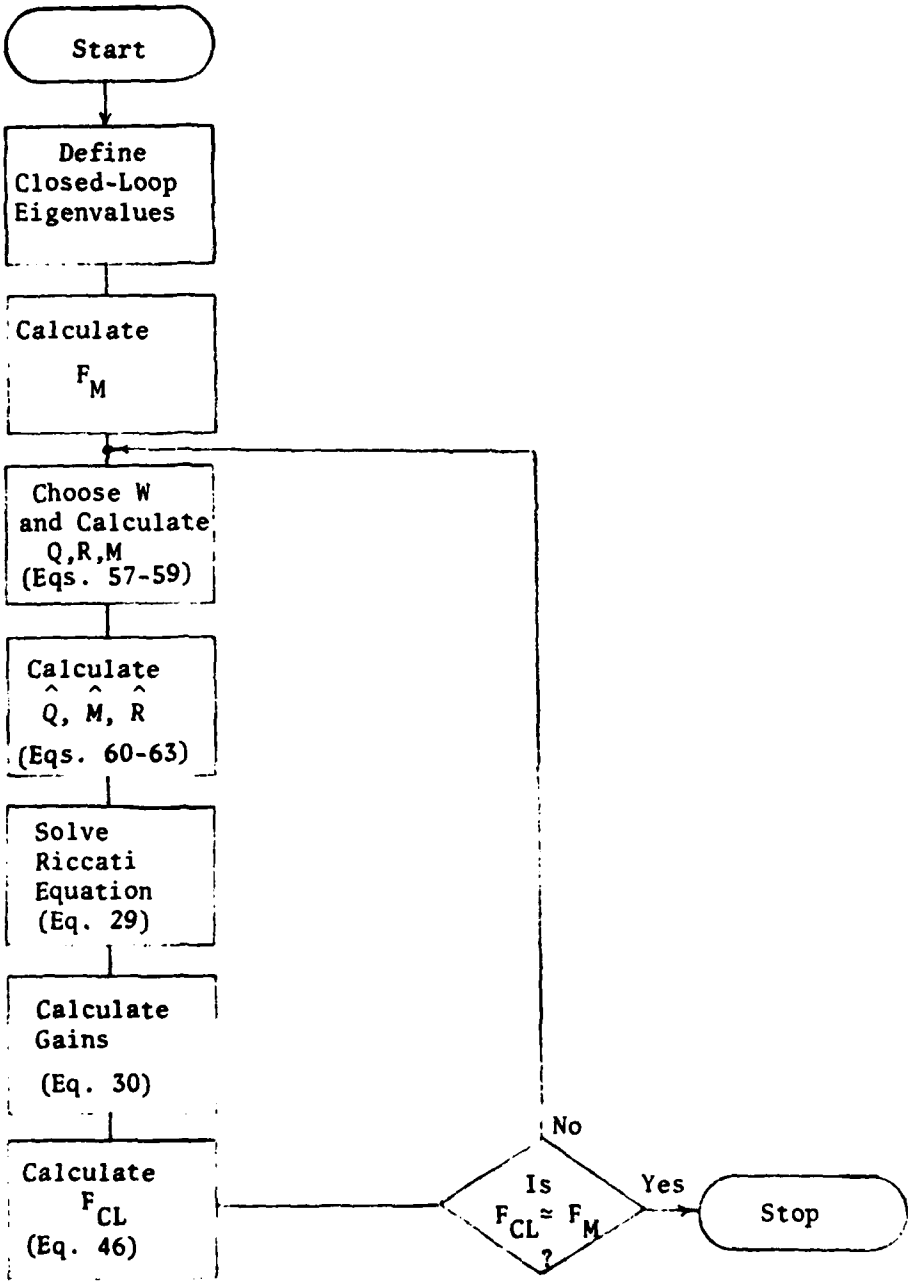

Figure 2-17. Sequence for Implicit Model-Following.

elements of F (M_q and M) are the values to be found. Using Eq. 48, F_M is found to be:

$$F_M = \begin{bmatrix} -.36 & -1.71 \\ 1 & -2 \end{bmatrix}$$

Choosing the diagonal weighting matrix W to initially be a (2x2) identity matrix, I_2, and completing the rest of the method outlined in Fig. 2-17,

$$F_{CL} = \begin{bmatrix} -.375 & -1.68 \\ 1.00 & -2.01 \end{bmatrix}$$

For this particular example, it is not possible to make F_{CL} close to F_M just by changing W, so the F_M used in the calculations is changed instead, keeping $W = I_2$. After a few iterations, it is found that,

$$F_M = \begin{bmatrix} -.34 & -1.73 \\ 1 & -2 \end{bmatrix}$$

will yield,

$$F_{CL} = \begin{bmatrix} -.360 & -1.71 \\ 1.01 & -2.01 \end{bmatrix} .$$

For reference, the weighting matrices and resulting gains are listed in Table 2-4.

The next chapter outlines the hardware and software aspects of the Micro-DFCS. It describes how the control laws derived in this chapter are actually implemented, and gives test results and analysis for a hybrid simulation.

TABLE 2-4

Weighting Matrices and Gains for Implicit Model-Following Example

Continuous-Time Weightings	Discrete-Time Weightings and Gains
$Q = \begin{bmatrix} 3.03 & 11.5 \\ 11.5 & 43.7 \end{bmatrix}$	$\hat{Q} = \begin{bmatrix} .338 & .965 \\ .965 & 2.83 \end{bmatrix}$
$M = [21.8 \quad 82.6]$	$\hat{M} = [2.08 \quad 6.03]$
$R = 156.3$	$\hat{R} = 12.9$
	$C = [.161 \quad .467]$

3. CONTROL LAW IMPLEMENTATION AND HYBRID TESTING

The control law developed in Chapter 2 is coded in the software of the Micro-DFCS for implementation on-board the VRA. The type and configuration of the Micro-DFCS equipment specifies, to a large extent, in what manner and how well these control laws will operate with the existing VRA FBW system. The efficiency and versatility of the equipment and software determines the complexity of control laws that may be used. The control law designs therefore have an impact on the equipment selected and organization of the software. This chapter outlines some of the specific aspects of the Micro-DFCS that support the implementation of the control design. The equipment and software are tested with an analog simulation of the VRA as a logical step before actual flight tests.

3.1 EQUIPMENT CONFIGURATION OF THE MICRO-DFCS

The primary task of the Micro-DFCS hardware is to accept analog information to calculate the control laws, and to generate analog commands for aircraft controls at periodic instants in time. This definition of the computer's main function suggests some desirable characteristics for the hardware to possess. Since the control law must be calculated in short intervals of time, the computations must be very fast but also have precision at least as great as the resolution of the digital data words generated by the analog to digital (A/D) converter. The computational speed is determined by the

instruction cycle time, the bit length of the data word, and the speed of the mathematical operations. The A/D and digital to analog (D/A) converters should have as much resolution as the sensors will provide and the control surfaces will move (real sensors and actuators do not have infinite precision because of stiction). An interrupt structure with at least one interrupt which can be triggered by a resetable timer is needed to initiate the control law calculation at precise instances in time. Other factors to consider include the cost, the range of compatible components which may be used to expand or upgrade the computer at a latter date, the standardization and flexibility of the bus structure (which determines the availability of components compatible with the system), the power requirements, and the software available to support the microcomputer.

The Micro-DFCS for this study is based on the Intel Single Board Computer (SBC) using the Intel 8085 Central Processing Unit (CPU) (Ref. 23). The SBC system is a modular design where the main functions of the computer are divided onto separate circuit boards. These boards may be combined to configure the desired system. Multiple CPU's may be used in a system when more processor time is needed. This is not the case at this time, but may be necessary as more complex command modes are implemented. As shown in Fig. 3-1, the Micro-DFCS is built around the SBC 80/05 central processing board. This is supported by a high-speed mathematics unit, random-access and programmable read-only memory (RAM and PROM), A/D and D/A conversion boards, and a hand-held control-display unit (CDU). The CPU works

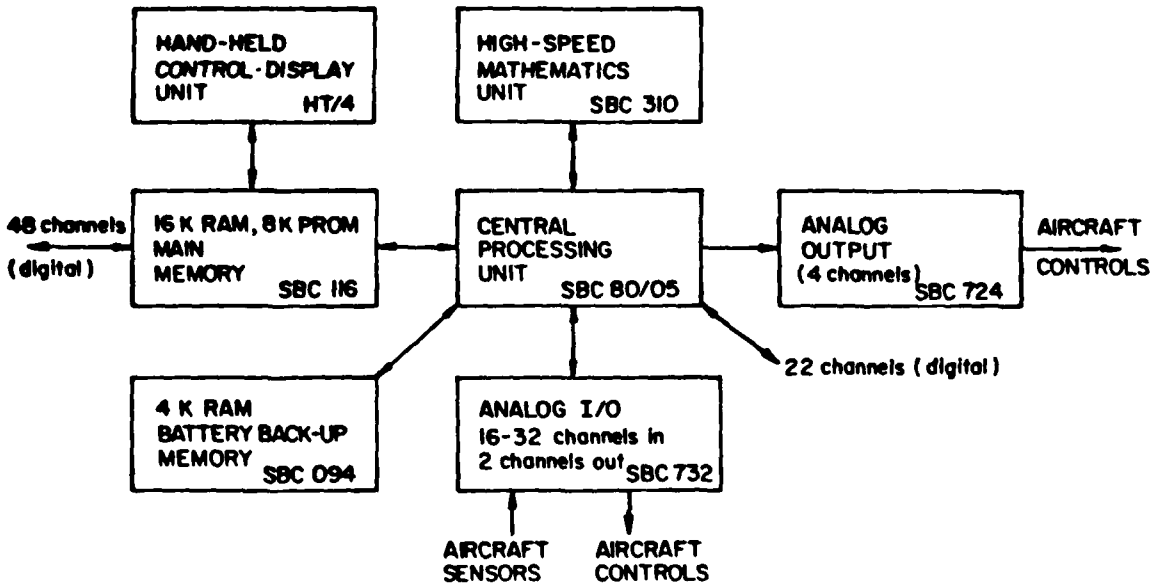

Figure 3-1. Micro-DFCS Microcomputer Configuration.

with 80 different machine instructions, has an 8-bit data word length, and an instruction cycle time from 2 to 6.1 μsec (depending on the instruction). A detailed description of the microcomputer components is contained in Appendix D.

The Micro-DFCS is functionally related to the VRA's FBW system as shown in Fig. 3-2. The Micro-DFCS can operate in parallel with the existing analog system or either can operate separately. This is an important aspect of the Micro-DFCS installation because, in this configuration, it is possible to model another aircraft with the VRA using the analog system and then test a digital control design (for the modeled aircraft) using the Micro-DFCS. Two pilots fly each test flight for reasons of safety and experimental efficiency. The safety pilot has conventional aircraft controls with

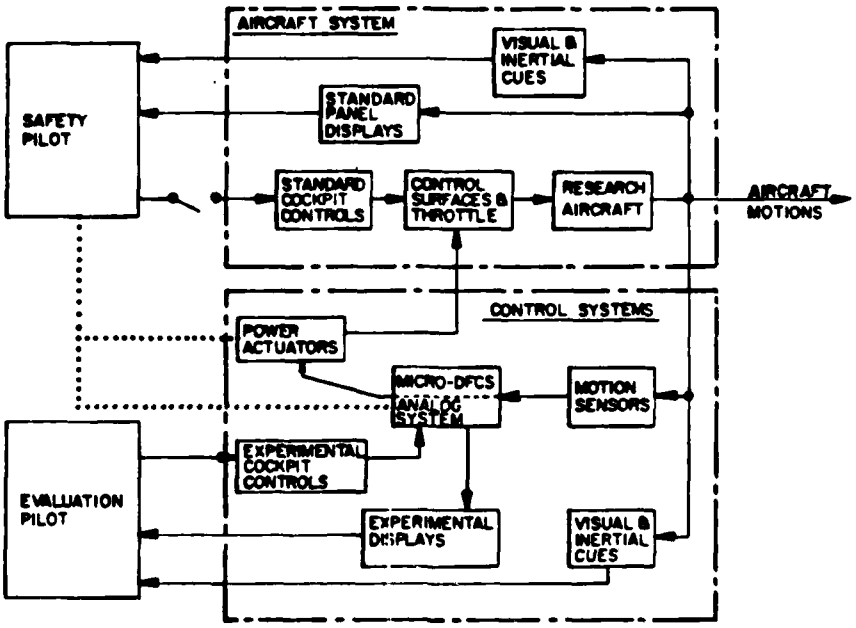

Figure 3-2. Overview of the VRA/Micro-DFCS System.

mechanical linkage connecting to the control surfaces. The Evaluation-pilot operates the experimental controls, which in this case, include a center control stick and the CDU.

The VRA's motion is measured by various air data and inertial sensors and sent to a ground station via 42 channels of telemetry. A more detailed explanation of the VRA's systems and ground station is contained in Appendix C.

3.2 THE OPERATIONAL MICROCOMPUTER SOFTWARE

The calculations for the control laws are performed by a set of software programs that execute every sampling instant. These Flight

Control routines are specific to their function in order to minimize the execution duty cycle. The Flight Control routines are supported by two sets of programs called the Executive and Utility routines. They are designed to be very flexible allowing new Flight Control routines to be easily added. These three categories together make up the operational software entitled CAS-1. The routines of CAS-1, arranged in Chapter format, are listed with memory requirements in Table 3-1. The Executive routines handle initialization, CDU interface, and one of three error detection methods used in CAS-1. This error detection routine checks the contents of memory every 50 samples to insure the coding of CAS-1 has not changed. A second error detection method checks for mathematical errors on every operation. The third method indicates when a Flight Control routine is executing properly by flashing a light at a steady rate on the pilot's panel. A more detailed description of the error detectors and a brief description of all routines is given in Appendix E.

The flexibility of the Executive and Utility routines is derived mainly from the modular construction of the program. Major and often performed tasks are divided into subroutines that are very general in nature. All user-definable parameters and variables that change in the operation of CAS-1 are stored in RAM outside the body of CAS-1. Therefore any part or all of CAS-1 may be stored in PROM. Developing new Flight Control programs for the Micro-DFCS can be done quickly and efficiently by using these existing routines. A detailed explanation on defining new keyboard commands and flight control modes is contained in Appendix E.

TABLE 3-1

CAS-1 PROGRAM TABLE OF CONTENTS AND MEMORY REQUIREMENTS

	Memory Words
1. EXECUTIVE ROUTINES	
1.1 INITIALIZATION	75
1.2 CDU INTERFACE AND COMMAND RECOGNITION	125
1.3 MEMORY CHECK	80
2. UTILITY ROUTINES	
2.1 ANALOG TO DIGITAL CONVERSION	18
2.2 ENTRY ERROR	53
2.3 BLINK	21
2.4 CLEAR LINE	8
2.5 CONSOLE OUTPUT	10
2.6 COUNT-UP DISPLAY	72
2.7 DECIMAL TO HEX CONVERSION	24
2.8 ERASE BLOCK MEMORY	7
2.9 MATH ERROR PROCESSOR	111
2.10 HEX TO DECIMAL CONVERSION	60
2.11 NUMERIC INPUT	66
2.12 INTERRUPT COUNT	19
2.13 LIMIT ANALOG OUTPUT	45
2.14 MATH UNIT DRIVER	38
2.15 MODE CHANGE	142
2.16 MOVE 4 WORDS	12
2.17 SERIAL OUTPUT	12
2.18 CALIBRATED STEP INPUT	294
3. FLIGHT CONTROL ROUTINES	
3.1 DIRECT CONTROL SET UP MODE 19	77
3.2 PITCH RATE CONTROL SET UP MODE 0	134
3.3 PITCH RATE CONTROL SET UP MODE 1	
3.4 PITCH RATE CONTROL SET UP MODE 2	95
3.5 PITCH RATE CONTROL SET UP MODE 3	
3.6 NORMAL ACCELERATION CONTROL SET UP MODE 10	135
3.7 DIRECT INTERRUPT SERVICE ROUTINE	94
3.8 PITCH RATE INTERRUPT SERVICE ROUTINE	323
3.9 NORMAL ACCELERATION INTERRUPT SERVICE ROUTINE	388
TOTAL =	2540

The selected control mode (Pitch Rate, Normal Acceleration, or Direct) determines which control law will be calculated at each sampling instant by the Flight Control routine. The control law calculation has the highest priority over all other tasks because the sampling interval is to be kept constant. Figure 3-3 presents a diagram of this priority structure and a description of the duty cycle for a nominal sampling interval of 0.1 sec.

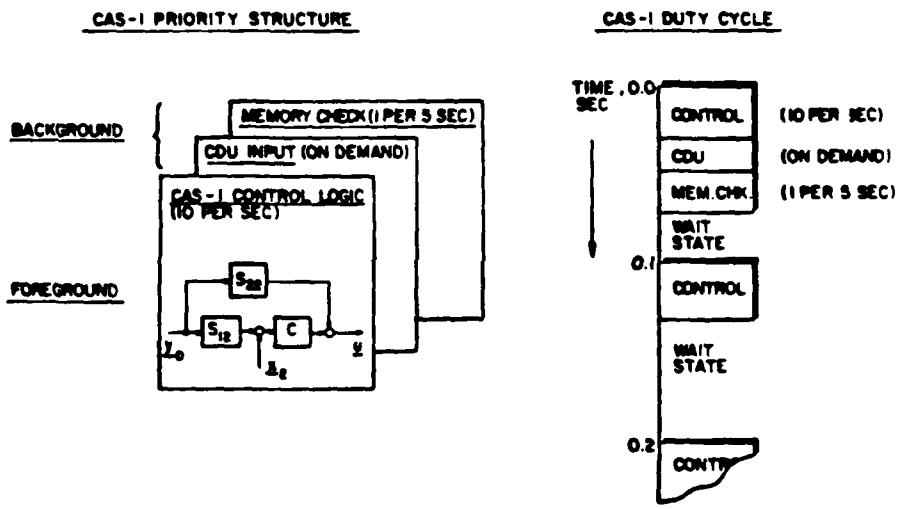

Figure 3-3. CAS-1 Program Organization

The control law calculation operates in the "foreground" and all other tasks are performed in the remaining available time (in the "background"). The duty cycle shows again that the routine containing the control logic is executed exactly every 0.1 second and any other routines fill in on the available "wait state" time.

The components of the software development system (Fig. 3-4) allow programs to be entered and tested efficiently. The ground chasis

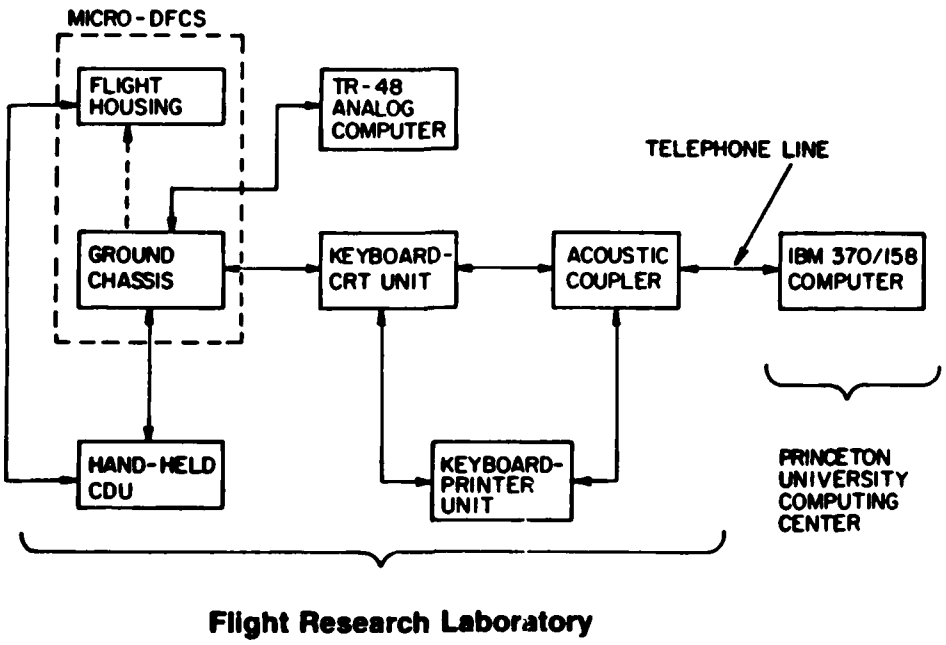

Figure 3-4. Equipment Layout for Micro-DFCS Software Development.

holds the microcomputer boards and provides them with power. The routines, when first coded in assembly language, can be entered into the microcomputer through the keyboard-CRT unit. The text of the routine can be edited to a limited extent on the microcomputer before it is sent to Princeton University's IBM 370/158 computer via an acoustic coupler and the telephone lines. The IBM computer provides more sophisticated text editing, cross-assembly of Micro-DFCS code, and permanent storage of all routines. The assembled routines can be loaded to the microcomputer from the IBM computer and then debugged using the keyboard-CRT unit. A further description of the software development system is contained in Appendix D.

For actual flight tests, the programs are transferred from the development system to the Flight Control Computer Unit (FCCU) mounted in the VRA. The programs can be transferred either on PROM or on a battery back-up 4K RAM board. The battery back-up RAM is the most convenient method, because program modifications made in RAM are much easier and quicker than programming a new PROM. CAS-1 presently occupies approximately 2.5K words of memory. When CAS-1 is expanded past the 4K limit, the routines that will require no changes (the Executive and most of the Utility routines) should be relocated in PROM. The Flight Control routines will probably be modified quite often and should be kept in battery back-up RAM if possible.

3.3 HYRBRID SIMULATION TESTS AND RESULTS

As a logical step between the analytic development and the flight tests, the Micro-DFCS hardware, software, and implemented control laws were tested by simulating the VRA's longitudinal dynamics on an EAI TR-48 analog computer. The voltage levels of the signals interfacing the analog computer to the A/D and D/A channels of the microcomputer were scaled to be of the same magnitude and sign as the outputs from the actual sensors in the VRA. This allows a "real-time" simulation of the Micro-DFCS which insures that all scalings, gains, and other parameters within the software have been set correctly. The analog computer diagram for the longitudinal dynamics of the VRA and a table of poteniometer settings is given in Appendix C (Fig. C-5 and Table C-2).

The simulation used the full fourth-order longitudinal equations of motion that give the effects of both the short-period and phugoid modes. The simulated VRA's q, α, n_z, and δ_s signals were connected to the analog input channels of the Micro-DFCS. The δ_E signal generated by the Micro-DFCS was connected to the control input of the modeled VRA. The states of the VRA and the δ_E output from the Micro-DFCS were recorded on a strip chart recorder.

The three flight control modes — Direct, Pitch Rate, and Normal Acceleration — were tested with different feedback gains and sampling rates (called control configurations). Each was investigated by generating a step input on δ_s and examining the response of the state variables. Specifically, the rise time and overshoot of the commanded state were compared to those predicted by the analytical results. The step of δ_s was generated internally in the microcomputer using the calibrated step routine explained in Appendix E. This insures that a true step is made for each input, and it eliminates differences in resulting plots that could be due to the input of δ_s.

The control law calculations were timed during these tests, and it was found that the Direct Mode routine takes 5 msec to execute, the Pitch Rate Mode takes 19 msec, and the Normal Acceleration Mode takes 6 msec. The Normal Acceleration Mode routine executes faster than the Pitch Rate Mode because the former is coded more efficiently to save execution time and not memory space. This is explained in more detail in Appendix E.

There are time plots at the end of this section for 15 different variations of the three basic flight modes. Each column of Fig. 3-5 represents one run. The flight control configuration, and the Δy_d used for each run are labeled at the top of each column. The different control modes are listed in Table 3-2. Each mode is for a certain control law and a set of weighting matrices. Whenever a control mode is used at different sampling rates, the gains are recalculated to account for the new sampling interval. So, for instance, Pitch Rate Mode B for 10 sps does not have the same optimal gains as Mode B for 7 sps (Table 3-3). All plots are for an initial condition of straight-and-level flight at 105 KIAS. For each run, the six variables Δq, $\Delta\theta$, Δn_z, $\Delta\alpha$, ΔV, and $\Delta\delta_E$ were plotted. The step input on $\Delta\delta_s$ was set and then released after approximately two seconds.

TABLE 3-2

Control Modes Used in Hybrid Tests

CAS	Mode	Q Weightings q_{11}, q_{22}	R Weightings
Direct	-	-	-
Pitch Rate	A	3,20	33
"	B	25,25	33
"	C	50,50	33
"	D	75,25	33
Norm. Acc.	A	5,10	33
"	B	10,5	33
"	C	5,10	250

TABLE 3-3

Optimal Gains for the Control Configurations

Control Mode	Sampling Rate (sps)	Gains q	$\alpha(n_z)$
q Mode A	10	-.150	.036
q Mode B	10	-.427	.324
q Mode C	10	-.554	.360
q Mode D	10	-.620	.469
q Mode C	8	-.484	.377
q Mode D	8	-.532	.475
q Mode B	7	-.358	.347
q Mode B	6	-.324	.355
q Mode B	5	-.282	.362
q Mode B	4	-.232	.366
n_z Mode A	10	-.533	(-.181)
n_z Mode B	10	-.474	(-.106)
n_z Mode C	10	-.238	(-.054)
n_z Mode A	8	-.494	(-.154)

The Direct Mode (Fig. 3-5a) demonstrates the predicted open-loop response of the aircraft. Pitch rate overshoots and decays, $\Delta\alpha$ reaches a new steady state, and ΔV decreases as the aircraft starts to climb. When Δy_d is set back to zero, $\Delta\alpha$ returns to its original value;the decreased ΔV leads to a negative Δq and a rapidly decreasing $\Delta\theta$.

The Pitch Rate Mode B (Fig. 3-5c) shapes the $\Delta\delta_E$ input, providing quicker Δq response with less overshoot. The Δq decay is reduced but not eliminated because the control law is not Type 1 and there is no throttle augmentation to control the decrease in ΔV. Upon releasing the stick, Δq returns closer to the original value than the previous case, and the rate of $\Delta\theta$ decrease is reduced. Comparing these plots to those generated in the analytic study (Fig. 2-7), it is seen the Micro-DFCS is operating as expected. The initial control deflection is approximately 3.5 degrees on both plots, and the responses of Δq, $\Delta\alpha$, and ΔV are similar. Increasing the weighting on Q for the Pitch Rate Mode C (Fig. 3-5d) shows the expected slight decrease in rise time for Δq, with about the same amount of overshoot. To obtain the faster rise time, the magnitude of the initial $\Delta\delta_E$ deflection has increased. With Pitch Rate Mode D, both rise time and overshoot have decreased as Fig. 2-5 predicts. Different sampling rates were used as shown in Fig. 3-5f-k. The optimal gains were recalculated for each set of weightings, taking into account the change in sampling interval. Comparing runs with the same weightings, but different sampling rates, shows identical state trajectories but quite different control inputs, $\Delta\delta_E$. The state trajectories are the same for different

sampling rates because, as mentioned in Chapter 2, the cost functional, J, is minimized continuously in time regardless of the sampling rate. The control input is different to account for the different sampling intervals. In all control configurations, the zero-order hold steps in $\Delta\delta_E$ are visible. The state responses to these control inputs are smooth because the rigid-body dynamics of the VRA filter out the higher frequency content of the sharp-edged steps.

The Normal Acceleration Mode A (Fig. 3-51) forces a large Δq overshoot to obtain rapid, well-damped Δn_z response. The $\Delta\delta_E$ deflection begins with a large impulse; this is followed by a gradual deflection which increases $\Delta\alpha$ to minimize Δn_z decay as ΔV decreases. Figure 3-5n gives the response for R = 250. The weighting R increases the importance of suppressing perturbations in $\Delta\underline{u}$ in the cost functional J. Comparing Fig. 3-5m to Fig. 3-5n, the $\Delta\delta_E$ deflection is initially less for R = 250, even though the step input used (Δy_d=.25g) is greater. Figure 3-5o was made with the sampling rate set at 8 sps. This plot shows once again that sampling rate does not effect the time response using sampled-data regulation theory.

The actual flight tests conducted for the Micro-DFCS are presented in the next chapter along with the results and analysis. This marks the next major step in the testing of the implemented control laws and the Micro-DFCS equipment.

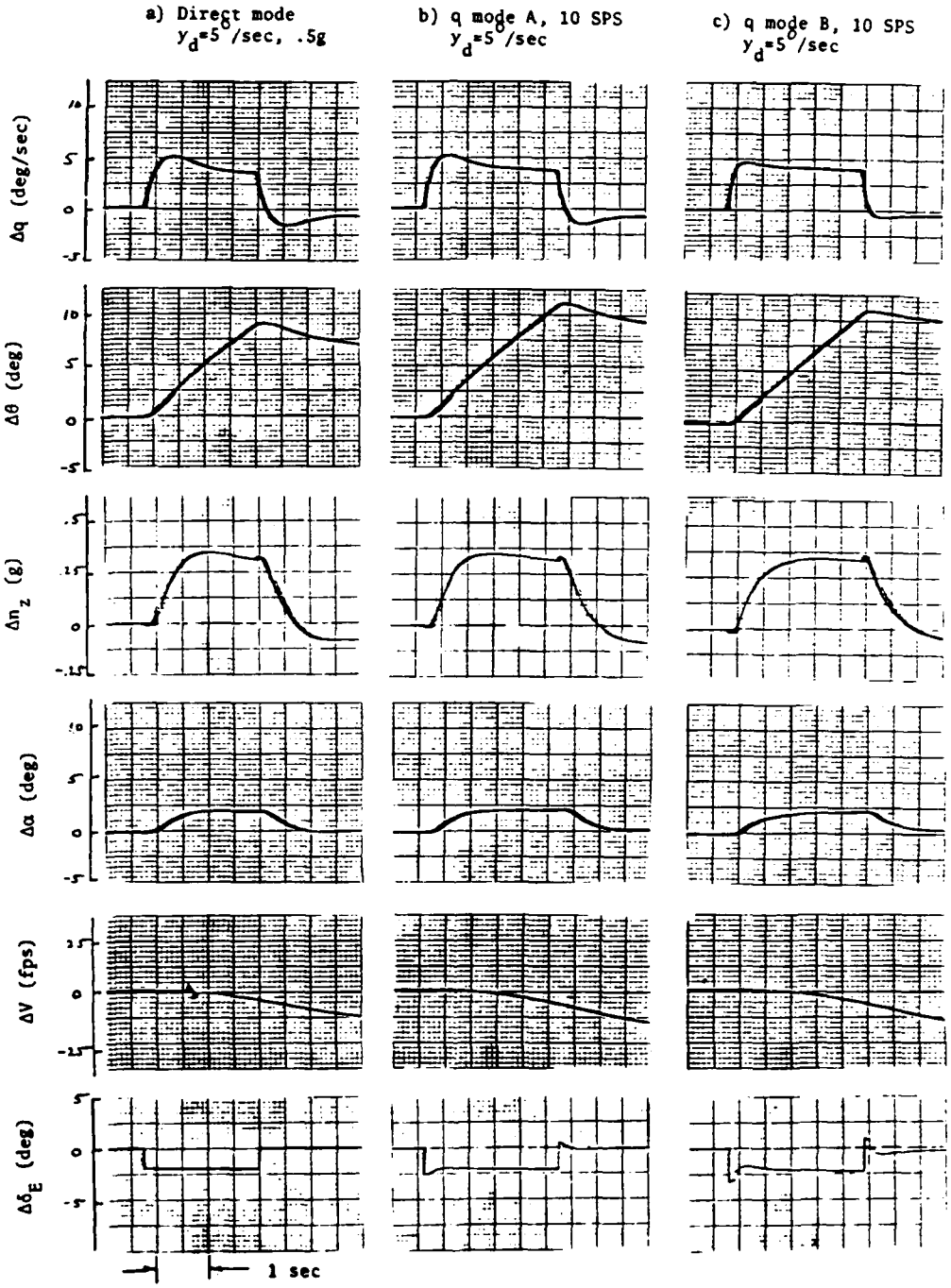

Figure 3-5. Hybrid Simulation Step Responses.

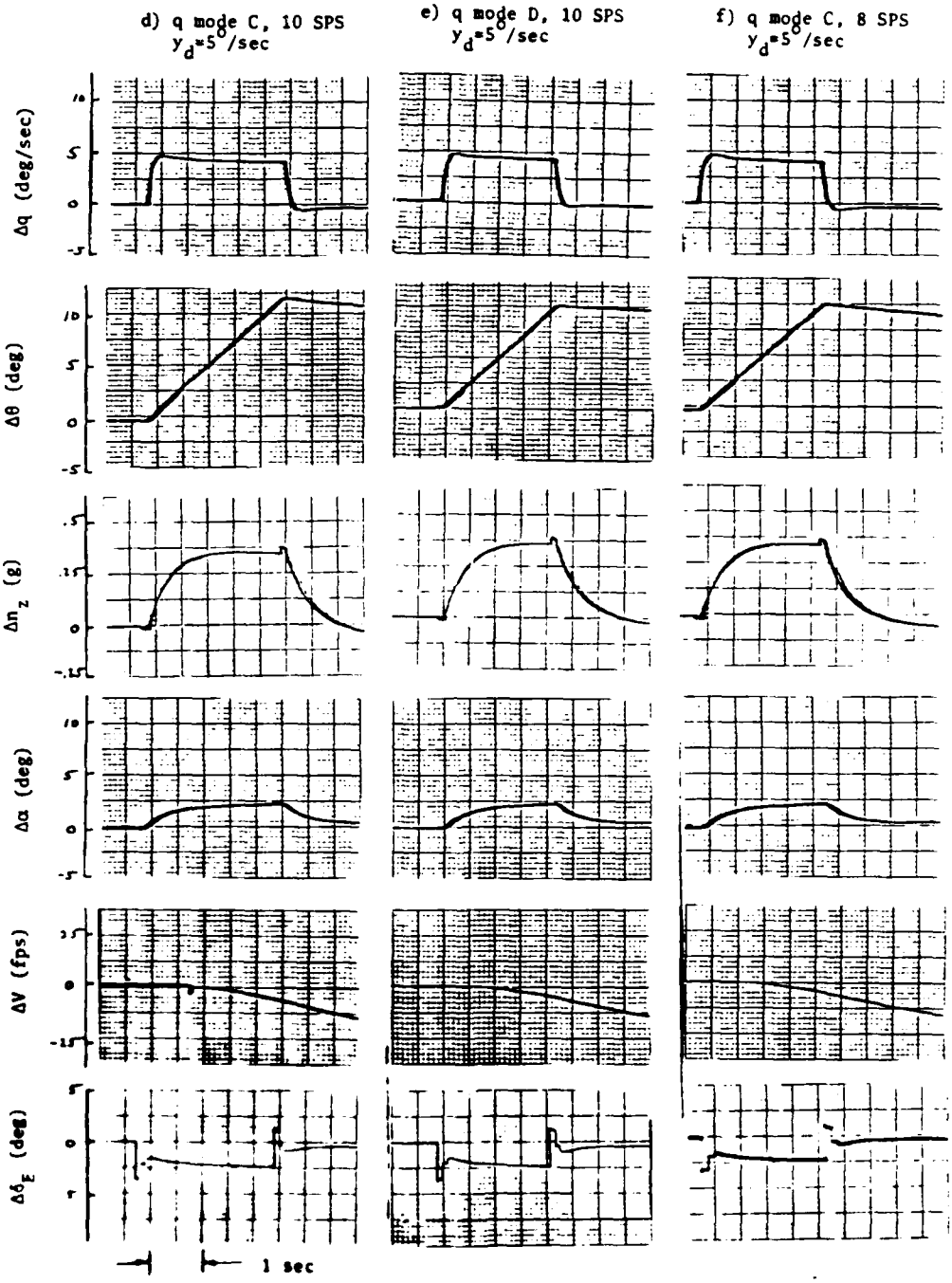

Figure 3-5. continued

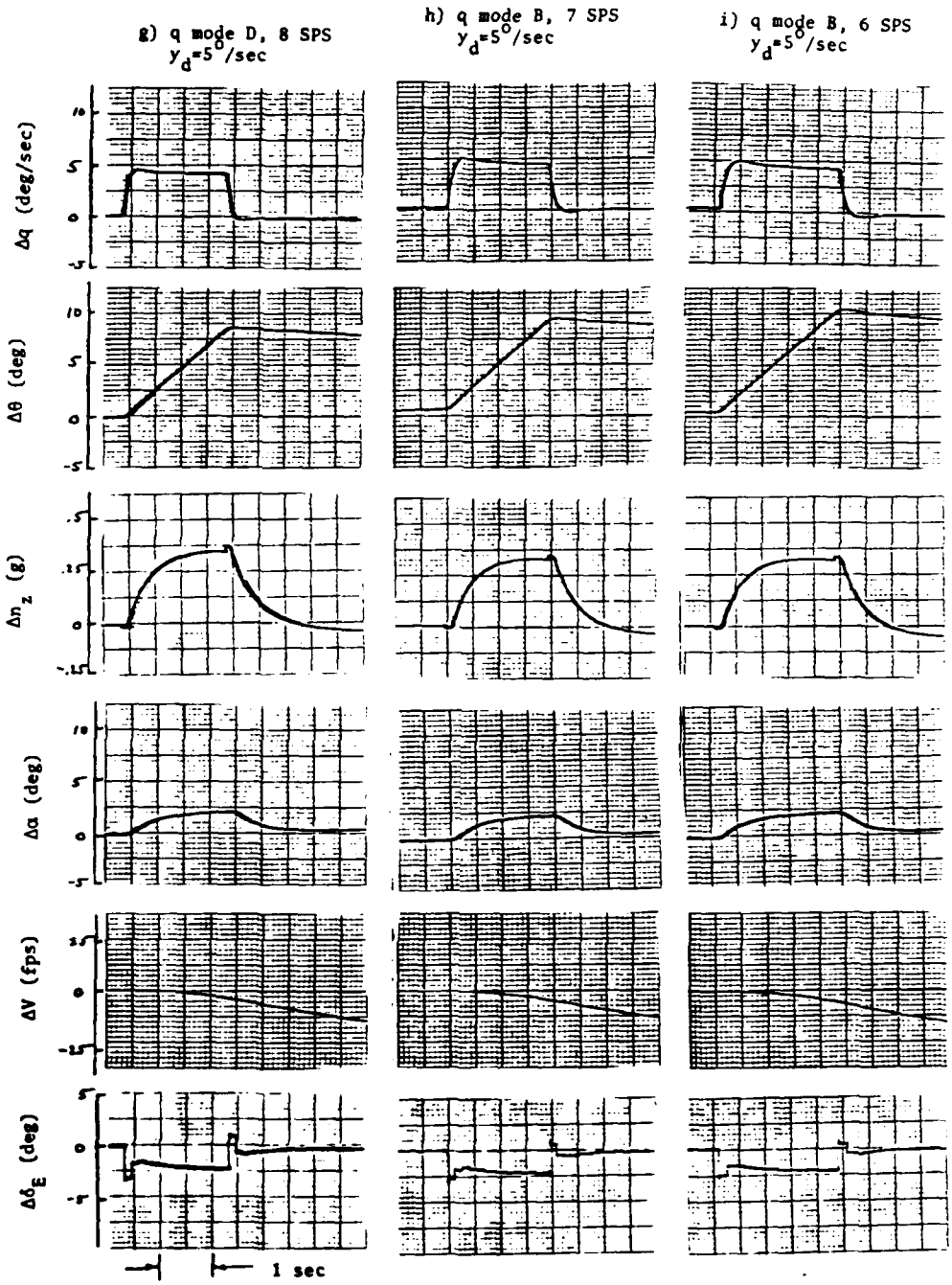

Figure 3-5. continued

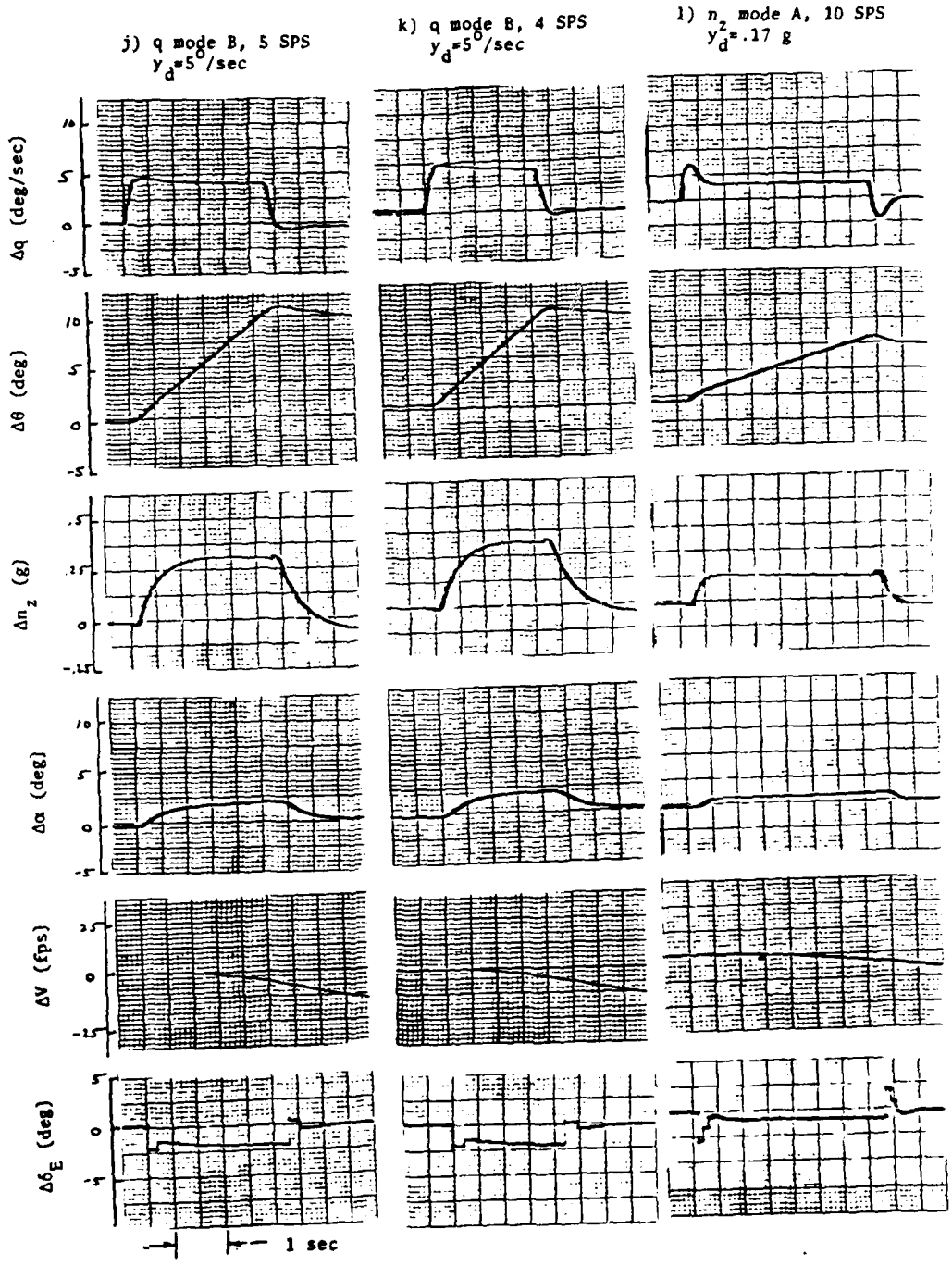

Figure 3-5. continued

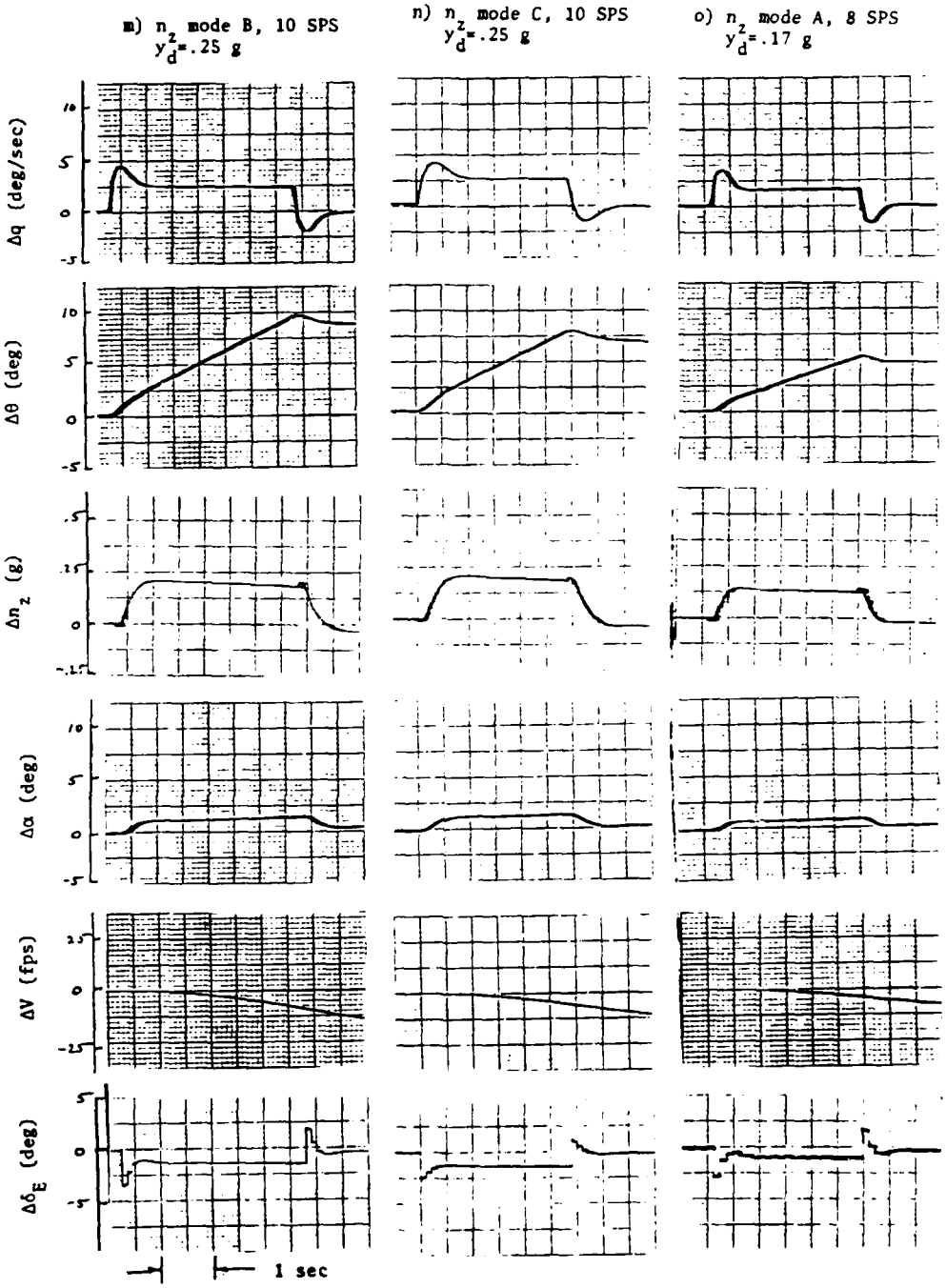

Figure 3-5. concluded

4. FLIGHT TESTING

Flight testing is an important segment of the Micro-DFCS implementation. Experiment and demonstration in flight are necessary for a full understanding of the relationships between control theory and practice. The qualitative and quantitative results obtained in this investigation show some interesting characteristics of DFC with low sampling rates (10 sps and below). The overall results indicate that low sampling rates of the Micro-DFCS do not cause destabilizing phase lags as would be expected with digitized analog control laws. These results are presented in Section 4.2. Section 4.1 outlines the test objectives and procedures.

4.1 TEST OBJECTIVES AND PROCEDURES

Two objectives were set for the flight tests. The first objective was to check out the Micro-DFCS installation, and its operation with the VRA fly-by-wire system. It was anticipated that problems may have occurred due to

- RF noise
- Sensor and channel noise
- Scaling factors set incorrectly within the software
- Difficulties in using the control display unit while in flight

The possibility existed that RF radiation from the telemetry or communication radios might effect the operation of the Micro-DFCS or vice-versa. Also noise might be present on the sensor signals (which

was not accounted for in the hybrid simulation) that would degrade the controller's performance. Noise at high frequencies (because of structural vibrations) that would not normally affect the performance of the VRA's analog control system, could be a problem with a digital controller. The digital system can cause the higher frequency content of the inputs to be "folded" down to the frequencies of interest because of sampling effects. Another problem could be caused by incorrectly set scaling factors that convert voltage levels of pilot controls and feedback sensors to the corresponding units of motion. Finally, there was a question whether the CDU's display could be seen well enough in direct sunlight, and if the method of keying in requests, defined in CAS-1, was adequate.

Examination of the effects of changing gains and sampling rates for the control laws used in the Micro-DFCS was the second major objective for testing. The influences of these parameters on

- Flying qualitites criteria
- Pilot's opinion of controllability, responsiveness, and other noted effects
- Step response as compared to the analytic and hybrid results
- Steady turn maneuvers

were specifically examined. The flying qualitites criteria from the Military Specification (Ref. 20) is given in terms of ζ_{sp} and $\omega_{n_{sp}}$ versus n_z/α. The closed-loop values of these parameters for each set of gains were determined in the analytical study; the flight tests were intended to verify the flying qualities classification. The pilot's opinion of controllability and responsiveness

is a subjective indication of flying qualities. The step response test was conducted with the same step inputs as the hybrid test. A step Δy_d command was entered on the CDU and the resulting motion response was telemetered to the ground for analysis. The last goal was to insure that this longitudinal controller did not significantly oppose steady-turn controller displacement.

The preparations for each flight test consisted mainly of identifying the control configurations (control mode and sampling rate) to be tested on each flight, and loading the flight control computer unit on its palet, which was mounted in the VRA (attached with quick release bolts). The FCCU was reinstalled for each test because CAS-1 usually needed slight modifications depending on the control configuration. Also the Micro-DFCS equipment and software were checked in the hybrid simulation prior to flight tests to verify that all scalings and gains were set correctly.

The testing procedure for each flight was basically the same. Once the VRA had attained the proper altitude (5000 feet MSL for most tests), the Micro-DFCS was engaged using the following sequence:

1. Attain straight-and-level flight at 105 KIAS
2. Select control configuration
3. Radio type of test to ground station
4. Engage VRA's FBW system
5. Accomplish test maneuver
6. Disengage FBW system
7. Set up for next test

The first step is necessary to put the VRA in the control design flight

condition. Some tests, however, were designed to find how the controller operates when under different flight conditions; in that case Step 1 was modified accordingly. The next step selects the control law, gains, and sampling rate by entering the requests through the CDU (see Appendix D for a detailed description for using the CDU). When a new control mode (different control law or set of gains) is requested using CAS-1, the feedback states at that instant are taken as the "set point" or nominal value about which the Micro-DFCS controls for zero $\Delta\delta_s$. Therefore, it is important that the flight condition desired for the run be maintained while Step 2 is being performed. Step 3 lets the ground station operator mark the strip chart plots and tape recording with the type of run. It is done just prior to the maneuver so the strip chart and tape recorder do not run needlessly during the set-up. Next, the FBW system is engaged, allowing the δ_E output from the Micro-DFCS to operate the elevator actuator. Up to this point in the sequence, the Micro-DFCS calculates a δ_E but the actuator is not enabled to follow the δ_E signal. When the FBW system is engaged, the Micro-DFCS δ_E signal is automatically biased so that it corresponds to the actual elevator position just before the engagement. This insures a smooth transition from the normal mechanical controls to the FBW controls. The maneuver is performed and the test data for that run then is collected. The FBW system is disengaged, and the sequence is repeated for the next test run.

The tests yielded both qualitative and quantitative results. In one set of tests, the pilot performed a defined task and rated the responsiveness and controllability for each control configuration.

Quantitative tests were conducted, where the response of the VRA to a step input on δ_s was telemetered for analysis. Figure 4-1 shows the breakdown of the test methods used.

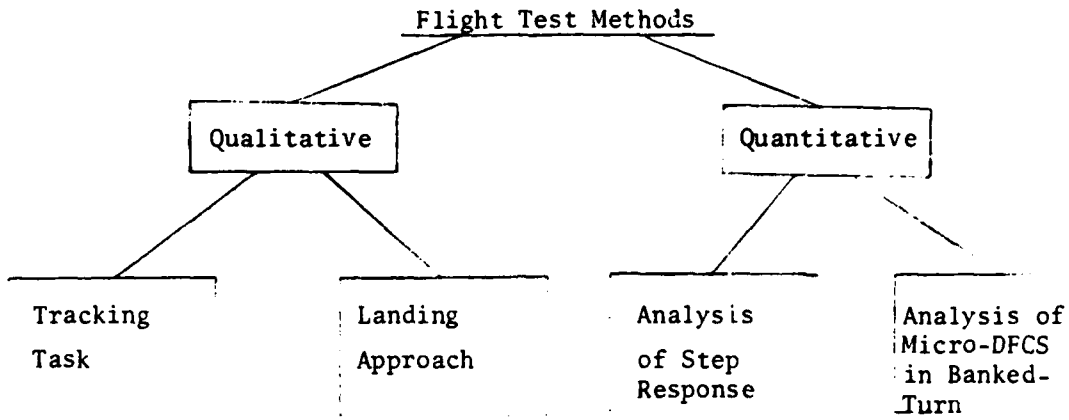

Figure 4-1. Breakdown of Test Methods Used.

The tracking task was conducted by engaging the Micro-DFCS and then attempting to position a "pip" or mark on the windshield over an arbitrary point on the horizon. Every few seconds another point on the horizon was picked and the pilot's success in tracking the new point was recorded as the results for that test. The pilot also was asked to comment on his impression of the discrete elevator movements. The tracking task was performed for the Direct Mode and Pitch Rate Mode B at sampling rates of 10, 8, 7, 6, 5, and 4 sps. It was also done for all Normal Acceleration Modes and Pitch Rate Modes C and D at 10 sps.

The landing approach test was conducted only in the Direct Mode because both control modes were developed only for a 105 KIAS flight condition. Only the effects of the sampling delay were being examined in the landing test. The testing period for each landing started right after the turn to the final approach until touchdown. Sampling rates of 10, 7, 5, 3, 2, and 1 sps were used.

Analysis of the response of the commanded state (either Δq or Δn_z) to a step input of $\Delta\delta_s$ was examined as in the hybrid tests. The same step inputs were used so a comparison could be made. All control configurations presented in Section 3.3 were tested in flight. In addition, the Pitch Rate Mode B operating at 10 sps was tested in straight-and-level flight at 80 KIAS and again at 120 KIAS.

The last testing method was performed to analyze the effects of this longitudinal controller when attempting to hold a steady co-ordinated turn with bank attitudes (ϕ) of 30 and 50 deg. The test was done using the Direct Mode and the Pitch Rate Mode B at 10 sps. The questions to be answered for this test were:

1. How large an effect does the pitch rate damping have on steady-state control position?
2. Is this deflection objectionable to the pilot?

4.2 FLIGHT TEST RESULTS AND ANALYSIS

Three flights were made to collect the data. The first flight was used to test the components of the VRA/Micro-DFCS combination. The components did not interfere with each other's operation except in one case. Whenever the telemetry transmitter was turned off, the FCCU

of the Micro-DFCS was halted. It was not clear if this was due to an RF pulse or a pulse on the power lines. This did not create a problem for testing the control laws, so it was not corrected.

The general operation of all but the Normal Acceleration Mode was tested on the first flight because the n_z accelerometer signal was too noisy to allow the control law to function. Stick-gearing for the Pitch Rate Modes was found to be too low for effective handling qualities evaluation. It was originally set to command 2.7 deg/sec per inch of stick deflection in the steady-state. The pilot considered this too much movement of the stick for the desired Δq. The stick-gearing was doubled which gave adequate control power at the 105 KIAS flight condition. The Normal Acceleration Mode stick-gearing was also doubled from its previous value to 0.52 g/inch. The stick-gearings were set low on Flight 1 for overflow protection; for some control modes, a large stick deflection can cause the Micro-DFCS to temporarily command more than the maximum δ_E allowable. This causes the D/A output to overflow, resulting in a jump in output voltage, as described for the LIMIT routine in Appendix E. The routine LIMIT was added to CAS-1 after Flight 1 to prohibit D/A overflow.

Noise on the sensor channels was a problem for the n_z accelerometer. Structural vibrations with frequencies of 10-Hz or more were superimposed on the n_z signal. A first-order low-pass analog filter with 4-Hz bandwidth was added to the n_z channel before the A/D converter input. For the short-period natural frequency (f_{sp}=0.56Hz), this filter causes a one percent attenuation and an 8 deg phase lag in the n_z signal. The filter completely eliminated the effects of

the structural vibration on the Micro-DFCS in the remaining test flights.

The second and third flights tested the modifications made after Flight 1 and provided data for the qualitative and quantitative tests outlined in Section 4.1.

Tracking at Altitude

The results for the tracking task are given in Table 4-1. The pilot's comments for each control mode and sampling rate used are listed. The temperature was 17°C, the altitude was 4500 to 5500 ft MSL, and barometric pressure was 30.16 inches. The tests were conducted in essentially calm air. Normal Acceleration Mode A was expected to give an undesirable response because the closed-loop $\omega_{n_{sp}}$ for this mode ($\omega_{n_{sp}}$=8.85 rad/sec, ζ_{sp}=.73) places the flying qualities in the Level 2 region of Fig. 2-3. Figure 2-3 is presented again in Fig. 4-2 with all control modes marked. Normal Acceleration Mode B is also in Level 2 with $\omega_{n_{sp}}$ = 7.62 rad/sec. The flying qualities on n_z Mode C is in Level 1 with $\omega_{n_{sp}}$ = 5.5 rad/sec; this rating is also reflected in the pilot's comments. The discrete pulsing movements of the elevator can be felt and heard in varying degrees, depending on the sampling rate and control mode. Low sampling rates or control modes that command large initial deflections make the discrete nature of the movements very noticeable. The vibrations seem very unnatural and are likened to the sound and feel of a stall buffet. The phenomena is very annoying and a DFCS with zero-order hold outputs at less than

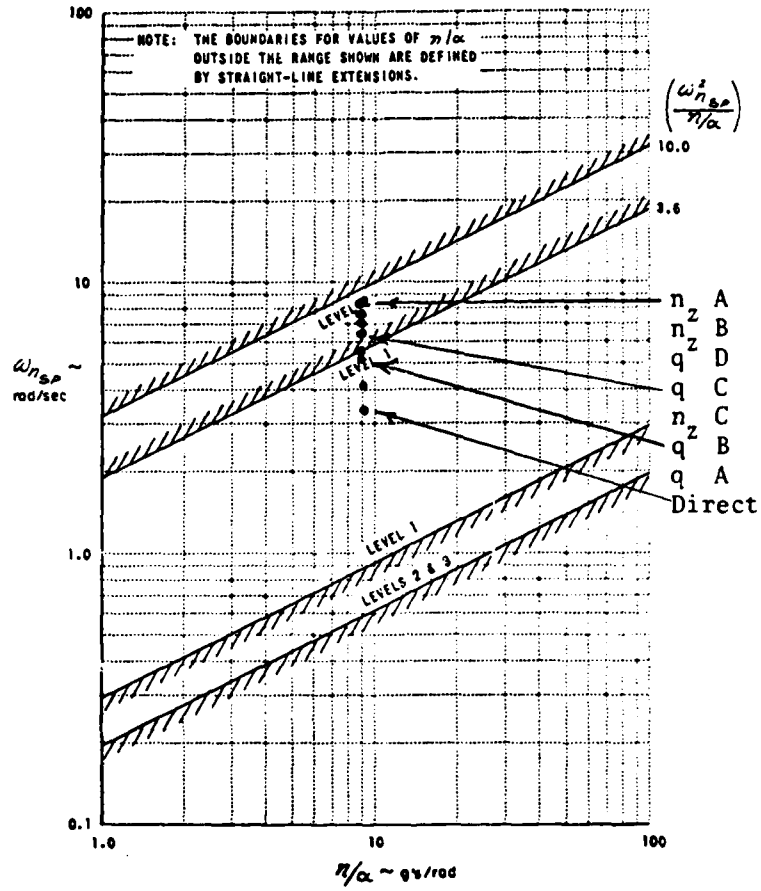

Figure 4-2. Short-Period Frequency Requirements with All Control Modes Marked.

10 sps could probably not be tolerated in an operational design for this flight condition using the control structure defined in Section 2.1; however, no conclusion can be reached regarding the suitability of these low sampling rates with more advanced control designs that smooth control rates.

The Direct Mode operating at 10 sps gives the normal open-loop response of the aircraft with no noticeable sampling effects.

TABLE 4-1

Results for Tracking Task

Sampling Rate (sps)	Control Mode	Pilot's Comments
10	n_z Mode A	Movements too abrupt. Over sensitive to command inputs. Large initial δ_E pulses are felt and heard. FBW system disengages on large input commands.
10	n_z Mode B	Better than Mode A, but initial response still too fast. Discrete δ_E deflections still noticeable.
10	n_z Mode C	Good response with "crisp" tracking. Discrete δ_E movements sound and feel like the stall buffet. This seems very unnatural.
10	Direct Mode	No noticeable difference from the normal continuous open-loop response except for slight rumble of δ_E deflection.
10	q Mode B	Good response. Easier to attain track of mark and hold then Direct Mode. "Rumble" from elevator about same as Direct Mode.
10	q Mode C	Seems the same as q Mode B.
10	q Mode D	Response and control the same as q Modes B and C, but rumble from elevator more noticeable. Not really distracting, but obviously present.
8	Direct Mode	The same response as Direct Mode for 10 sps. Rumble may be slightly more apparent.
8	q Mode B	The same response as q Mode B for 10 sps. Rumble may be slightly more apparent.

(continued)

TABLE 4-1. (continued)

Sampling Rate (sps)	Control Mode	Pilot's Comments
7	Direct Mode	A little overshoot noticed on tracking task but does not interfere with performance significantly. Rumble of δ_E movements more noticeable.
7	q Mode B	No overshooting of mark. Rumble as in the Direct Mode above.
6	Direct Mode	Continual overshoot of mark in tracking task. Very objectionable, but tolerable.
6	q Mode B	Overshoot of mark noticed, but tracking attained more quickly than Direct Mode at 6 sps. Rumble now more of a "thumping"; more noticeable than Direct Mode.
5	Direct Mode	Response seems better than Direct or q Mode at 6 sps. Thumping very noticeable (sound and vibrations.
5	q Mode B	Worse than Direct Mode. Tendency to overshoot mark, but can eventually get there. δ_E thumping about the same as above.
4	Direct Mode	Performance very bad. Very large overshoots in tracking task.
4	q Mode B	Pilot senses delay from command until motion, but no trouble in attaining and keeping the track. No overshoot, just a very objectionable delay. δ_E thumping same as 5 sps.

The elevator movements are noted as a kind of "rumbling" sound. The Pitch Rate Modes B and C at 10 sps give a better response than the Direct Mode because the overshoots and rise times in q, arising from short-period modal characteristics, are decreased. Pitch Rate Mode D gives a similar response, but initial elevator deflections are larger with Mode D, which causes the deflections to be more noticeable. The flying qualities criterion set by Fig. 4-2 shows Level 2 response for Modes C and D with $\omega_{n_{sp}}$ = 6.5 rad/sec, and 7.2 rad/sec respectively (taken from Table 2-2). The pilot's comments indicate, however, that the response and controllability are very good for these two modes. An explanation may be that when the ζ_{sp} is very high (in this case 1.5 and 1.8), Fig. 4-2 may not necessarily apply. The Military Specification gives no necessary relationship between $\omega_{n_{sp}}$ and ζ_{sp}; possibly one is needed.

The remaining tests listed in Table 4-1 are for sampling rates 8 through 4 sps, comparing the response for the Direct Mode and Pitch Rate Mode B. As the sampling rate is decreased, the elevator vibrations get worse and are described as a "thumping" sound. The deflections can also be felt. The Pitch Rate Mode is always worse in this respect than the Direct Mode (at the same sampling rate). Down to 8 sps, the response is considered the same as for 10 sps for both the Direct Mode and Pitch Rate Mode B. At 7 sps and below, a definite degradation in performance is noted in the Direct Mode because of a tendency for the pilot to overshoot the mark. This overshoot probably is caused by the pilot expecting an immediate pitching motion that is instead delayed by the sampling interval. When the anticipated

motion does not occur, the pilot moves the stick slightly more, which causes too much δ_E when the sampling instant does occur. Each Pitch Rate Mode B is better than the Direct Mode for the same sampling rate, except for the 5 sps case, a seemingly anomalous result. At 4 sps, the pilot definitely can sense a delay but comments that he has no trouble attaining and holding a track on the mark. This could be a learning effect which occurred during these particular tests. The pilot may control overshoot better with Pitch Rate Mode B at 4 sps because he finally realizes why he is overshooting the mark when a definite delay is sensed. The pilot may not recognize the problem with the Direct Mode, because the overshoots in Δq could be attributed to the lighter damping of the unaugmented short period mode.

As mentioned above, the Direct Mode, for some reason, seems better than the Pitch Rate Mode at the 5 sps rate. The 5 sps tests were repeated to assure that no error in set-up was made, each time with the same result. No explanation has been found for the degraded 5 sps results. Possible (unverified) causes include calculation of gains done incorrectly, or that there is some type of interaction between the sampling frequency and the frequency of the pilot's inputs.

Landing Approach

The results for the landing approach test are given in Table 4-2. The atmospheric conditions are the same as for the tests listed in Table 4-1. The tests were conducted in essentially calm air. Analysis of this test shows the flare maneuver to be less sensitive to sampling

AD-A090 895 AIR FORCE INST OF TECH WRIGHT-PATTERSON AFB OH F/G 1/3
A FLIGHT INVESTIGATION OF DIGITAL CONTROL USING MICROPROCESSOR --ETC(U)
JUN 79 J C SEAT
UNCLASSIFIED AFIT-CI-79-188T NL

2 OF 2
AD A
090895

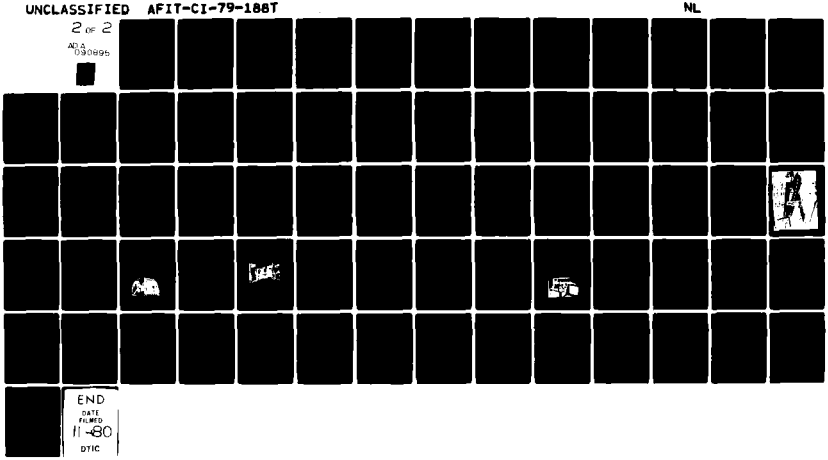

TABLE 4-2

Results for Landing Approach Using the Direct Mode

Sampling Rate (sps)	Pilot's Comments
10	No problem: not aware of sampling on δ_E vibrations.
7	Slight overshoot in response on short final, but no problem in flare.
5	Larger overshoots on short final, but still no problem in flare.
3	Overshoots very objectionable on short final, flare still no problem.
2	The marginal case: overshoots cause poor control on both short final and flare.
1	Not possible in this configuration: pilot moves stick far enough in 1 sec to send a step to δ_E that disengages the safety feature of the FBW system of VRA.

rate than the short final approach or tracking task. This might be explained by examining the pilot's reaction to delayed response. In the tracking task at 105 KIAS or on short final at 70-75 KIAS, the control surfaces generate a larger moment than in the slower flare (60 KIAS). The pilot, therefore, expects an immediate response to his commanded inputs when at cruising speed or on the short final approach, but he has learned there will be slower, more sluggish movements in the flare. He anticipates a natural delay in response on the flare which in effect "masks" the delay of the sampling rate.

When the aircraft does not move immediately in response to a commanded input, the pilot expects this and does not over correct with a larger command.

Pitch Rate in Steady Turn

The telemetry records for the banked turn test shows that the longitudinal controller does oppose the execution of a coordinated, banked turn. The results are given in Table 4-3.

TABLE 4-3

Results for Banked Turn Test

Control Mode	Bank Angle (deg)	Elevator Deflection (deg)	Steady Longitudinal Stick Deflection Required, (inches)
Direct	30	-1	.24
q Mode B	30	-1	.5
Direct	50	-3	1.2
q Mode B	50	-3	1.7

More δ_s is needed for the Pitch Rate Mode than the Direct Mode at both bank angles. This is true because the Micro-DFCS pitch rate feedback is trying to suppress the positive Δq developed in a steady turn. With the stick-force per g characteristic used in these tests, the pilot was not aware of the additional deflection needed, so the longitudinal controller did not seem to degrade lateral-directional maneuvering of the VRA in any significant way.

Step Response Analysis

The final results obtained from the flight tests are the responses to commanded step inputs. The telemetry records of the step responses are presented in Fig. 4-3. Because of a technical malfunction of the ground station, many of the step response runs were not recorded on tape correctly to be played back for better analysis. The only telemetry records available are those that came off the strip chart recorder at the time of the actual test. The sense of these plots is opposite to that of the analytical and hybrid tests. The axes are labeled correctly, so comparisons still can be made.

The analysis of the step responses from the flight and hybrid tests is done in the same manner. Since there is a corresponding hybrid plot for each flight test plot (except for the 120 and 80 KIAS cases), and the hybrid plots were analyzed in Section 3.3, only the different or important aspects of the flight test plots are examined here. Pitch Rate Modes B, C, and D (Fig. 4-3c,d,e) at 10 sps improve the Δq response essentially the same amount. Mode D commands a larger initial $\Delta\delta_E$ deflection, as expected. As the sampling rate is decreased for Pitch Rate Mode B (Fig. 4-3g,h,i,j,k), the Δq response stays the same, but the initial $\Delta\delta_E$ deflections are smaller, to account for the decrease in sampling rate. In Fig. 4-3k it is easy to see the 0.25 sec sampling interval in $\Delta\delta_E$. Comparing plots from Fig. 4-3l and m to Fig. 4-3c, there is not much difference in Δq response from speeds of 80 to 120 KIAS. At 80 KIAS it is apparent, however, that more $\Delta\delta_E$ is needed to hold the commanded Δq as velocity falls to even lower values.

An important difference between the Pitch Rate Mode plots of the hybrid and flight tests is the presence of small disturbances on the latter. It is probably not noise generated in the FBW or telemetry systems because the Normal Acceleration Mode responses are relatively smooth (Fig. 4-3n). Most likely it is small air disturbances at the wing tips picked up by the α vanes. These disturbances can be seen in the $\Delta\alpha$ plots in Fig. 4-3g and m. The α signal feeds to the elevator, which in turn causes the small perturbations in Δq. This is a good example of why air data sensors might not be the best choice for some designs. In this case, however, the pilot is not aware of these small perturbations and gives the Pitch Rate Modes B-D good ratings at 10 sps.

The Normal Acceleration Modes have plots in Fig. 4-3 similar to the hybrid plots. Normal Acceleration Mode A has an initial $\Delta\delta_E$ deflection that is too large to use a commanded input of $y_d = .25g$. To test Normal Acceleration Mode A, a commanded input of $y_d = .17g$ is used to keep the FBW system from disengaging. The large overshoots in Δq are present as expected.

The next and final chapter summarizes the major results of all the previous chapters. Recommendations are made for continuation of research in this project.

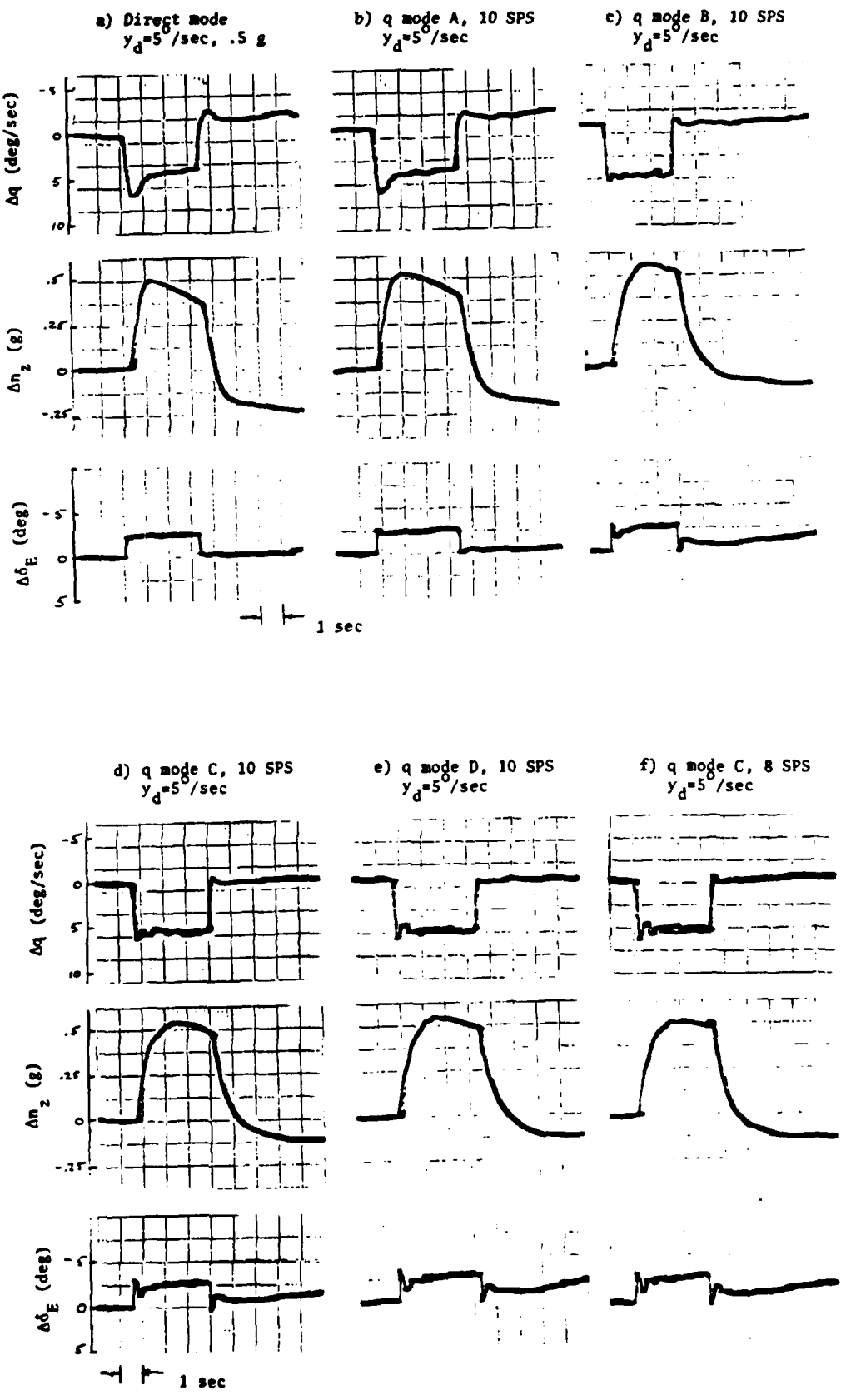

Figure 4-3. Flight Test Step Responses.

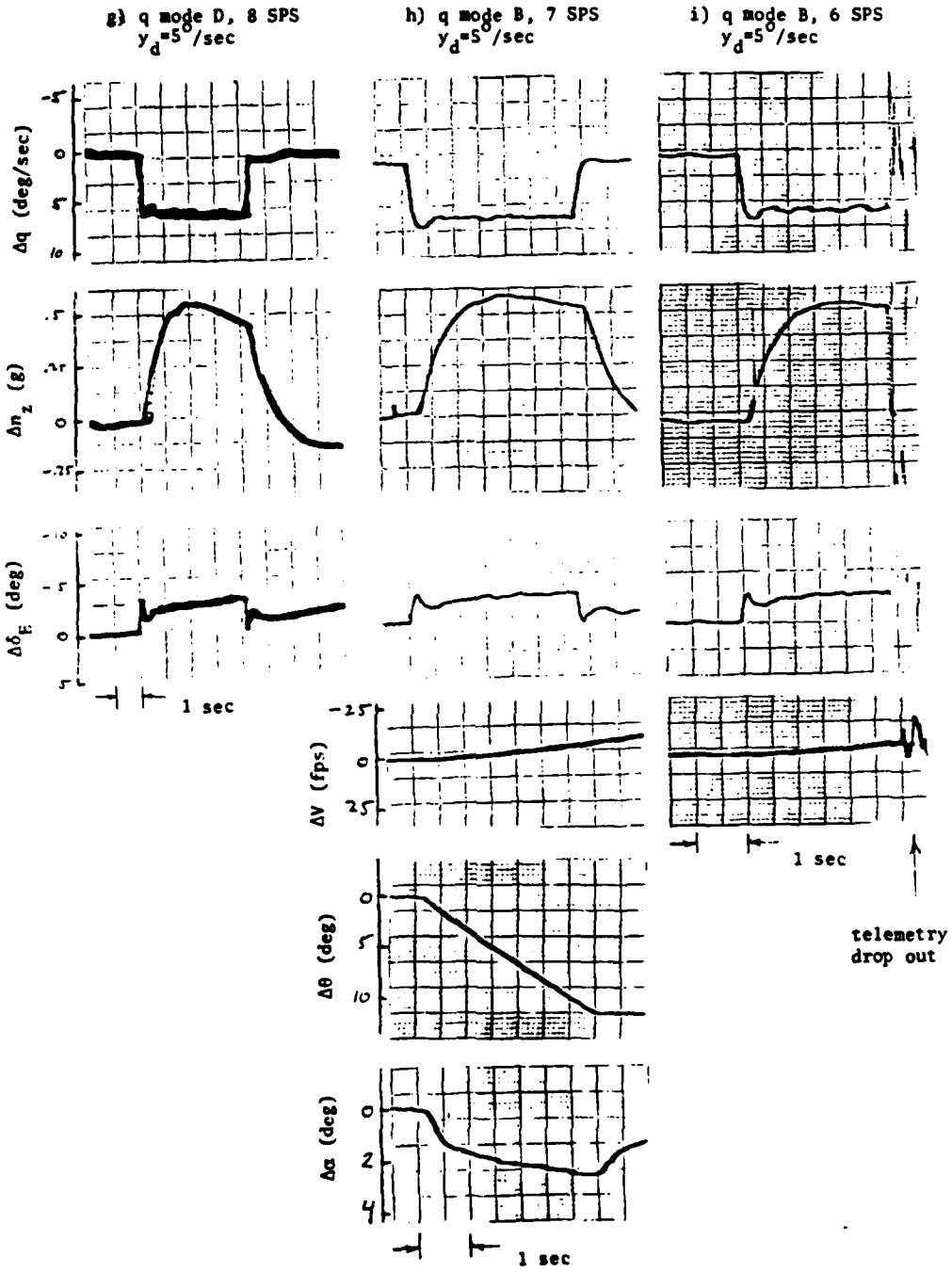

Figure 4-3. continued

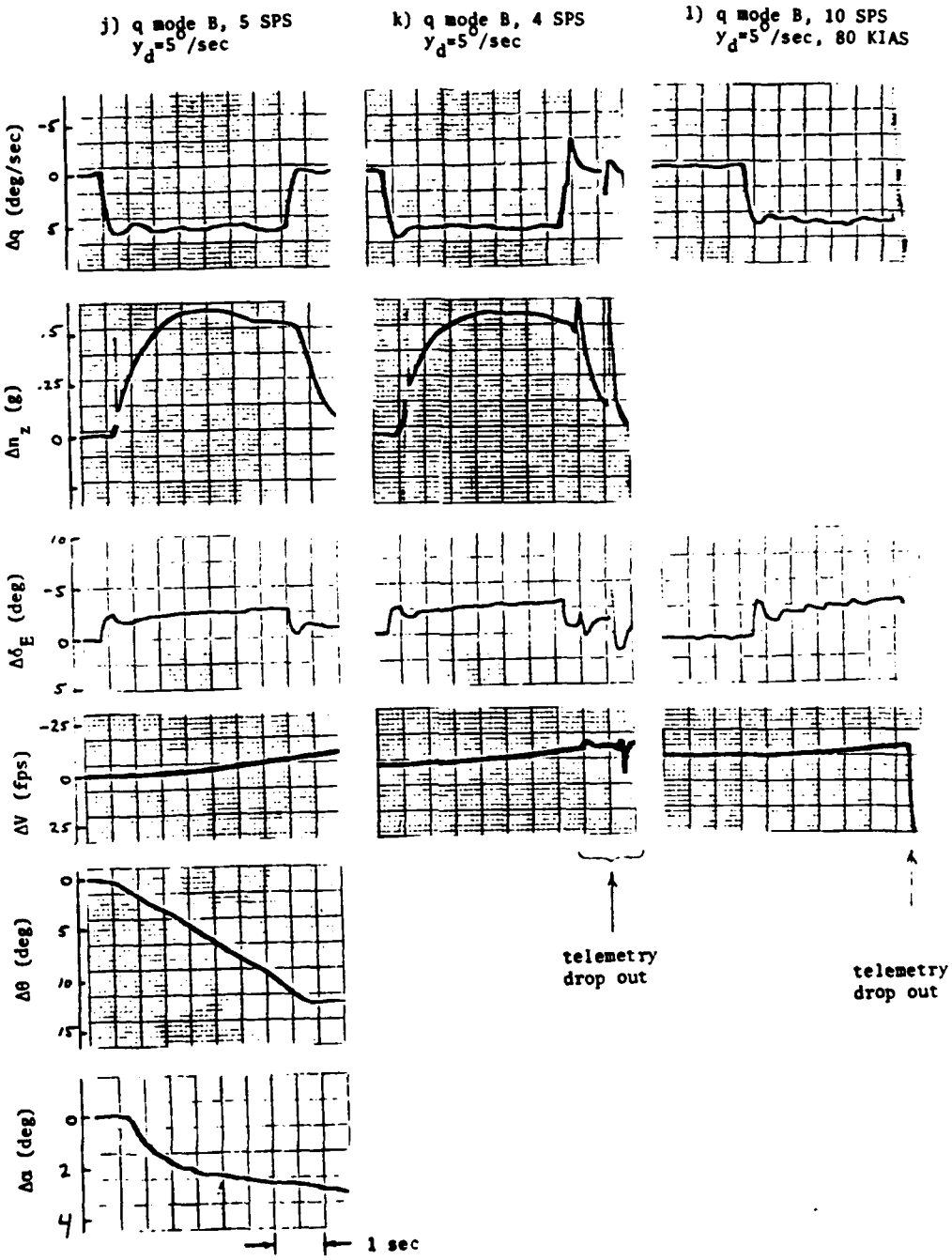

Figure 4-3. continued

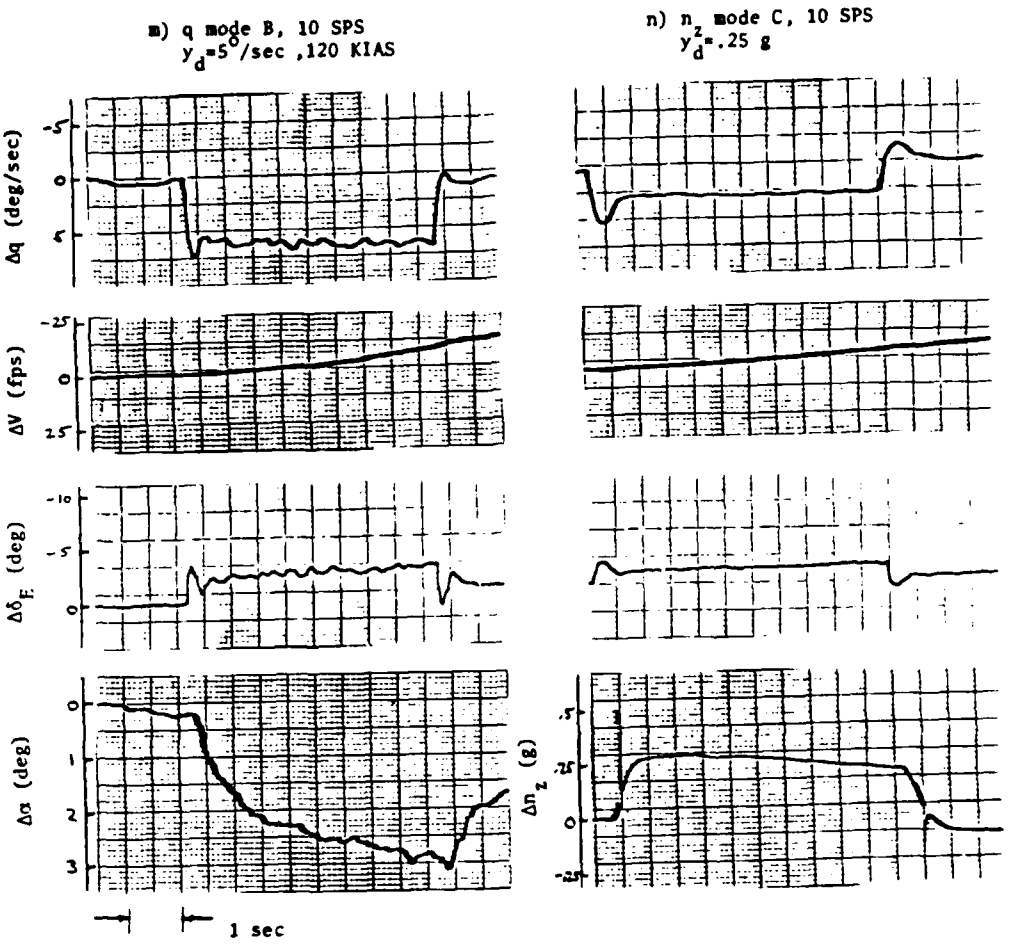

Figure 4-3. continued

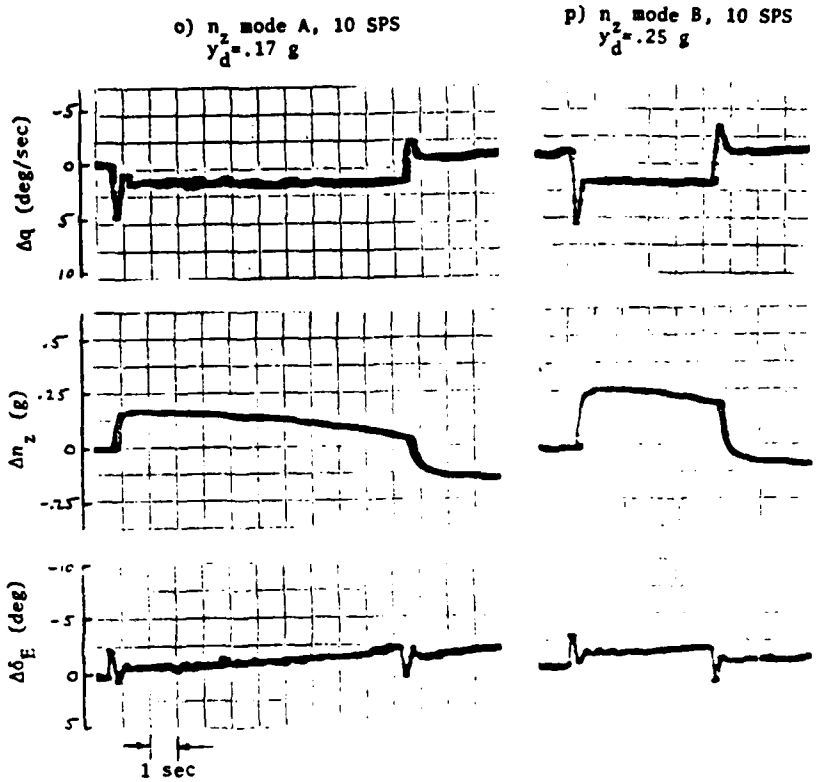

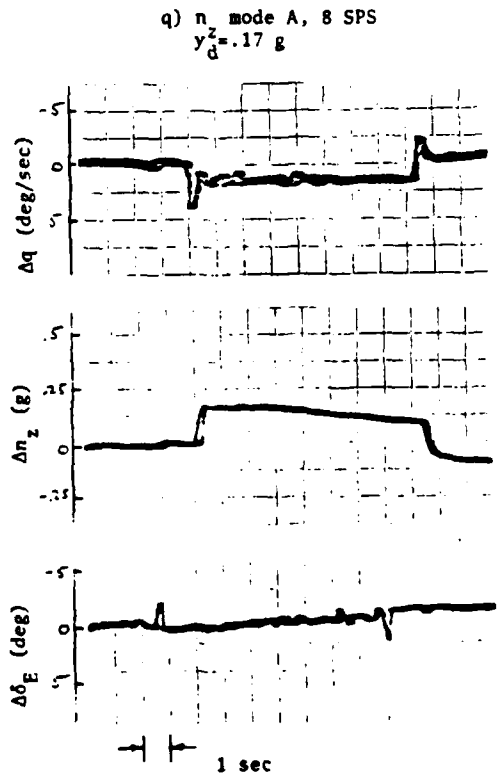

Figure 4-3. concluded

5. CONCLUSIONS AND RECOMMENDATIONS

5.1 CONCLUSIONS

The results of this study provide a basis for low-cost flight testing of advanced concepts in digital flight control using both modern control theory and microprocessor technology. The proof-of-concept control laws, derived using optimal control theory, allow very low sampling rates to be used (10 sps or less). This is because the gains for the simple Type 0 pitch rate and normal acceleration CAS structures are derived by minimizing an analog performance index even though the control law is calculated at discrete instances in time. This gives a large improvement in sampling requirements over the conventional method of simply digitizing an analog control law. The resulting lower sampling rates decrease the computational burden associated with the controller and would allow more advanced control modes to be implemented on the microprocessor based system. The Micro-DFCS is integrated with the VRA; the system is completely operational and ready for further digital flight control research. New flight test programs can be developed quickly because all hardware is installed, and a basis for further software development is present in CAS-1.

The objectives of this project, as outlined in Chapter 1 were to add a Micro-DFCS to the VRA's FBW analog control system and provide initial results with actual flight testing. The

objectives have been met with all results and analysis given in the text of this report. A summary of the major conclusions follows.

- The step response plots from the digital model, analog simulation, and flight tests all show that the major response features of the closed-loop system are not affected by sampling rate when sampled-data regulator theory is used. This verifies that the lag which results from sampling the feedback variables is indeed accounted for in the control law calculation. The lower limit on sampling rate in this study is, therefore, not determined by the phase lag inherent in the sampling process.

- The microcomputer used in this study has the speed to execute much more complicated and advanced control laws at the sampling rates examined. For example, Type 0 fourth-order longitudinal and fourth-order lateral-directional control laws require 84 calculations per sampling interval compared to 20 for the two-state feedback control laws examined here (including all scalings). This implies that the control laws for an eight-state feedback longitudinal, lateral-directional controller can be calculated in less than 26 msec (84/20 x 6 msec). For a nominal sampling rate of 10 sps, over 74% of the available duty cycle still is not being used.

- Commercially available microcomputer equipment provides substantial capability for conducting advanced research in DFC. Additional memory, analog channels, or other peripheral devices can be added quickly to the system. The ease of this expansion, coupled with the speed of the machine, makes it very versatile for further research.
- The software development system provides an efficient means of writing and testing the Micro-DFCS software. The rudimentary text editor of the microcomputer allows easy entry of assembly language programs. Editing the programs on the microcomputer is a cost-effective alternative to using the time-sharing computer for this purpose.
- Modifying the commanded state's response by changing the weighting factors in the Q and R matrices is not difficult, but it is an iterative procedure, and it is not always obvious how the weightings should be changed to attain the desired response. Figures 2-5 and 2-12 show the relationships between weightings and response for the particular CAS structures of this study, but, in general, there is no standard relation between step response and quadratic weighting factors. These figures may, however, give some indication of what can be expected for similar control law developments.

- The pilot is not aware of the sampled nature of the Micro-DFCS at 10 sps for the Pitch Rate Modes and Direct Mode. At this rate, no effects on flying qualities, due to sampling, are seen, and the sound and vibrations from the step elevator movements are barely noticeable. For the pitch rate CAS at 105 KIAS, performance degradation is not noted down to 7 sps; however, the elevator movements are rather annoying. They sound and feel similar to the cues sensed in a stall buffet. A sampling rate of 3 sps is found to be acceptable using the Direct Mode on the flare of the landing, but a minimum of 10 sps is needed for the short final segment of the approach.
- The n_z response cannot be speeded up effectively at the 105 KIAS flight condition with only an elevator control input. For any appreciable decrease in n_z rise time, the closed-loop $\omega_{n_{sp}}$ increases to a value which places the response of the system in the Level 2 category. The pilot perceives the response as being too touchy and oversensitive. If n_z response is to be speeded up at this flight condition, direct lift control is needed.

The Micro-DFCS, using modern control theory, definitely has a place in future flight control applications because of its low-cost

and flexibility. The modern control theory allows more computations per sampling interval which, in turn, implies a capability to execute complex control functions. This increases the desirability of the DFCS and especially a low-cost Micro-DFCS. In this way, microprocessor technology and modern control theory will complement one another and promote each other's use.

5.2 RECOMMENDATIONS

From lessons learned in this study, five recommendations are made for continuing research in microprocessor based digital flight control:

- At sampling rates below 8 sps, some type of output to the control effectors, other than zero-order hold, may be needed if control laws with control rate restraint are not used. The sound and the vibrations are too objectionable at the lower sampling rates. Possible corrections of the problem could include low-pass filtering of the controller output or using output rates higher than the input rates. It must, however, be remembered that the sampled-data regulator theory used in this study assumes zero-order hold on the controller output when minimizing the analog performance index, J.

- It may be necessary to filter the signals from the sensors or pilot's controls before the A/D conversion to prevent higher frequency noise from effecting the performance of the Micro-DFCS. The sampling process folds the higher frequency content of the signal onto the lower frequencies of interest and can make the sampled signal useless if the higher frequency content is large in magnitude compared to the low frequency information. For an operational design, all controller inputs would probably need to be filtered to guard against noise that may develop. Only the n_z accelerometer was filtered in this investigation.

- Some provision for trimming would be very useful and improve efficiency in flight tests. Once the fly-by-wire system is engaged in the VRA, there is presently no digital mechanism to change the set point about which the Micro-DFCS regulates with the simple system of this study. This means either that the FBW system must be disengaged and controls reset everytime the aircraft drifts from the desired flight condition or that the VRA's analog system must be used to achieve trim. The slow integration of a trim switch deflection, summed into y_d may provide the necessary control.

- The Flight Control routines should be written to conserve time and not memory. The computational speed is very important, so the least number of program instructions should be executed on each calculation. This implies avoiding the use of generalized sub-routines, and making the Flight Control routines very specific to their function.

- The battery back-up memory board has been a big asset in the development and use of the microcomputer software. The transfer of programs from the software development system to the FCCU is accomplished very easily, and program modifications are much simpler and faster than would be the case using PROM. For routines that seldom need to be changed, PROM storage would be the cheapest and most convenient method. For this initial programming effort, more battery back-up memory will benefit the research program.

There are many other variations and capabilities of the Micro-DFCS that need to be investigated. A few that were recognized from the results of this study are given below.

- A lower limit on sampling rate needs to be established in the presence of worst-case turbulence.

The limits on sampling rate given in this study are set only by the pilot's acceptance criteria explained in Section 2.2. The limit set by error build-up remains to be found.

- The pilot's comments on Pitch Rate Mode D show it to exhibit good response, yet the Military Specification on Flying Qualitites (Ref. 19) rates this mode in the Level 2 category because of the high $\omega_{n_{sp}}$. This mode has a rather large ζ_{sp} which might indicate that the military specification's criterion is not true at high values of ζ_{sp}. Some relation may be needed in the specification between $\omega_{n_{sp}}$ and ζ_{sp} to make the criterion valid.

- Because of the zero-order hold on the controller outputs, the control actuators always are commanded to move in steps, at infinite rates. The question is raised as to what kind of stress this places on the actuator mechanism when it always is moved at its maximum rate.

- In the tracking task of the flight tests, the pilot preferred 5 sps in the Direct Mode to 5 sps in the Pitch Rate Mode. This is contrary to the preference at other sampling rates. While it is

possible that a mistake was made in calculating or entering the gains in CAS-1, the step response test for the Pitch Rate Mode at 5 sps was accomplished during the same flight, with the same gains, and those results are as expected (Fig.4-3j). Further investigation of this anomaly is warranted.

APPENDIX A

DERIVATION OF DISCRETE WEIGHTING MATRICES FROM CONTINUOUS IMPLICIT MODEL-FOLLOWING WEIGHTING MATRICES

The discrete weighting matrices, $\hat{Q}$, $\hat{M}$, and $\hat{R}$ derived in Ref. 15 use the continuous cost functional of Eq. 23. The implicit model-following presented in Section 2.6 calculates Q, M, and R matrices for the continuous cost functional of Eq. 56. In order to use the implicit model-following technique for a digital system, a transformation from Q, M, and R to $\hat{Q}$, $\hat{M}$, and $\hat{R}$ is needed. This relation is derived below with the same assumptions used for the derivations of Ref. 12.

The objective is to minimize the continuous-time cost functional, so it is necessary to find $\hat{Q}$, $\hat{M}$, and $\hat{R}$ that satisfy the relation

$$J = \int_{t_o}^{t_N} [\underline{x}^T(t)\ Q\ \underline{x}(t) + 2\ \underline{u}^T(t)\ M\ \underline{x}(t) + \underline{u}^T(t)\ R\ \underline{u}(t)]dt \tag{63}$$

$$= \sum_{i=0}^{N-1} \left(\underline{x}_i^T\ \hat{Q}\ \underline{x}_i + 2\ \underline{u}_i^T\ \hat{M}\ \underline{x}_i + \underline{u}_i^T\ \hat{R}\ \underline{u}_i \right)$$

N = number of samples

i = index

given the system dynamics, Q, M, and R. The continuous J can be decomposed into a sum of N integrals:

$$J = \sum_{i=0}^{N-1} \int_{t_i}^{t_{i+1}} (\underline{x}^T Q \underline{x} + 2 \underline{u}^T M \underline{x} + \underline{u}^T R \underline{u}) \quad dt \tag{64}$$

where the time dependency is understood. Setting Eq. 64 equal to the bottom line of Eq. 63 and making a substitution with

$$\underline{x}(t) = \Phi(t,t_i) \quad \underline{x}_i + \Gamma(t,t_i) \quad \underline{u}_i \tag{65}$$

the derivation proceeds as follows:

$$\underline{x}_i^T \hat{Q} \underline{x}_i + 2 \underline{u}_i^T \hat{M} \underline{x}_i + \underline{u}_i^T \hat{R} \underline{u}_i$$

$$= \int_{t_i}^{t_{i+1}} [(\Phi \underline{x}_i + \Gamma \underline{u}_i)^T Q(\Phi \underline{x}_i + \Gamma \underline{u}_i) + 2 \underline{u}_i^T M(\Phi \underline{x}_i + \Gamma \underline{u}_i)$$

$$+ \underline{u}_i^T R \underline{u}_i] \quad dt \tag{66}$$

$$= \int_{t_i}^{t_{i+1}} (\underline{x}_i^T \Phi^T Q \Phi \underline{x}_i) dt + 2 \int_{t_i}^{t_{i+1}} (\underline{u}_i^T \Gamma^T Q \Phi \underline{x}_i$$

$$+ \underline{u}_i^T M \Phi \underline{x}_i) dt + \int_{t_i}^{t_{i+1}} [\underline{u}_i^T R \underline{u}_i + \underline{u}_i^T \Gamma^T Q \Gamma \underline{u}_i$$

$$+ 2 (\underline{u}_i^T M \Gamma \underline{u}_i)] \quad dt \tag{67}$$

Because $\underline{x}_i$ and $\underline{u}_i$ are not functions of the integration variable, t, they may be taken outside the integrals. Matching like variables from both sides of the equation we have the desired relation:

$$\hat{Q} = \int_{t_i}^{t_{i+1}} \Phi^T(t,t_i)\ Q\ \Phi(t,t_i)\ dt \tag{68}$$

$$\hat{M} = \int_{t_i}^{t_{i+1}} [\Gamma^T(t,t_i)\ Q\ \Phi(t,t_i) + M\ \Phi(t,t_i)]\ dt \tag{69}$$

$$\hat{R} = \int_{t_i}^{t_{i+1}} [R + \Gamma^T(t,t_i)\ Q\ \Gamma(t,t_i) + 2\ M\ \Gamma(t,t_i)]\ dt \tag{70}$$

APPENDIX B

DESCRIPTION OF APL FUNCTIONS FOR GENERATING OPTIMAL GAINS AND TIME HISTORIES

The equations from modern control theory (given in Chapter 2) are coded in APL functions. The functions are listed in Table B-1. A short description of each function is given below:

FCLOOP - Calculates the closed-loop F matrix for a second-order system given Φ, Γ, and the gains, k. F_{CL} is returned in variable FCL. Uses Eq. 46.

FCL4 - Calculates the closed-loop F matrix for a fourth-order system given the fourth-order Φ and Γ, and the second-order gains, k. F_{CL} is returned in variable FCL.

FOLLOW - Calculates continuous-time Q, M, and R for implicit model-following given the matrix F of the model, matrices F and G of the VRA and a weighting matrix, W. Uses Eqs. 57-59.

GAIN - Calculates optimal gains using Eq. 30. Gains are passed to variable k. The dimension of k is changed in k4 for use in FCL4.

GAMMA - Calculates the discrete control effects matrix, Γ, for a second-order system. It is a monadic operator that uses the second-order Φ(STM). Variable GAM holds the result. Uses Eq. 12.

GAMMA4 - Calculates fourth-order Γ. It is a monadic operator that uses the fourth-order Φ(STM4).

GENSTM - Generates 100 Φ matrices using time intervals in 1 percent increments of the sampling interval. These matrices are for use in function QMR for calculating discrete weighting matrices.

IDENT - Forms an identity matrix. A monadic operator that uses the matrix dimension as the argument. Result returned in variable I.

QMR - Calculates discrete weighting matrices $\hat{Q}$, $\hat{M}$, and $\hat{R}$ from continuous Q and R. Uses simple Euler integration in 100 steps. Uses Eqs. 26-28.

QMRF - Calculates discrete weighting matrices $\hat{Q}$, $\hat{M}$, and $\hat{R}$ from continuous Q, M, and R. Uses simple Euler integration in 100 steps. Uses Eqs. 60-62.

RICCATI- Solves Riccati equation (Eq. 29). Result returned in variable P.

SONETWO- Calculates relation between $\Delta \underline{y}_d$ and $\Delta \underline{x}^*$:S_{12}. It uses the result from STWOTWO. Uses Eq. 18.

STMDYN - Calculates Φ given sampling interval and F matrix. Result is returned to variable specified by using the "back arrow." Uses Eq. 11.

STWOTWO- Calculates relation between $\Delta \underline{y}_d$ and $\Delta \underline{u}^*$: S_{22}. Uses Eq. 19.

SYSMODEL-Generates a time history for the second-order system. The function will ask if a printed table is desired (answer yes or no). The time history will run for 5 sec. unless 'BREAK' is depressed. The time history is stored in vectors ΔQ, ΔALPHA, TIME, and DELU. Vector ΔQ contains elements $\Delta \underline{x}_{1_k}$, ΔALPHA contains $\Delta \underline{x}_{2_k}$, TIME contains the time instances spaced by the sampling interval, and DELU contains $\Delta \underline{u}_k$. These vectors are used in the 10 LINPLOT functions to plot the time histories. Uses Eqs. 10 and 22.

SYSMOD4-Same as SYSMODEL except 4th-order time history is generated using the 2nd-order gains. Additional vectors for plotting are Δv and ΔGAM. Vector Δv contains $\Delta \underline{x}_{3_k}$ and ΔGAM contains $\Delta \underline{x}_{4_k}$.

```
      ∇FCLOOP[⎕]∇
      ∇ FCLOOP;SM;R;FACTOR;INDEX;I;IFCL
[1]   ⍝ CALCULATES C.L. F MATRIX FOR SECOND ORDER SYSTEM
[2]    R←(⍉,STM)*0.5
[3]    I←(⍳R)∘.=⍳R
[4]    N←0
[5]    FCL←I-I
[6]    STMCL←STM-GAM+.×K
[7]    STMI←I
[8]   LO:N←N+1
[9]    STMI←(STMCL-I)+.×STMI
[10]   FACTOR←((¯1)*N+1)×STMI
[11]   IFCL←FCL+FACTOR÷N
[12]   INDEX←(+/|,FCL-IFCL)÷R*2
[13]   FCL←IFCL
[14]   →(N=100)/STP
[15]   →(INDEX>0.00001)/LO
[16]   →CONT
[17]  STP:'DID NOT CONVERGE ON C.L.F  MATRIX IN 100 ITERATIONS.'
[18]  CONT:FCL←FCL÷DT
      ∇
      ⋄

      ∇FCL4[⎕]∇
      ∇ FCL4;SM;R;FACTOR;INDEX;I;IFCL
[1]   ⍝ CALCULATES C.L. F MATRIX FOR FOURTH ORDER SYSTEM
[2]    R←(⍉,STM4)*0.5
[3]    I←(⍳R)∘.=⍳R
[4]    N←0
[5]    FCL←I-I
[6]    STMCL←STM4-GAM4+.×K4
[7]    STMI←I
[8]   LO:N←N+1
[9]    STMI←(STMCL-I)+.×STMI
[10]   FACTOR←((¯1)*N+1)×STMI
[11]   IFCL←FCL+FACTOR÷N
[12]   INDEX←(+/|,FCL-IFCL)÷R*2
[13]   FCL←IFCL
[14]   →(N=100)/STP
[15]   →(INDEX>0.00001)/LO
[16]   →CONT
[17]  STP:'DID NOT CONVERGE ON C.L.F  MATRIX IN 100 ITERATIONS.'
[18]  CONT:FCL←FCL÷DT
      ∇
      ⋄

      ∇FOLLOW[⎕]∇
      ∇ FOLLOW
[1]   ⍝ CALCULATES CONTINUOUS TIME Q, M, R
[2]   ⍝ FOR IMPLICIT MODEL-FOLLOWING GIVEN
[3]   ⍝ THE MATRIX F OF THE MODEL.
[4]    Q←(⍉F-FM)+.×W+.×F-FM
[5]    M←(⍉G)+.×W+.×F-FM
[6]    R←(⍉G)+.×W+.×G
      ∇
```

Table B-1. Listing of APL Functions.

```
      ∇GAIN[⎕]∇
      ∇ GAIN
[1]   ⍝ CALCULATES OPTIMAL FEEDBACK GAINS
[2]    K←(⍉FH+(⍉GAM)+.×F+.×GAM)×((⍉GAM)+.×F+.×STM)+⍉MH
[3]    K4← 1 4 ⍉(0,0,K)
      ∇
      ⋄

      ∇GAMMA[⎕]∇
      ∇ GAMMA STM
[1]   ⍝  CALCULATES GAMMA MATRIX
[2]    GAM←STM+.×(⍉F)+.×(I-(⍉STM))+.×G
      ∇
      ⋄

      ∇GAMMA4[⎕]∇
      ∇ GAMMA4 STM
[1]   ⍝  CALCULATES 4TH ORDER GAMMA MATRIX
[2]    GAM4←STM+.×(⍉F4)+.×(I-(⍉STM))+.×G4
      ∇
      ⋄

      ∇GENSTM[⎕]∇
      ∇ GENSTM;STEP
[1]   ⍝ GENERATES 100 TRANSITION MATRICES FOR QMF
[2]    T←STEP←DT÷100
[3]    GSTM←I
[4]   AGAIN:STMI←T STMDTN F
[5]    GSTM←GSTM,STMI
[6]    →(T=DT)/0
[7]    T←T+STEP
[8]    →AGAIN
      ∇
      ⋄

      ∇IDENT[⎕]∇
      ∇ I←IDENT N
[1]   ⍝  MAKES IDENTITY MATRIX OF SIZE N
[2]    I←⍳N
[3]    I←I∘.=I
      ∇
      ⋄
```

Table B-1. continued

```
      ∇QMR[⎕]∇
      ∇ QMR;STEP
[1]   ⍝  CALCULATES Q HAT, M HAT , R HAT
[2]    MH←GAM-GAM
[3]    QH←I-I
[4]    RH←0
[5]    T←STEP←DT÷100
[6]    C←1
[7]   LOOP:C←C+2
[8]    D←C+1
[9]    STATETM← 2 2 ⍴GSTM[1;C],GSTM[1;D],GSTM[2;C],GSTM[2;D]
[10]   GAMMA STATETM
[11]   IQ←STEP×(⍉STATETM)+.×Q+.×STATETM
[12]   QH←QH+IQ
[13]   IM←STEP×(⍉STATETM)+.×Q+.×GAM
[14]   MH←MH+IM
[15]   IR←STEP×R+(⍉GAM)+.×Q+.×GAM
[16]   RH←RH+IR
[17]   →(T=DT)/0
[18]   T←T+STEP
[19]   →LOOP
      ∇
      ⍎

      ∇QMRF[⎕]∇
      ∇ QMRF;STEP
[1]   ⍝  CALCULATES Q HAT, M HAT , R HAT
[2]   ⍝ FROM CONTINUOUS Q, M, R
[3]    MH←⍉GAM-GAM
[4]    QH←I-I
[5]    RH←0
[6]    T←STEP←DT÷100
[7]    C←1
[8]   LOOP:C←C+2
[9]    D←C+1
[10]   STATETM← 2 2 ⍴GSTM[1;C],GSTM[1;D],GSTM[2;C],GSTM[2;D]
[11]   GAMMA STATETM
[12]   IQ←STEP×(⍉STATETM)+.×Q+.×STATETM
[13]   QH←QH+IQ
[14]   IM←STEP×((⍉GAM)+.×Q+.×STATETM)+M+.×STATETM
[15]   MH←MH+IM
[16]   IR←STEP×R+((⍉GAM)+.×Q+.×GAM)+2×M+.×GAM
[17]   RH←RH+IR
[18]   →(T=DT)/STOP
[19]   T←T+STEP
[20]   →LOOP
[21]  STOP:MH←⍉MH
      ∇
```

Table B-1. continued

```
      ∇RICCATI[⎕]∇
      ∇ RICCATI
[1]   ⍝ CALCULATES SS P FROM RICCATI EQUATION
[2]    P←QH
[3]    COUNT←0
[4]    ERROR←0.001
[5]   ⍝
[6]    GAMMA STM
[7]    GAMT←⍉GAM
[8]    MT←⍉MH
[9]   LOOP:GPS←MT+GAMT+.×P+.×STM
[10]   NP←QH+((⍉STM)+.×P+.×STM)-(⍉GPS)+.×(⍉RH+GAMT+.×P+.×GAM)+.×GPS
[11]   COUNT←COUNT+1
[12]   DIFF←NP-P
[13]   P←NP
[14]   A←(|DIFF)>ERROR
[15]   B←+/A
[16]   C←+/B
[17]   →(COUNT=100)/STOPS
[18]   →(C≠0)/LOOP
[19]   →0
[20]  STOPS:'DID NOT CONVERGE ON RICCATI SOLUTION IN 100 ITERATIONS.'
[21]   →0
      ∇
      ⋄

      ∇SONETWO[⎕]∇
      ∇ SONETWO
[1]    S12←-(⍉STM-I)+.×GAM+.×S22
      ∇
      ⋄


      ∇STMDTN[⎕]∇
      ∇ PHI←DT STMDTN A;R;N;FACTOR;INDEX
[1]   ⍝ CALCULATES TRANSITION MATRIX
[2]    R←(⍴A)×0.5
[3]    I←(↑R)∘.=↑R
[4]    N←0
[5]    PHI←I
[6]    FACTOR←I
[7]   L0:N←N+1
[8]    FACTOR←FACTOR+.×A×DT÷N
[9]    PHI←PHI+FACTOR
[10]   INDEX←(+/|,FACTOR)÷R×2
[11]   →(INDEX>EPS)/L0
      ∇
```

Table B-1. continued

```
      ∇STWOTWO[⎕]∇
      ∇ STWOTWO
[1]   S22←⌹((-HX+.x(⌹(STM-I))+.xGAM)+HU)
      ∇
      ∇SYSMODEL[⎕]∇
      ∇ SYSMODEL YD
[1]   ⍝  GIVES RESPONSE OF 2ND ORDER SYSTEM TO INPUT YD
[2]   ⍝  AND STORES TIME HISTORY FOR GRAPHING
[3]   ⍝  NOTE: ANSWER WITH 'NO' IF TABLE IS NOT DESIRED.
[4]   T←ΔQ←TIME←DELU←ΔALPHA←0
[5]   ΔX← 2 1 ⍴ 0 0
[6]   'IS A PRINTED TABLE DESIRED?'
[7]   →('N'=1↑ANS←⎕)/LOOP
[8]   'TIME                    ΔQ                    ΔALPHA          ΔU'
[9]   LOOP:ΔU←(-(K+.x(ΔX-S12xYD)))+S22+.xYD
[10]  →('N'=1↑ANS)/SKIP
[11]  T,ΔX[1;],ΔX[2;],ΔU
[12]  SKIP:ΔX←(STM+.xΔX)+GAMxΔU
[13]  →(T=5)/STOP
[14]  T←T+DT
[15]  ΔQ←ΔQ,ΔX[1;]
[16]  ΔALPHA←ΔALPHA,ΔX[2;]
[17]  TIME←TIME,T
[18]  DELU←DELU,ΔU
[19]  →LOOP
[20]  STOP:DELU←1↓,DELU
      ∇
      ∇SYSMOD4[⎕]∇
      ∇ SYSMOD4 YD
[1]   ⍝ GIVES RESPONSE OF 4TH ORDER SYSTEM TO INPUT YD
[2]   ⍝  AND STORES TIME HISTORY FOR GRAPHING
[3]   ⍝  NOTE: ANSWER WITH 'NO' IF TABLE NOT DESIRED.
[4]   T←ΔQ←TIME←DELU←ΔALPHA←ΔGAM←ΔV←0
[5]   ΔX← 4 1 ⍴ 0 0 0 0
[6]   'IS A PRINTED TABLE DESIRED?'
[7]   →('N'=1↑ANS←⎕)/LOOP
[8]   'TIME        ΔQ            ΔALPHA          ΔU                    ΔV
[9]   LOOP:ΔQALF← 2 1 ⍴ΔX[3;],ΔX[4;]
[10]  ΔU←(-(K+.x(ΔQALF-S12xYD)))+S22+.xYD                    ΔGAM'
[11]  →('N'=1↑ANS)/SKIP
[12]  T,ΔX[3;],ΔX[4;],ΔU[1;],ΔX[1;],ΔX[2;]
[13]  SKIP:ΔX←(STM4+.xΔX)+GAM4xΔU
[14]  →(T=5)/STOP
[15]  T←T+DT
[16]  ΔQ←ΔQ,ΔX[3;]
[17]  ΔALPHA←ΔALPHA,ΔX[4;]
[18]  TIME←TIME,T
[19]  DELU←DELU,ΔU
[20]  ΔV←ΔV,ΔX[1;]
[21]  ΔGAM←ΔGAM,ΔX[2;]
[22]  →LOOP
[23]  STOP:DELU←1↓,DELU
      ∇
      ∇
```

Table B-1. concluded

There are two separate methods for finding the optimal gains using these functions. The first method involves changing the weighting matrices in the cost functional to obtain the desired response. The sequence for using the APL functions in this manner is given in Fig. B-1. For example, say the gains are to be found for a pitch rate controller using the second-order model given in Eq. 39. It can be specified as a pitch rate controller by letting

$$H_x = [1\ 0] \quad \text{and} \quad H_u = 0 \tag{71}$$

The weightings for this example will be

$$Q = \begin{bmatrix} 25 & 0 \\ 0 & 25 \end{bmatrix}, \quad R = 33 \tag{72}$$

and a sampling interval of 0.1 sec is used.

The public workspace 3 EIGENVAL is copied for use in calculating eigenvalues from F_{CL}. Following the sequence of Fig. B-1:

```
ar]

      V S   A F L

CLEAR WS
      )LOAD OPTIMAL
SAVED 12:21:33 08/03/78
      )COPY 3 EIGENVAL
SAVED 23:49:25 08/18/[illegible]
      .

      F←2 2⍴¯2.08 ¯8.35 1 ¯2
      .

      G←2 1⍴ 12.5 0
      .

      HV←1 2⍴1 0
      UU←0
      .

      I ←IDENT 2
      .

      DT←.1
      .

      STM←.1 STMUTH F
      .



      STM
 0.7784429646   ¯0.6[illegible]
 0.08041631265   0.7648[illegible]
      .

      GAMMA STM
      .

      GAM
¯1.113699322
¯0.05424770696
      .
```

```
      STWOTWO
      •

      S22
¯0.5004
      •

      SONETWO
      •

      S12
1
0.5
      •


      GENSTM
      •

      R←35
      •

      R←2 2⍴25 0 0 25
      •

      QSO
      •

      FICCATI
      •

      GAIN
      •

      K
¯0.4264245713  0.3235125049
```

```
      SYSMODEL .1
IS A PRINTED TABLE DESIRED?
YES
TIME                    ΔQ                    ΔALPHA          ΔU
  0                 0                 0                ¯0.07650683188
  0.1                0.0852056068      0.004150320196 ¯0.04151574802
  0.2               0.1097769243      0.01236154268 ¯0.03369436764
  0.3               0.114679987       0.02035797915 ¯0.03419052844
  0.4               0.1136798987      0.02705539419 ¯0.03678368817
  0.5               0.1112922323      0.03237228587 ¯0.03952192871
  0.6               0.1089129806      0.03650192393 ¯0.04187248965
  0.7               0.1069057333      0.03967936074 ¯0.04375636378
  0.8               0.1053077085      0.04211403623 ¯0.04522545177
  0.9               0.1040650297      0.04397614249 ¯0.04635777873
  1                 0.1031083829      0.0453991598  ¯0.04722607982


      FCLOOP
      .

      FCL
¯11.45688255    ¯5.92595 372
  1.096801468   ¯1.958250392
      .

      .001 EIGVAL FCL
 10.72116992    0
¯2.69596312     0
      .



      F4+4 4F¯.073 ¯32.2 0 0 .002 0 0 2 .002 0 ¯2.08 ¯8.35
      .
                                                  ¯.002 0 1 ¯2


      F4
¯0.073 ¯32.2      0        0
 0.002   0        0        2
 0.002   0       ¯2.08    ¯8.35
¯0.002   0        1       ¯2
      .
```

```
      G4←4 1↑0 0 ¯12.5 0
      •

      G4
   0
   0
¯12.5
   0
      •

      STM4←.1 STMDYN F4
      •

      GAMMA4 STM4
      •

      FCL4
      [illegible]

      .001 EIGVAL FCL
¯1[illegible]  0
¯2.680229258  [illegible]
¯0.0444667[illegible]  0.1[illegible]
¯0.0444667675  ¯0.13[illegible]
```

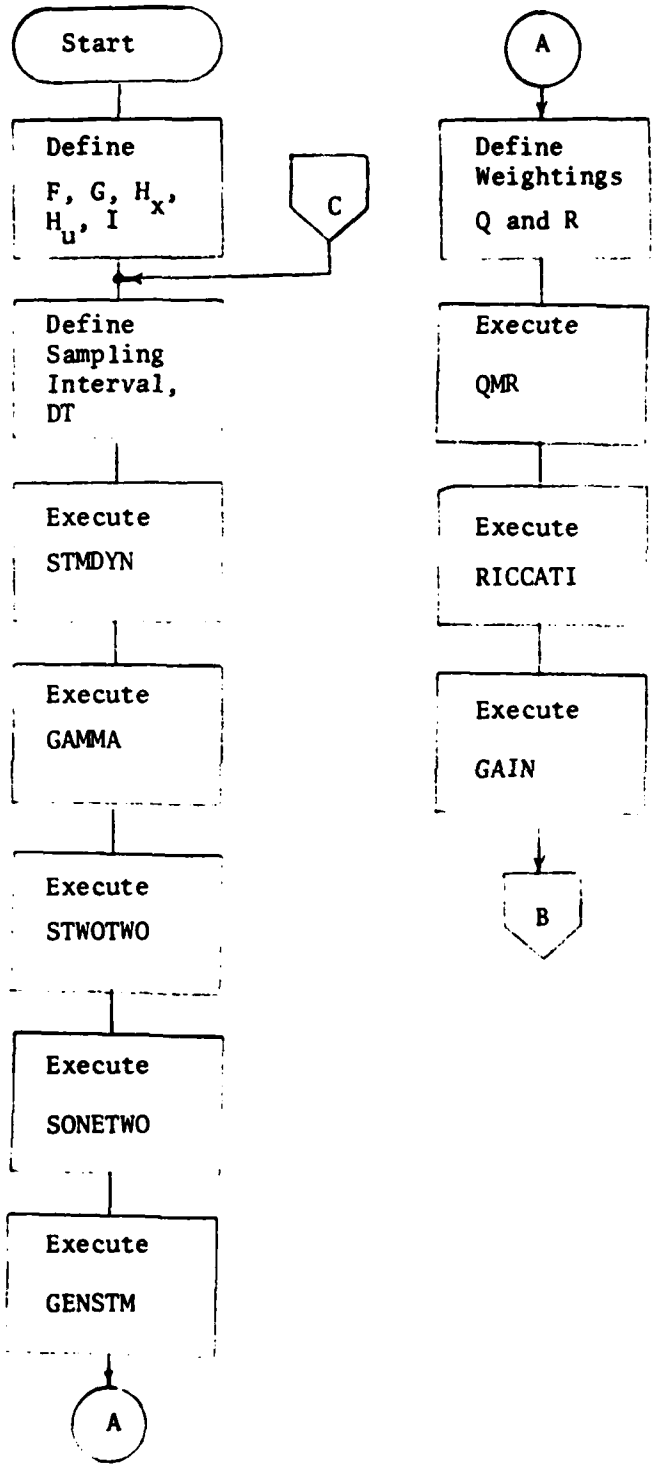

Figure B-1. Sequence for Calculating Gains by Changing Weighting Matrices.

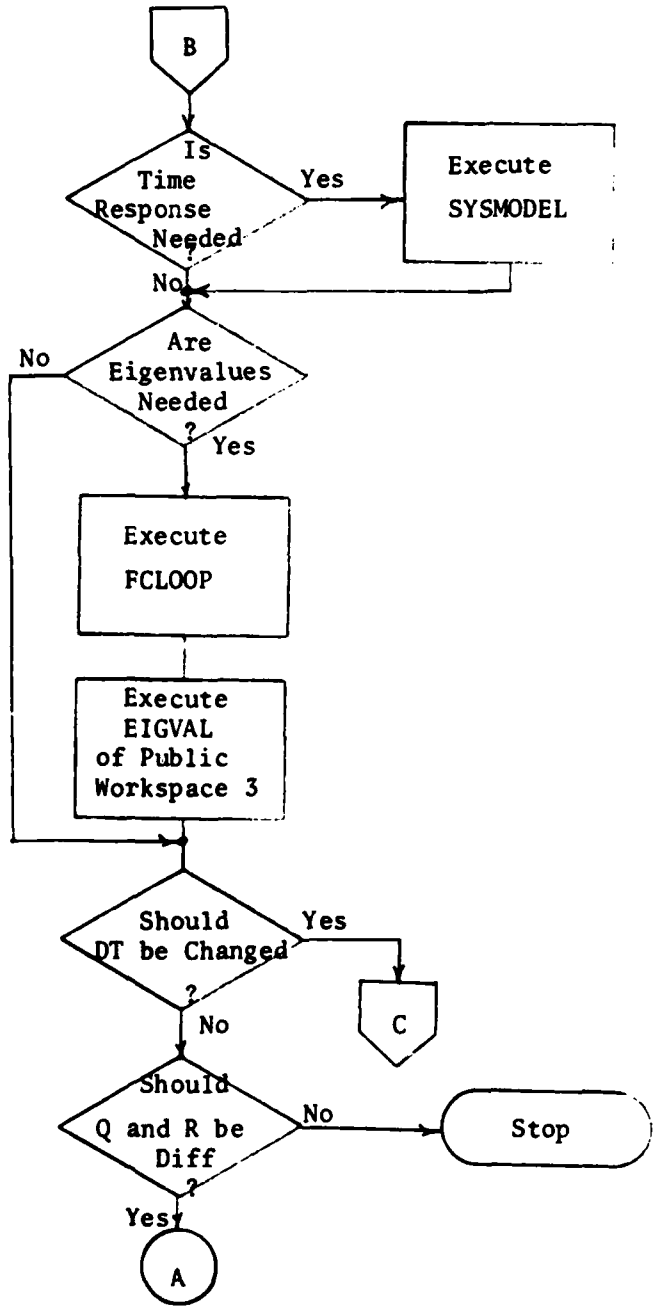

Figure B-1. continued

The second method for calculating gains uses implicit model-following. For instance, say the VRA is to match the short-period modal characteristics of an aircraft with the reduced second-order model

$$\Delta\dot{\underline{x}} = \begin{bmatrix} -.5 & -6 \\ 1 & -2 \end{bmatrix} \begin{bmatrix} \Delta q \\ \Delta\alpha \end{bmatrix} + \begin{bmatrix} M_{\delta_E} \\ 0 \end{bmatrix} \Delta_{\delta_E} \tag{73}$$

A weighting matrix, W, should initially be set to the identity matrix. Following the sequence given in Fig. B-2:

```
F←2 2⍴¯2.08 ¯8.35 1 ¯2
⋄

G←2 1⍴¯12.5 0
⋄

FM←2 2⍴¯.5 ¯6 1 ¯2
⋄

DT←.1
⋄

STM← .1 STMDTN F
⋄

GAMMA STM
⋄

GENSTM
⋄

W←I
⋄

FOLLOW
⋄
```

```
QMEF
.

RICCATI
.

GAIN
.

K
0.1304705484 0.1334808096

ECLOOP
ECL
¯0.5054028136 ¯5.983308109
 1.001310358   ¯2.011826687
.
```

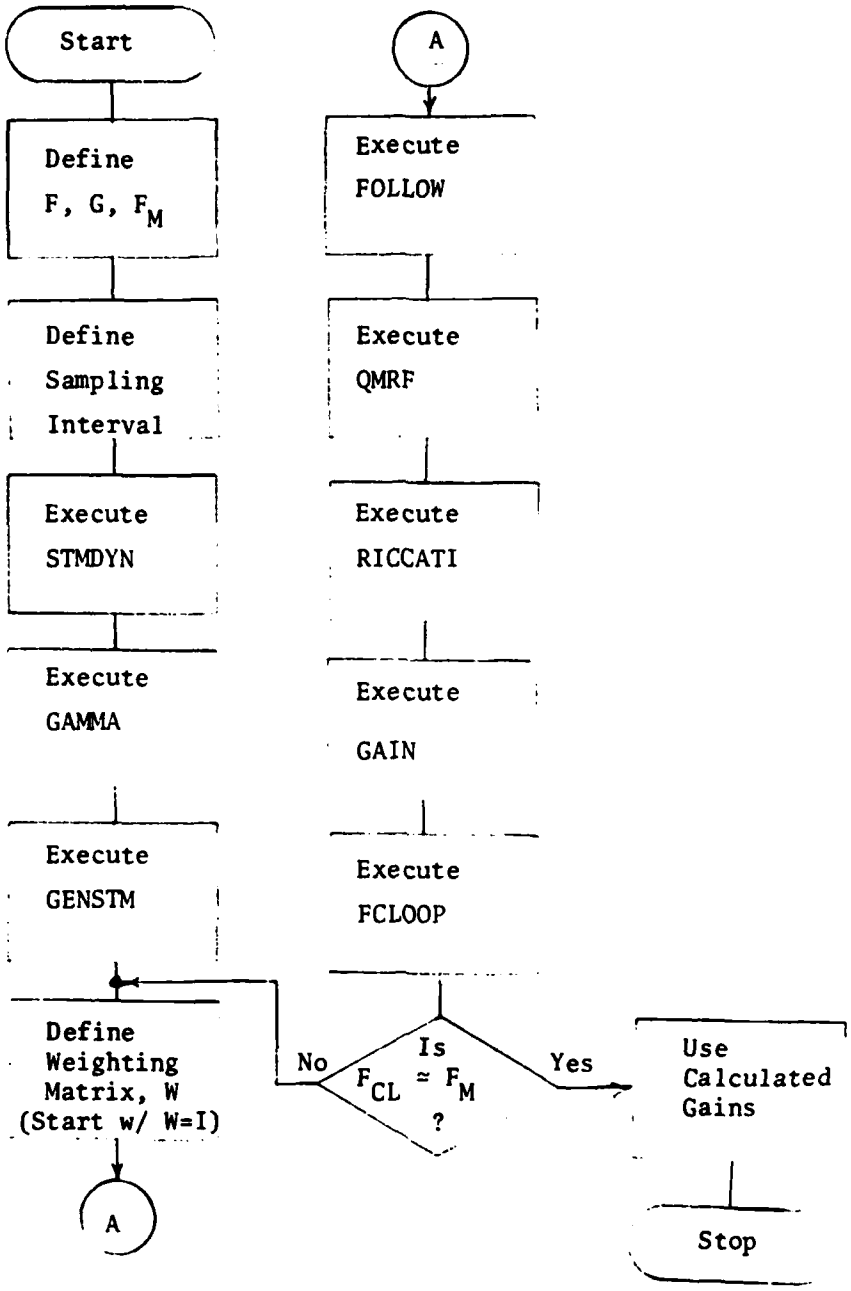

Figure B-2. Sequence for Calculating Gains Using Implicit Model-Following.

APPENDIX C

RESEARCH SYSTEMS

C.1 VARIABLE-RESPONSE RESEARCH AIRCRAFT (VRA)

The VRA is a highly modified Navion equipped with inertial, air data, and navigation sensors, as well as six independent force and moment controls. The VRA, shown in Fig. C-1, has been used to conduct a broad range of experiments in aircraft flying qualities, human factors and control in the past. The aircraft has played a major role in establishing current military and civil flying qualities criteria, and with the addition of the Micro-DFCS, the VRA is equipped to expand this type of research, as well as to investigate advanced digital control concepts (Ref. 23).

Independent control of three forces and three moments is provided by commands to the elevator, ailerons, rudder, throttle, direct-lift flaps, and side-force panels (Fig. C-2). The control surfaces are driven by hydraulic servos originally fitted to the B-58 aircraft. The modified VRA units incorporate solenoid-actuated valves with force-override features for quick disengagement. Characteristics of the control effectors are summarized in Table C-1. Surface rate limits are seen to range from 60 to 110 deg/sec. Bandwidths are given for flat response and 6 db attenuation (in

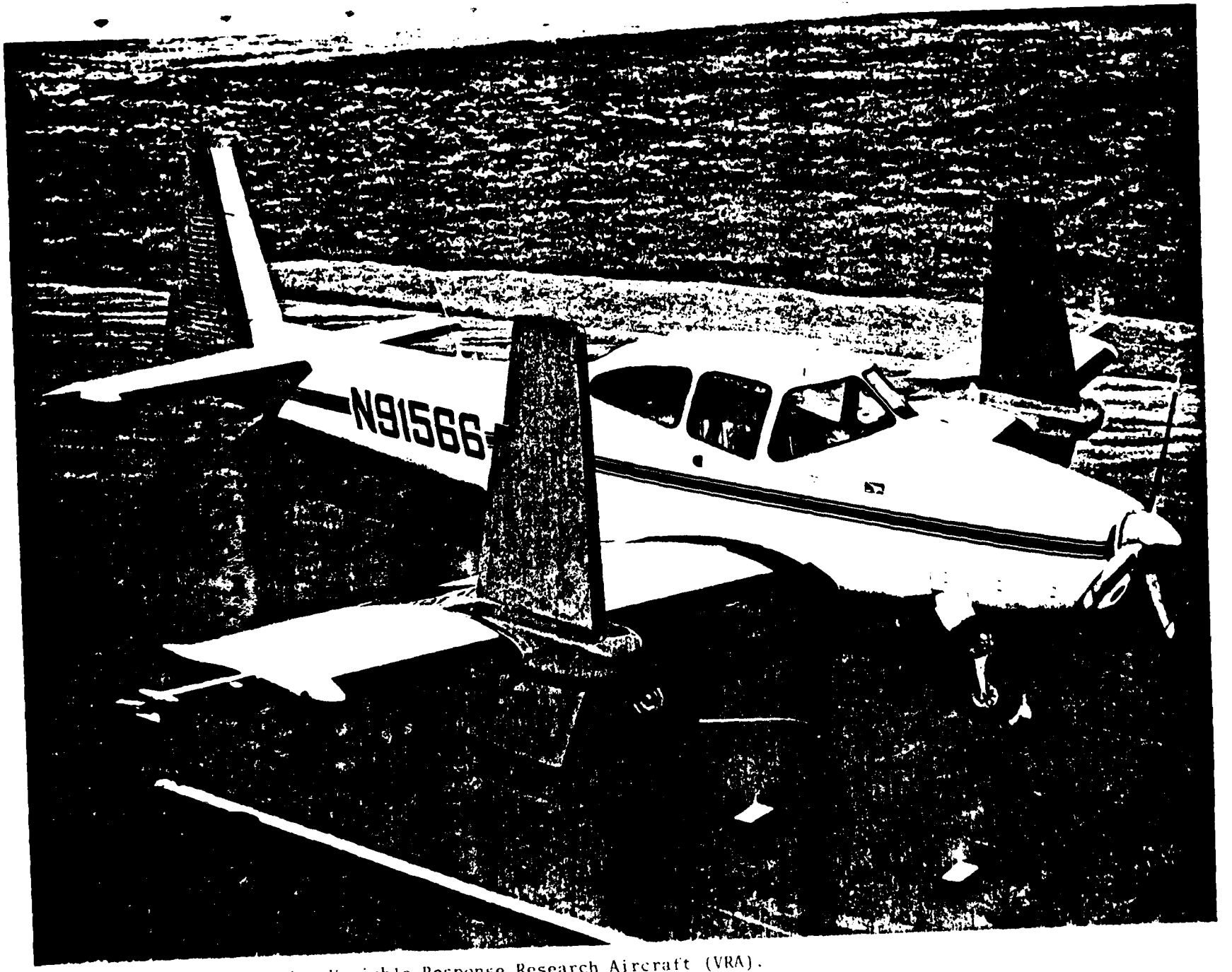

Figure C-1. Variable-Response Research Aircraft (VRA).

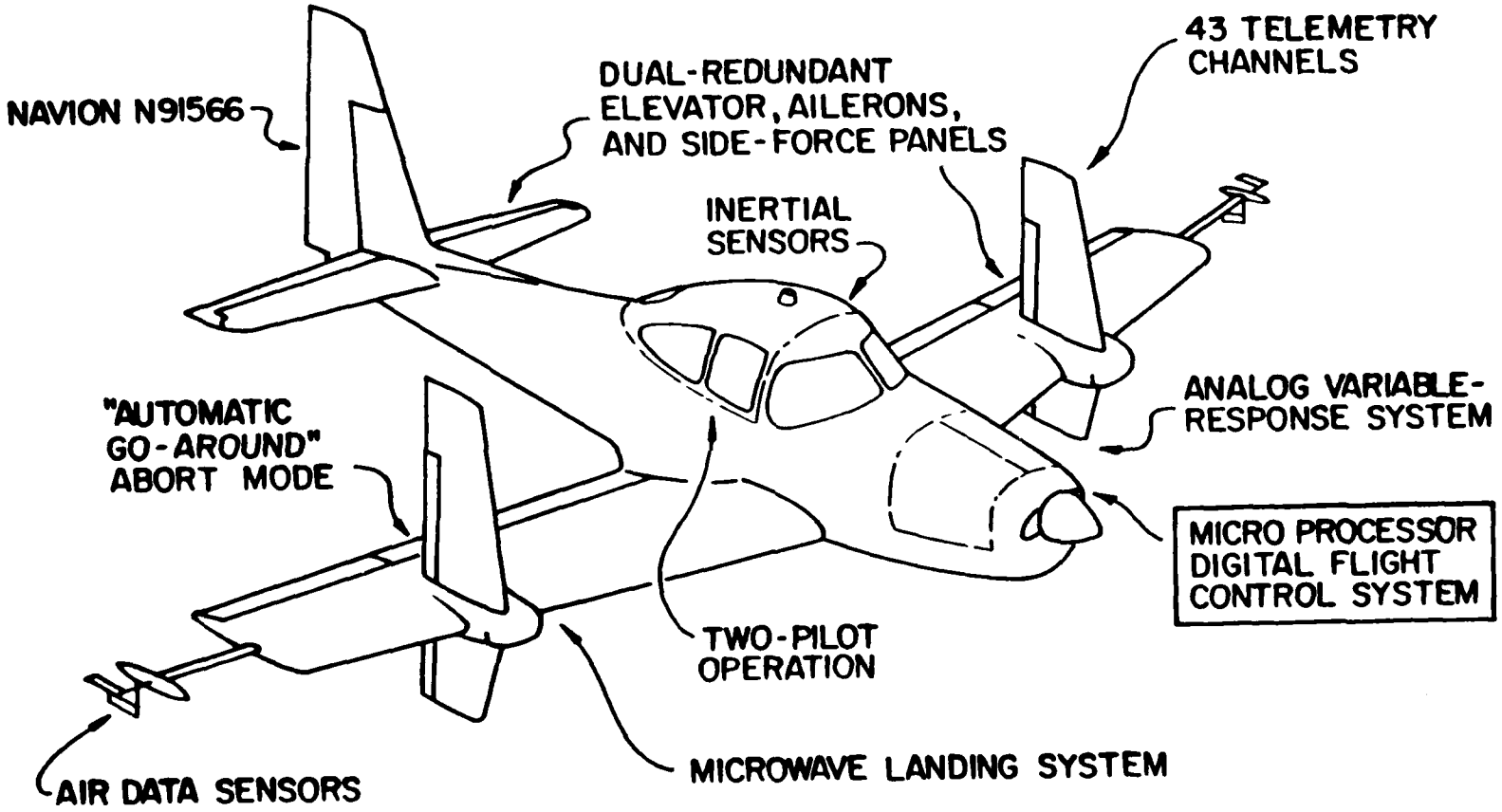

Figure C-2. Major Components of VRA.

parentheses), except that thrust bandwidth is specified by the frequency for 3 db attenuation. The aircraft's normal operating speed range is 65 to 120 kt; maximum specific forces and moments ("control power") are given for 70 kt airspeed. At IAS = 105 kt, maximum direct lift and side-force accelerations are 1g and 0.5g, respectively.

The sensors used for most flight testing include angular rate gyros and linear accelerometers for all three axes, vertical and heading gyros, dual angle-of-attack and sideslip-angle vanes, radar altimeter, indicated airspeed, control surface positions, and cockpit control positions. Several other signals (e.g., air temperature, barometric altimeter, altitude rate, and TALAR microwave landing system signals) are available for system feedback or telemetry recording. The present telemetry system allows 42 data channels to be multiplexed and transmitted to the FRL ground station described below.

TABLE C-1

VRA Control Characteristics

Control	Displacement Limit, deg	Rate Limit, deg/sec	Bandwidth, H_z	Maximum Specific Force or Moment (IAS = 70kt)
Roll	30.	70.	5 (10)	4.1 rad/sec^2
Pitch	-30. +15	70.	5 (10)	4.4 rad/sec^2
Yaw	15.	70.	5 (10)	1.9 rad/sec^2
Thrust	-	-	0.6	0.1 g
Side Force	35.	60.	2 (3)	0.25 g
Normal Force	30.	110.	2 (3)	0.5 g

The aircraft is flown by a two-man crew during all research. This provides a number of advantages in comparison to single-pilot operation from the standpoint of flight safety and experimental efficiency. The instrument panel and controls are shown in Fig. C-3. The conventional mechanical aircraft system is flown by the safety pilot in the left seat, while the fly-by-wire aircraft system used for research is flown by the evaluation pilot seated at the right. This system includes the Micro-DFCS and redundant aileron, elevator, and side-force actuators for protection against system failures. The evaluation pilot's station is tailored to the experiment; for the Micro-DFCS program, this station includes a center control stick, thumb switches for trim and direct force modes, rudder pedals,

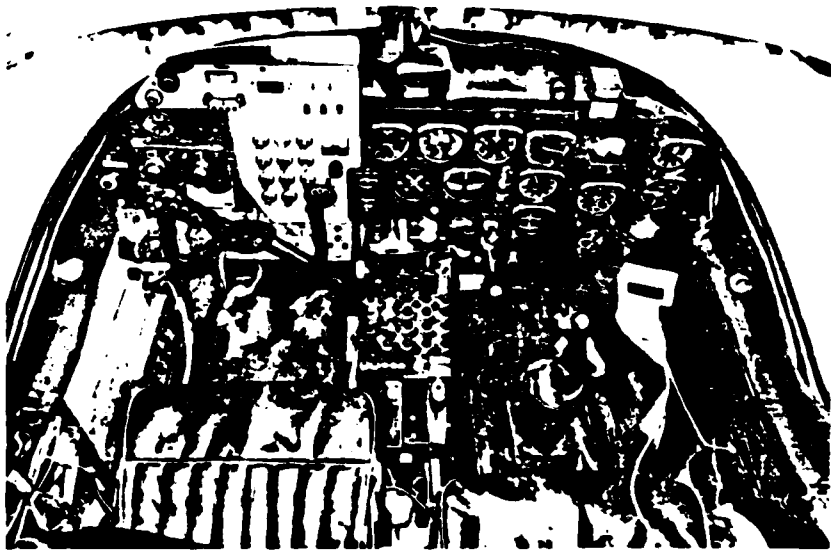

Figure C-3. Instrument Panel and Controls of VRA.

sideslip and side-force-panel meters, and conventional instruments.

The safety pilot is the in-flight test conductor, monitoring systems and adjusting all experimental parameters. He has several electrical and hydraulic mechanisms for disengaging the Micro-DFCS and the variable-response system in the event of a malfunction, as well as an "automatic go-around" abort mode which makes safe experimentation through touchdown possible. The abort mode commands a 20-deg flap setting and climb power when activated; at 70-kt (36 m/s) airspeed on a 6-deg glideslope, an up-flap "hardover" failure can be corrected and climbout can be initiated with a maximum altitude loss of 10 ft (3 m).

C.2 EXPERIMENTAL FACILITIES

The VRA is operated from the flight test facility at Princeton University's James Forrestal Campus. The facility includes the FRL hangar, laboratories, and shops, plus a 3000-ft Basic Utility II runway. TALAR 3 and 4 fixed-beam microwave landing systems (MLS) furnish precision approach-path guidance.

The ground station (Fig. C-4) at the FRL is used to receive, record, and analyze the telemetered data from the VRA. It includes a Honeywell seven channel tape recorder, an FM or AM receiver presently operating at 1458 MHz in the FM mode, a telemetry demultiplexer with five translators, an EAI TR-48 analog computer, a radio telephone, and a six channel paper strip chart recorder. The PDM

telemetry system provides 42 data channels, each sampled at a rate of 20 sps. The telemetry data from the receiver can be recorded on tape and demultiplexed five channels at a time for plotting on the strip chart recorder. The analog computer scales and buffers all input channels from the translators to the strip chart recorder.

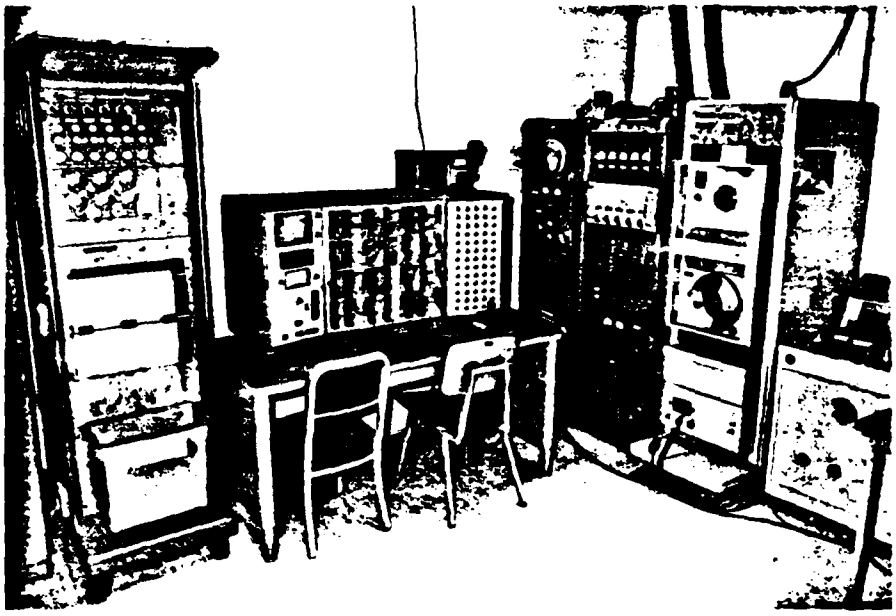

Figure C-4. FRL Ground Station.

In addition to the analog computer's function in analyzing telemetered data, it is also used for ground-based simulations of the VRA and other dynamic systems. In the Micro-DFCS study, it is used to model the VRA for ground testing the microcomputer software. The schematic and corresponding potentiometer settings are presented in Fig. C-5 and Table C-2, respectively.

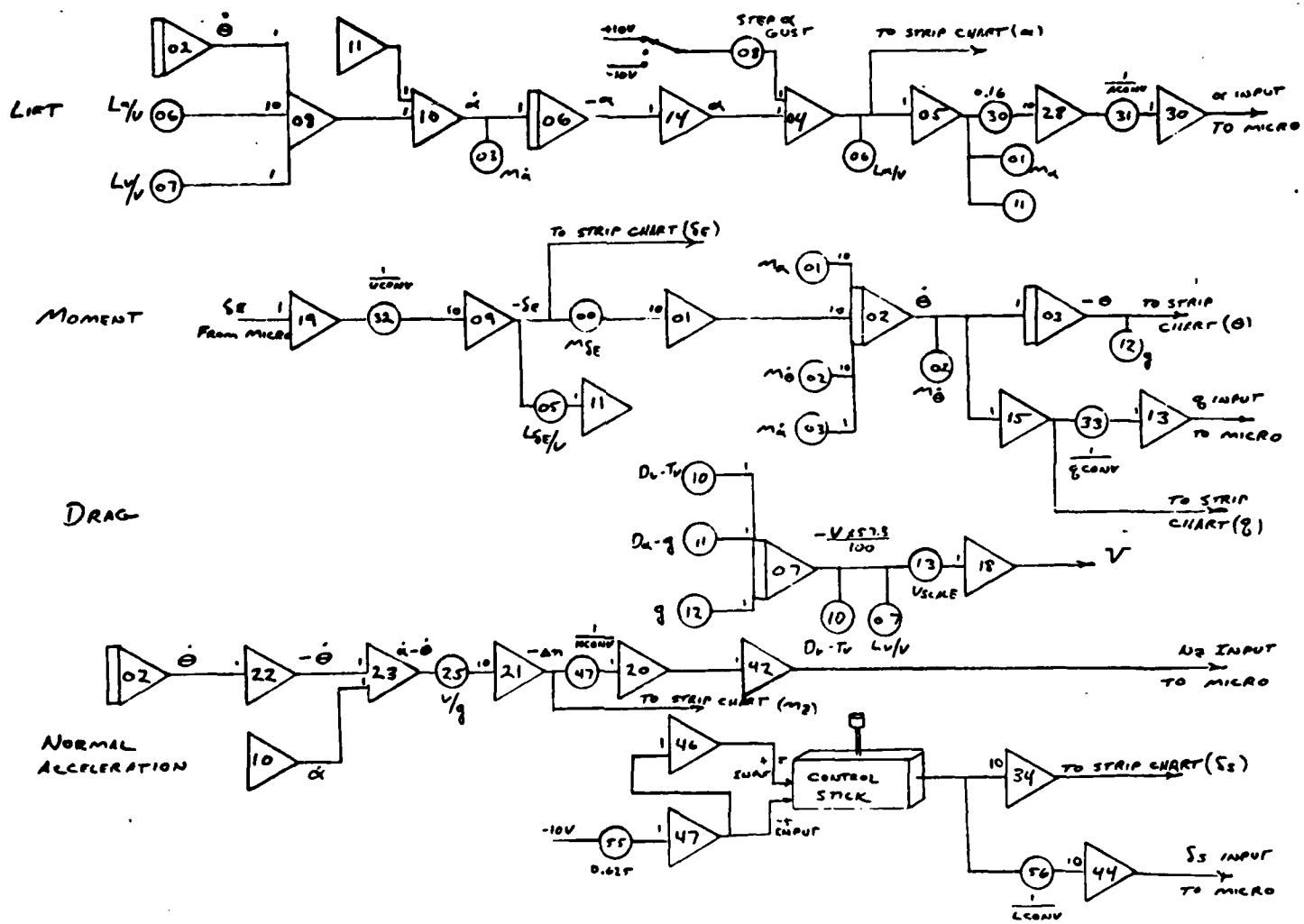

Figure C-5. Schematic of Simulated VRA at 105 Kts
With Scaling for Microcomputer Interface.

TABLE C-2

COMPUTER POTENTIOMETER SETTINGS
FOR VRA LONGITUDINAL MODEL (105 KIAS)

Pot	Parameter	Scaling	Setting
00	M_{δ_E}	$M_{\delta_E}/100$	.125
01	M_α	$M_\alpha/10$	.835
02	$M_{\dot\theta}$	$M_{\dot\theta}/10$	.208
03	$M_{\dot\alpha}$		.910
05	L_{δ_E}/V		.125
06	L_α/V	$L_{\alpha/V}/10$	.200
07	L_V/V	$100\ L_V/_V$	.200
08	Step Gust Scaling		.100
10	D_V-T_V		.073
11	D_α-g	D_{α}-g/100	.060
12	g	g/100	.322
13	V_{scale}	$\frac{100}{57.3x5}$	.349
25	V/g	$V/g \times \frac{2x10}{57.3}$	.190
30	α_M scaling error	$\alpha_{MSE}/10$	.160
31	$\frac{1}{ACONV}$		.345
32	$\frac{1}{UCONV}$	$\frac{1}{UCONVx10}$	.144
33	$\frac{1}{QCONV}$		.225
47	$\frac{1}{NCONV}$		.188
55	Stick Range		.625
56	Stick Scaling		.592

Nominal Scaling: 1 volt = 1°, 1°/sec, 5 ft/sec, .05 G's

APPENDIX D

THE MICRO-DFCS HARDWARE

D.1 DESCRIPTION OF MICROCOMPUTER COMPONENTS

In addition to the brief description of the microcomputer equipment given in Chapter 3, the following information is provided. The CPU board has 22 parallel lines of input and output (I/O), 4.5 K of memory and one hardware interval timer which may be wired to an interrupt line of the 8085. The timer's time interval may be changed under software control. The mathematics unit does 16- and 32-bit fixed-point and 32-bit floating-point operations, where the typical time needed to do one floating-point operation (including the time to pass arguments to the mathematics unit) is 137 μsec. The mathematics unit provides the computational speed necessary to calculate the control law within the sampling interval. The main memory contains 16K words of RAM and also provides an interface for the CDU. The battery back-up memory allows programs and data to be stored with the power off for up to 96 hours. This board is used to transfer the microcomputer programs from the software development system to the FCCU mounted in the VRA. The analog I/O boards provide 16 (expandable to 32) input channels and 6 output channels each with 12-bits of resolution. The A/D has a conversion rate of 28KHz and can be interrupt- or software-driven. The CDU provides input for all ASCII characters and can display two lines of 12 characters each.

It is functionally equivalent to a conventional 1200-baud keyboard/ display terminal, although its display is limited, and multiple key strokes are required to enter most characters.

The FCCU consists of the six computer circuit boards and two 4-board cardcages into which the boards plug. It is housed in an RF-shielded, shock-mounted aluminum box. The mount is located in the cockpit behind the two pilots. The FCCU therefore experiences the same environment the pilots do, and no special provisions are made in using these commercially available microcomputer components. The Micro-DFCS components installed in the VRA, including the power supplies, cost approximately $6900 when purchased in February, 1978. There are four cables that interface the FCCU with the rest of the VRA's FBW system. One cable supplies the ± 5 and ± 12 volts necessary to operate the Intel SBC boards. These voltages are obtained by regulating the VRA's primary 28vdc. A second connector links the CDU to the FCCU. A two-position switch and program monitor light mounted on the pilot's instrument panel each have connections made through a third cable. One position of the switch resets the computer's program counter, and the other position gives the CPU program control. The light is part of an error detection system. When the light flashes at a steady rate, it indicates that the control law is being calculated every sampling interval. The fourth cable supplies the inputs from the motion sensors and pilot controls, and the outputs to the control surface actuators. The voltage range of these signals (± 10v) is compatible with that used by the A/D and D/A converters of the microcomputer.

The status of the Micro-DFCS is output on one of the D/A channels and this information is sent on a telemetry channel. This status channel indicates what control mode is running (if any) and also flags any errors found by the two software error detection methods described in Section 3.2. The telemetered data can be recorded and plotted on a strip chart recorder.

The components of the Micro-DFCS and development system are pictured in Fig. D-1. The FCCU and CDU are at the upper left, resting on the ground chassis and power supply. The keyboard-CRT terminal, acoustic coupler, and telephone extension are to the right of the chassis. A keyboard-printer unit (not shown in Fig. D-1) is used to obtain copies of program listings and other computer output.

Figure D-1. Components of the Micro-DFCS and Software Development System.

D.2 DIRECTIONS FOR USING CONTROL DISPLAY UNIT

The Control Display Unit (CDU), shown in Fig. D-2, allows the pilot to monitor the Micro-DFCS and input commands. The display is two lines of 12 characters each. The keyboard allows all 128 ASCII characters to be entered; most by multiple key strokes.

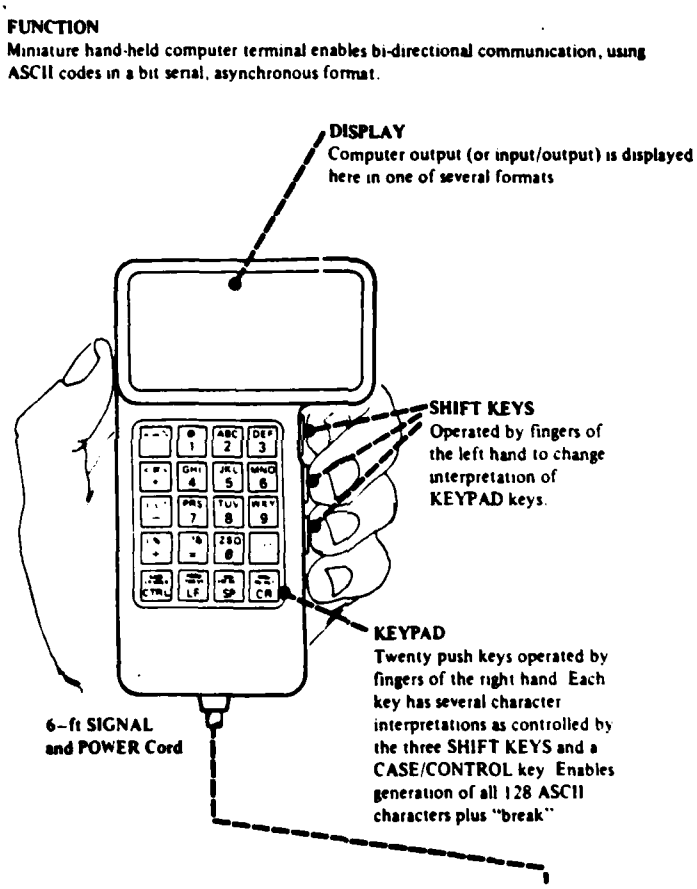

Figure D-2. Control Display Unit (CDU).

There are three levels of entry on the CDU (Fig. D-3). The System Monitor level is entered by flipping the two-position switch on the instrument panel (marked RESET/RUN) to the RUN position. The

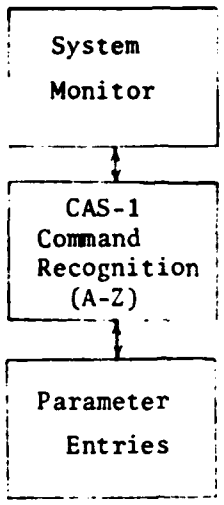

Figure D-3. Levels of Entry on CDU.

CDU display will show "80/05 MON" indicating the first entry level. Any of the normal 80/05 System Monitor commands outlined in the Intel SBC 80P05 User's Guide can be used at this level.

The second level of entry may be entered by jumping to location 8000H. This is accomplished by pressing the keys:

G, 8, 0, 0, 0, CR

where CR is the CDU's "carriage return". This starts execution of CAS-1 and enters the CAS-1 Command Recognition level. Twenty-six different commands may be entered at this level, each selected by pressing a key with a letter of the alphabet. Only four commands are presently defined in CAS-1: HALT, INITIALIZE, MODE CHANGE, and STEP INPUT.

The third level sets parameters necessary to complete the command entered at the second level. For example, if MODE CHANGE was entered by pressing "M", then the third entry level is automatically set and the next two key strokes will specify which mode is selected (a number 00-19). Once the mode number is entered, then the CDU again operates at the second entry level waiting for another command. STEP INPUT also requires the third entry level after the "S" is pressed. The analog channel to be stepped (00-15) is entered followed by the voltage this channel is to be stepped (in the format ±DD.DD, where D represents some base ten number).

The upper line of the display shows the mode CAS-1 is operating in at all times. In the case where CAS-1 is first entered, the mode is Initialization and the top display line reads "8085 READY". If the mode is changed by using the MODE CHANGE command, the new mode is displayed on the upper line (e.g. "OPEN LOOP", PITCH RATE", or "NORMAL ACC"). The entries made at the second level are displayed on the bottom line. If an entry error is made at any time while using the CDU, "ENTRY ERROR" will be displayed on the bottom line for ten sampling intervals.

To reenter the System Monitor level, the switch on the instrument panel is placed in the RESET position and then back to RUN.

APPENDIX E

THE MICRO-DFCS SOFTWARE

E.1 DESCRIPTION OF CAS-1 ROUTINES

The routines of CAS-1 are divided into three categories, depending on their function: Executive, Utility and Flight Control. Each of these routines has detailed documentation included in the source listing consisting of line comments and a header. The header explains the purpose of the routine, how variables should be passed to it, and what parameters of the microcomputer are effected by the routine's execution.

A brief explanation of the major elements of CAS-1 is given below.

EXECUTIVE ROUTINES - Initialization, CDU interface, and one of the three error detection methods are contained in this section (Fig. E-1). INITIALIZATION involves setting up the mathematics unit, the analog board, the parallel I/O ports, the serial port, the hardware interrupt timer, the registers to be used as counters and flags, and clearing storage area in RAM. CDU INTERFACE routine allows the user to set the operation of CAS-1 by inputs from the keyboard. MEMORY CHECK is one of two software error detection methods employed in the program. Every 50 samples, the entire contents of CAS-1 is summed in an 8-bit register (ignoring overflow) and compared to the known sum. If the two differ, some part of

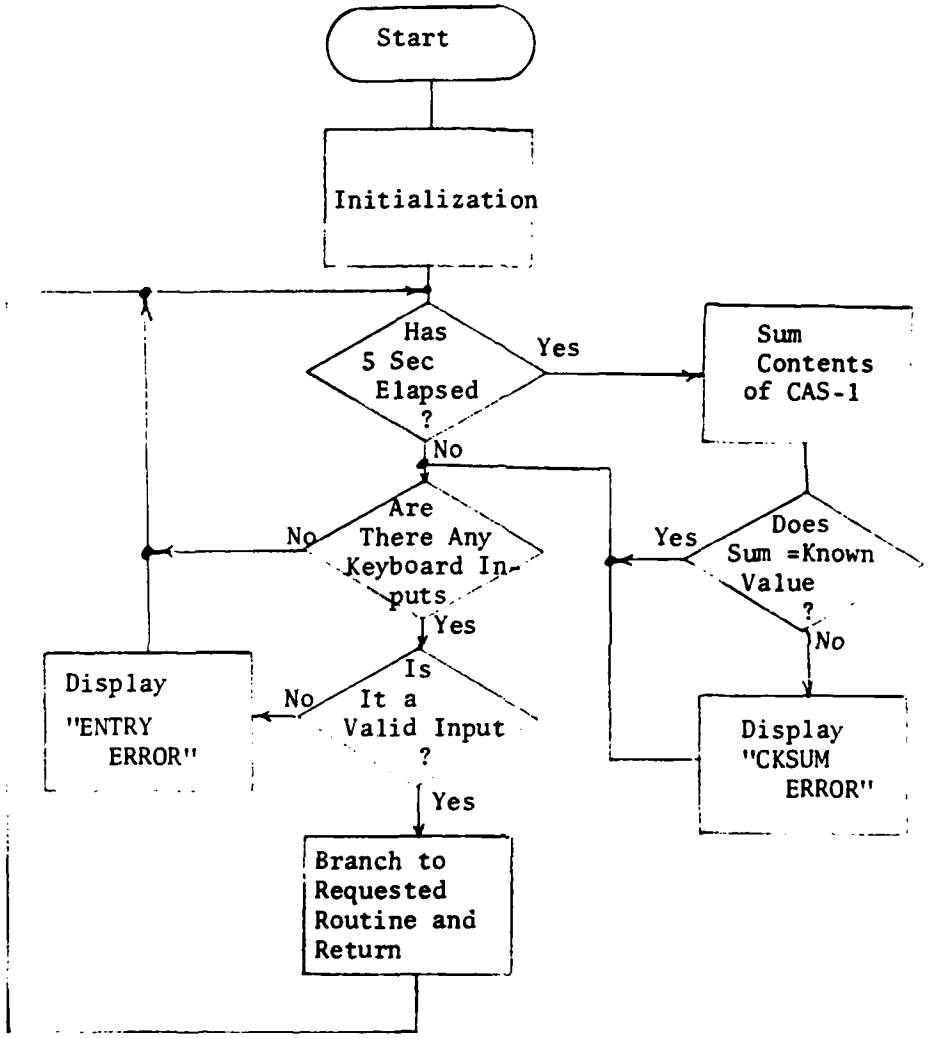

Figure E-1. Flowchart of Executive for CAS-1.

the program has changed; this condition is displayed on the CDU, and sent via telemetry to the ground station.

UTILITY ROUTINES - The routines CLEAR LINE, CONSOLE OUTPUT, NUMERIC INPUT, ENTRY ERROR, and SERIAL OUTPUT are used for displaying and entering data on the CDU. BLINK is part of the hardware error detection method that flashes a light on the safety pilot's instrument panel to indicate that the flight control function of CAS-1 is running. BLINK is called once in every flight control interrupt service routine. ANALOG TO DIGITAL CONVERSION selects the proper analog input channel, initiates the conversion, and stores the results. COUNT-UP DISPLAY generates an increasing sequence of numbers 1-9 (reset each 10 sec) on the bottom line of the CDU. This is to indicate that the hardware interrupt (used for timing purposes) is working, the program has initialized correctly, and the D/A channels are operational. An increasing sequence of voltage outputs from a D/A channel is telemetered to the ground station to indicate in what mode the Micro-DFCS is operating. INTERRUPT COUNT increments a counter every time an interrupt service routine is executed. This counter is used for timing purposes in routines such as MEMORY CHECK (which must execute every 50 samples). LIMIT ANALOG OUTPUT prevents the analog output channels from instantly switching from +10 volts to -10 (or vice versa). This condition occurs when the control law calculates a value for control surface deflection which corresponds to a voltage greater than 10 volts or less than -10 volts. It is because of the method used for converting floating point numbers to fixed point format. This routine was not added until after flight

testing had begun. MODE CHANGE allows the user to select 1 of 20 possible flight control modes. Presently only six modes are defined; four pitch rate command modes with different feedback gains, one normal acceleration command mode, and one direct mode where longitudinal stick is fed directly to the elevator through a stick gearing factor. MATH UNIT DRIVER loads the high-speed mathematics unit with the two arguments to be operated on, initiates the mathematical operation, and stores the results in RAM. It is very general and slow (normally 230 μsec). Therefore, it should not be used for time critical functions; i.e. not in flight control interrupt service routines. MATH ERROR PROCESSOR is the second software error detection method. It is used to check for errors that occur in the mathematics unit (such as divide by zero or an overflow condition). The type of error that has occurred and the number of mathematics unit uses since the last interrupt service routine began execution is displayed on the CDU. The type of error is also sent to the ground station via telemetry. This information should allow the user to find which mathematical operation is causing the problem, should one exist. CALIBRATED STEP INPUT allows the pilot to apply a step input on any one of the analog input channels. After entering the desired step value, the input is initiated by depressing the CDU's "carriage return" key. The step input is nulled by depressing any CDU key.

FLIGHT CONTROL ROUTINES - These are of two types: control set-up routines and the timed interrupt service routines. The control set-up routines are called from MODE CHANGE and set the

parameters necessary for the interrupt service routines to operate. A set-up routine will store the starting location of a service routine in the timed interrupt branch point, and it will set the optimal gains for the control law. A set-up routine will also store the nominal values of all analog inputs for use in calculating perturbation values by the service routine. The microcomputer status channel is set to indicate what flight control mode the computer is executing.

The flight control interrupt service routines are executed on every timed interrupt. They contain the control logic that calculates the control inputs, $\Delta \underline{u}$, for every sampling interval. Once a set-up routine has set the timed interrupt branch point to execute a particular service routine on every timed interrupt, then that service routine has the highest priority over all other routines and will be executed on every timed interrupt, regardless of where the program is running at the time.

The DIRECT INTERRUPT SERVICE ROUTINE takes in commands from longitudinal stick, adds the step bias, multiplies this input by a stick gearing factor, and sends this value to the elevator actuator. The stick gearing used for flight tests was three degrees elevator deflection per inch of longitudinal stick, δ_s, deflection. At 105 KIAS, this corresponds to a steady-state Δq of 5.3 deg/sec per inch or a steady-state Δn_z of 0.52g per inch of δ_s.

The PITCH RATE INTERRUPT SERVICE ROUTINE calculates an elevator command, δ_E, for measured values of δ_s, α, and q. The inputs

must be formatted and scaled before the control law can begin its calculation (Fig. E-2). First the analog voltage signal for a particular input is converted to a 12-bit fixed-point binary number, which is then converted to a 32-bit floating-point representation. The nominal value for the channel (stored by the control set-up routine) is subtracted from the current input value to form the perturbation value. At this point, if a step bias value has been specified for a particular input channel by CALIBRATED STEP INPUT, that value is added to the input. The control law must be calculated with the inputs scaled to the proper units. A scaling factor that converts units of voltage to the proper units of motion is the last step before actual calculation of $\Delta \underline{u}$. In the case of the pilot's inputs, this scaling factor can be thought of as a stick gearing. For $\Delta\alpha$, there is one more scaling to be done that takes into account the difference between the α vane deflection and the aircraft's actual α. The output from the control law is converted from units of radians to volts, converted to fixed-point notation, then converted to an analog voltage, and sent to δ_E.

The control law is calculated using Eq. 22 where the mathematical operations are performed by calling MATH UNIT DRIVER. This mathematics routine is actually too slow and general for calculating the control law. The PITCH RATE INTERRUPT SERVICE ROUTINE takes, on the average, 19 msec to execute including all formating and scaling. The normal acceleration command version of this routine is written not using MATH UNIT DRIVER in order to decrease execution time.

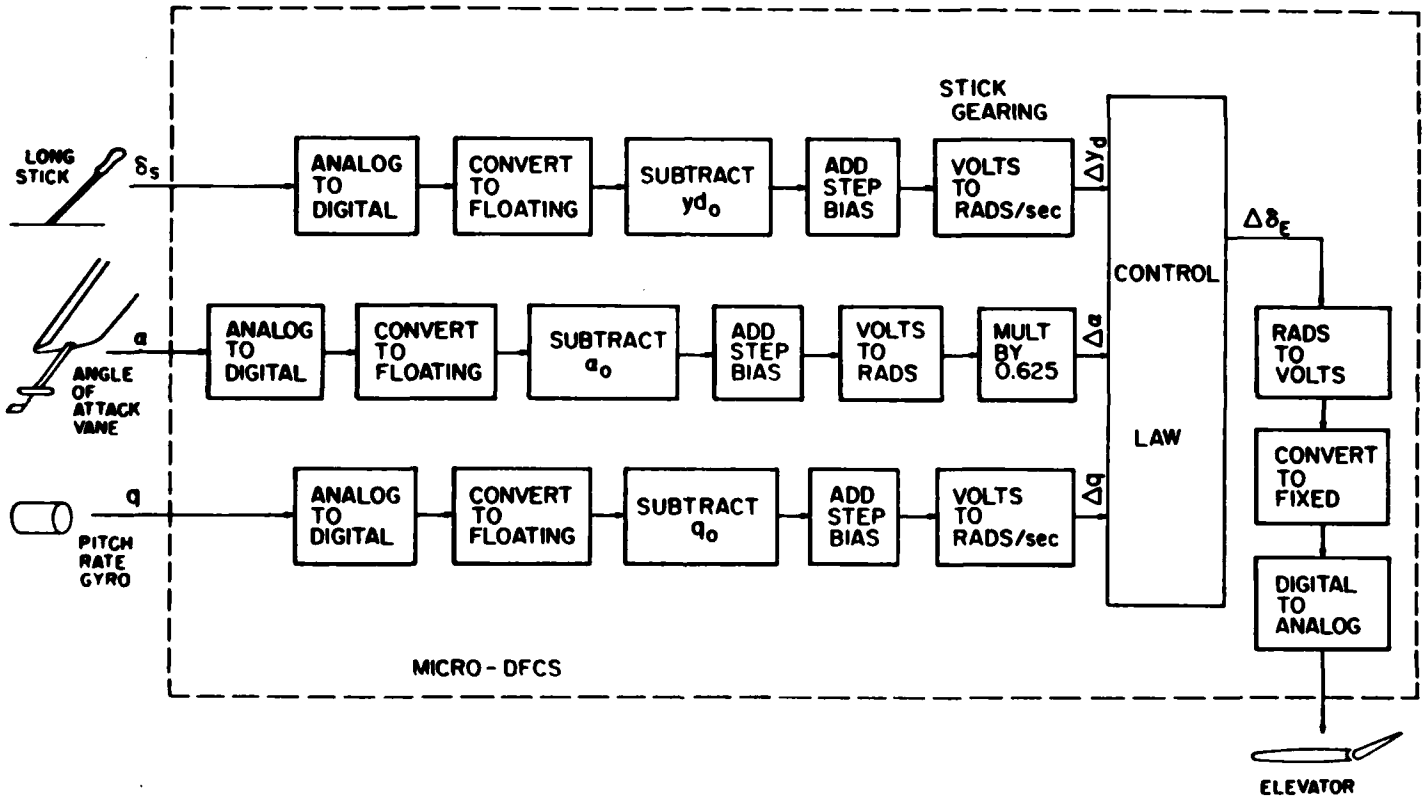

Figure E-2. Formating and Scaling of Sensor and Pilot Inputs.

The NORMAL ACCELERATION INTERRUPT SERVICE ROUTINE calculates a δ_E command for measured values of δ_S, n_z, and q. The task of this routine is similar to the pitch rate service routine, but the method of making calculations is fundamentally different in two ways. First, the MATH UNIT DRIVER is not used to perform the calculations. Instead, this service routine sets up the mathematics unit and initiates the mathematical operations itself. While the mathematics unit is doing the calculation, the service routine gets the next calculation ready. Also, only one argument is loaded to the mathematics unit per calculation because the answer from the last calculation is always used as the second argument. By comparison, MATH UNIT DRIVER always loads two arguments and stores the answer regardless of the next operation to be performed. By not using MATH UNIT DRIVER, this service routine takes more storage but each calculation is speeded up by a factor 1.7 (137 μsec per calculation). The second difference in calculations comes from using a reduced form of Eq. 22 for the control law. The equation can be rearranged to the form

$$\Delta \underline{u}_k = (S_{22} + CS_{12})\, \underline{y}_{d_k} - C\, \Delta \underline{x}_k \tag{74}$$

For the two-state feedback and single pilot input CAS studied here, Eq. 74 breaks down further to

$$\Delta \delta_{E_k} = c_1\, \Delta \delta_s - c_2\, \Delta q - c_3\, \Delta\, n_z \tag{75}$$

which only takes five mathematical operations to calculate compared to nine for Eq. 22. By not using MATH UNIT DRIVER and using Eq. 75 for the control law, execution time of the NORMAL ACCELERATION INTERRUPT SERVICE ROUTINE is reduced to 6 msec. PITCH RATE INTERRUPT SERVICE ROUTINE could also be rewritten to run at this speed because it has the same number of calculations as the normal acceleration routine. The scaling factors for the inputs and outputs can be incorporated in the gains of Eq. 75 to speed up the service routines even more. This was not done in CAS-1 to help isolate any problems that might have occurred in its initial use.

E.2 SOFTWARE DEVELOPMENT

Each routine for the Micro-DFCS software was developed using the method shown in Fig. E-3. The routines are written in the assembly language for the Intel 8085 CPU. This language consists of 80 different mnemonics that represent the machine operation codes. The assembly language is cross-assembled to the machine language and loaded to the microcomputer for debugging. Initially, the routines are tested separately, i.e., without the other program modules. This procedure helps identify problems that may occur when the routines are combined to operate in the program.

E.3 ADDING FLIGHT CONTROL ROUTINES TO CAS-1

New or modified Flight Control routines can easily be added to CAS-1. The procedure consists of 1) defining a new mode in the Mode Branch Table of CAS-1, 2) writing an appropriate mode set-up

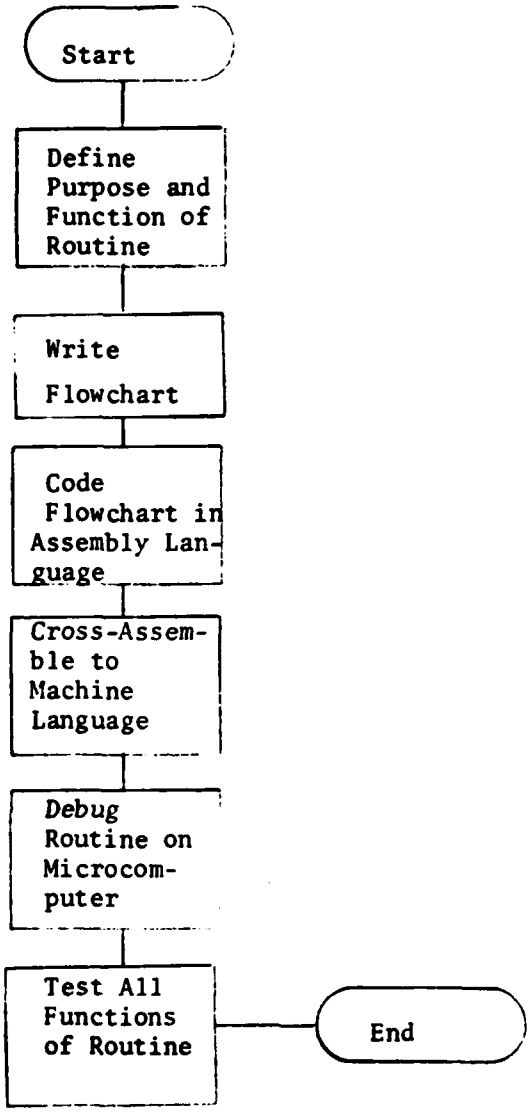

Figure E-3. Sequence for Developing Micro-Computer Routines.

routine, and 3) writing the flight control interrupt service routine in a form that makes it compatible with the operation of CAS-1. Step one is the only modification necessary to the coding of CAS-1. It consists of replacing the operand "BADEN" at the correct location in the Mode Branch Table with the label for the new mode set-up routine.

In the second step, the mode set-up routine is written to set the timed interrupt branch point and store parameters for the interrupt service routine. The branch point for the timed interrupt starts at 3FECH in RAM. A typical mode set-up routine is structured as in Fig. E-4. All registers are saved to insure the routine does not change any parameters for CAS-1. The interrupt is disabled so the interrupt service routine does not execute before the gains and other parameters can be changed. The mode type (e.g. OPEN LOOP, PITCH RATE, etc.) is displayed on the bottom line of the display and a corresponding voltage level is set on the analog status channel. After storage is set for the service routine, all registers are restored and the interrupt is enabled to allow the newly specified service routine to execute on the occurence of each timed interrupt.

The third step of the procedure is to structure the flight control interrupt service routine as shown in Fig. E-5. The interrupt is disabled to guarantee the routine completes before the next service routine starts. All registers are saved because the timed interrupt may break the program flow of CAS-1 at any point, and therefore the status of the program at the break must be saved.

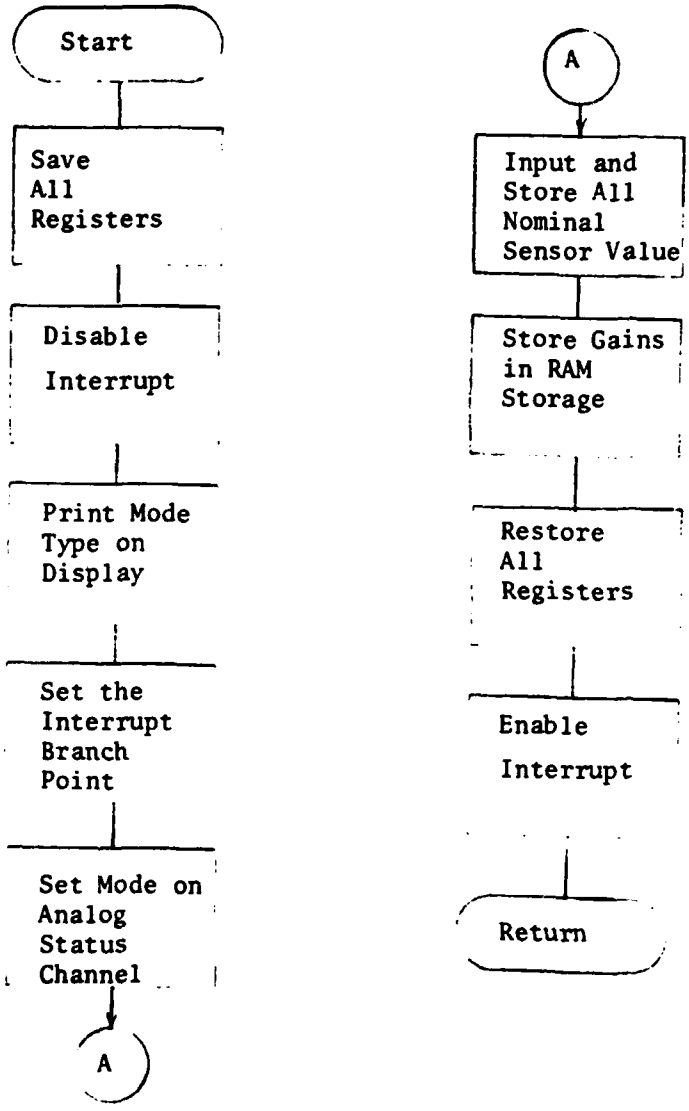

Figure E-4. Flowchart for Typical Mode Set-Up Routine.

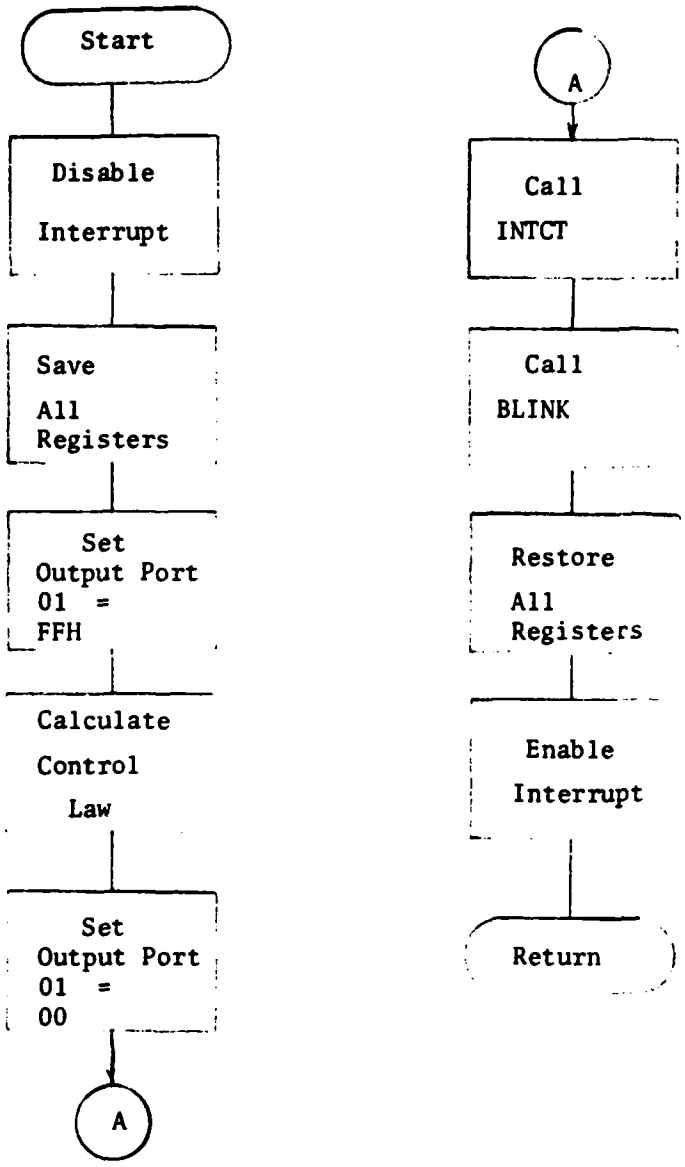

Figure E-5. Flowchart for Typical Flight Control Interrupt Service Routine.

Output port 01 is set to FFH to indicate the start of the control law inputs and calculations. The port is set to 00 to mark the end of the calculations. The time of the calculations can be measured by connecting an oscilloscope to this output port and observing the pulse length. The routine INTCT is called to increment a counter that keeps track of interrupts. The routine BLINK is called to flash the instrument panel light at one-tenth the sampling rate.

There is basically only one restriction on the Flight Control routine for the proper operation of CAS-1. The routine must complete execution within the sampling interval or no other routines will run. In such a case, there would be no available time for keyboard inputs, display outputs, or memory checks. See the CAS-1 source listing (not included in the thesis) for detailed examples of using mode set-up and flight control interrupt service routines.

REFERENCES

1. Konar, A. F., et.al., "Digital Flight Control Systems for Tactical Fighters", AFDL-TR-74-69, July 1974.

2. Yechout, T. R., and Oelschlaeger, D. R., "Digitac Multimode Flight Control System", AIAA Paper No. 75-1085, Aug. 1975.

3. Seacord, C. L., and Vaughn, D., "Computer Technology Forecast Study for General Aviation", NASA CR-137889, June 1976.

4. Gallagher, J. T., Saworotnow, I., Seeman, R., and Gossett, T., "A Model-Following Variable Stability System for the NASA ARC X-14B", Journal of Aircraft, Vol. 9, No. 7, July 1972, pp. 461-469.

5. Stein, G., Hartmann, G. L., and Hendrick, R. C., "Adaptive Control Laws for F-8 Flight Test", IEEE Transactions on Automatic Control, Vol. AC-22, No. 5, Oct. 1977, pp. 758-767.

6. Tobie, H. N., and Ramby, K. W., "A Practical Solution to Automatic Landings Using Digital Flight Control Computers", AIAA Paper No. 70-1032, Aug. 1970.

7. Mathews, M. A., Jr., "SAAB Digital Flight Control", AIAA Paper No. 74-26, Jan. 1974.

8. Osder, S. S., Mossman, D. C., and Devlin, B. T., "Flight Test of a Digital Guidance and Control System in a DC-10 Aircraft", AIAA Paper No. 75-567, April 1975.

9. Smyth, R. K., "Avionics and Controls State of the Art Survey (SOAS)", presented at the NASA Workshop on Avionics and Controls Research and Technology, Hampton, Va., June 1978.

10. Stengel, R. F., Broussard, J. R., and Berry, P. W., "Digital Controllers for VTOL Aircraft", IEEE Transactions on Aerospace and Electronic Systems, Vol. AES-14, Jan. 1978.

11. Motyka, P. R., Rynaski, E. G., and Reynolds, P. A., "Theory and Flight Verification of the TIFS Model-Following System", Journal of Aircraft, Vol. 9, No. 5, May 1972, pp. 347-353.

12. Dorato, P., and Levis, A. H., "Optimal Linear Regulators: The Discrete-Time Case", IEEE Transactions on Automatic Control, Vol. AC-16, No. 6, Dec. 1971, pp. 613-620.

13. McRuer, D., Ashkenas, I., and Graham, D., "Aircraft Dynamics and Automatic Control",Princeton University Press, Princeton, 1973.

14. Stengel, R. F., Broussard, J. R., and Berry, P. W., "The Design of Digital-Adaptive Controllers for VTOL Aircraft", NASA CR-144912, March 1976.

15. Stengel, R. F., Broussard, J. R., and Berry, P. W., "Command Augmentation Control Laws for Maneuvering Aircraft", AIAA Paper No. 77-1044, AIAA Guidance and Control Conf., Hollywood, Florida, August 1977.

16. Mrazek, J. G., and Robertus, D. P., "Considerations in the Design of a Digital Flight Control Function for a High Performance Aircraft", NAECON '74 Record, Dayton, Ohio, June 1974.

17. Berman, H., and Gran, R., "Design Principles for Digital Autopilot Synthesis", Journal of Aircraft, Vol. 11, No. 7, July 1974, pp. 414-422.

18. Gelb, A., Ed., Applied Optional Estimation, MIT Press, Cambridge, Mass., 1974.

19. Anon., "Flying Qualities of Piloted Airplanes", MIL-F-8785B(ASG), USAF/USN, August 1969.

20. Bryson, A. E., Jr., and Ho, Y. C., Applied Optimal Control, Ginn-Blaisdell Co., Waltham, Mass., 1969.

21. Stengel R. F., Broussard, J. R., and Berry, P. W., "Digital Flight Control Design for a Tandem-Rotor Helicopter", Proceedings of the 33rd Annual National Forum of the American Helicopter Society, Paper No. 77-33-44, Washington, May 1977.

22. Tyler, J. S., Jr., "The Characteristics of Model-Following Systems as Synthesized by Optimal Control", IEEE Transactions on Automatic Control, Vol. AC-9, No. 4, Oct 1964, pp. 485-498.

23. Stengel, R. F., "Digital Flight Control Research Using Microprocessor Technology", Flight Control Systems Criteria Symposium, Naval Postgraduate School, Monterey, Calif., August 1978.

N

DATE

ILME